Laser Surface Texturing of Multicrystalline Silicon to Reduce Solar Weighted Reflectance

Mehrnegar Aghayan

A Thesis

in

the Department

of

Electrical and Computer Engineering

Presented in Partial Fulfillment of the Requirements

for the Degree of Master of Applied Science at

Concordia University

Montréal, Québec, Canada

November 2015

CONCORDIA UNIVERSITY
SCHOOL OF GRADUATE STUDIES

This is to certify that the thesis prepared

By: Mehrnegar Aghayan

Entitled: "Laser Surface Texturing of Multicrystalline Silicon to Reduce Solar Weighted Reflectance"

and submitted in partial fulfillment of the requirements for the degree of

Master of Applied Science

Complies with the regulations of this University and meets the accepted standards with respect to originality and quality.

Signed by the final examining committee:

_____ Chair
Dr. R. Raut

_____ Examiner, External
Dr. M. Hojjati (MIE) To the Program

_____ Examiner
Dr. M. Z. Kabir

_____ Supervisor
Dr. S. Williamson

_____ Supervisor
Dr. S. Narayanswamy (MIE)

Approved by: _____
Dr. W. E. Lynch, Chair
Department of Electrical and Computer Engineering

_____20_____ _____
Dr. Amir Asif, Dean
Faculty of Engineering and Computer Science

ABSTRACT

Laser Surface Texturing of Multicrystalline Silicon to Reduce Solar Weighted Reflectance

Mehrnegar Aghayan

Increase in the global demand for energy, has put a lot of pressure on natural resources such as gas and oil that are predicted to be diminished in not too distant future. Global warming which is the consequence of burning fossil fuels is an alarming issue as well. Solar cells that can transform the clean and abundant solar energy into electricity have shown to be one of the promising solutions for supplying the energy demand which is the number one problem that we face today. However, efficiency along with costs associated with the material and fabrication of solar cells should be improved in order to make them a practical alternative to the fossil fuels. Silicon (Si) has proven to be the most dominant semiconductor used in optoelectronic devices. It is the second abundant element on the earth, which results in its lower production costs compared to other semiconductors. Furthermore, based on Shockley–Queisser limit calculations, maximum efficiency of a single junction solar cell occurs with a band gap of 1.34eV therefore, Si having a band gap of 1.12eV is highly recommended to produce maximum efficiency of a solar cell. Since solar technology is still not cost-effective and efficient enough to compete with the fossil fuels, researchers are investigating new methods to overcome the mentioned limitations.

In this work, multicrystalline silicon (mc-Si) which is less expensive compared to the single crystalline silicon (sc-Si), is textured with nanosecond laser; not only to decrease the optical loses due to reflection from the surface but also to increase the absorption by increasing the optical path length of the light. Texturing was performed on the mc-Si surface and the effect of laser fluence, spot overlap percentage, and number of scans on the Solar Weighted Reflectance (SWR) as well as surface morphology of mc-Si was studied. Statistical analysis was implemented to identify the most efficient laser parameters to reduce SWR and it was found that increase in average surface roughness (R_a) and depth decreases the SWR. R_a and depth were measured by means of scanning electron microscopy and optical interferometry.

The experiments were done both in ambient air as well in acetone confinement and a comparison was made in terms of R_a, depth and SWR. The technique of acetone-assisted laser texturing takes the advantage of bubble formation, which results in a debris free microfabrication where depth and consequently SWR is improved. Results validated the correlation of the higher number of pulses with the increased depth and R_a when texturing was conducted in acetone.

In order to understand if depth or R_a plays the major role in SWR reduction, a regression analysis was performed, and the results indicated that the increase in depth plays more significant role in reduction of SWR compared to increase in R_a. Finally, an attempt was made to fabricate the P-N junction and the electrodes with both textured and untextured mc-Si wafer surfaces. From the I-V characterization of these devices, it was seen that untextured wafer as well as wafers textured at 0% overlap produced output power.

Solutions are presented to improve the electrical properties of the fabricated cells that might be implemented in the future works.

Acknowledgment

I would like to express my special appreciation and thankfulness to my supervisor Dr. Sivakumar Narayanswamy and my co-supervisor Dr. Sheldon Williamson for their constant support along with patience and valuable guidance during my graduate research work.

In addition, I would like to thank Dr. Laszlo Kalman from Physics department, who let me use his lab facilities for performing my optical measurements and McGill Nanotools Microfab lab staff for their support during my fabrication stage. Furthermore, I would like to Thank Dr. Mohammad Keshmiri for his collaboration in developing the LabVIEW program.

Finally, I would like to express my deep gratitude to my parents and husband for their heartiest support and encouragement.

Table of Contents

List of figures

List of tables

List of Abbreviations

Si	-	Silicon
c-Si	-	Crystalline Silicon
sc-Si	-	Single Crystalline Silicon
mc-Si	-	Multicrystalline Silicon
DI		Deionized
IPA		Isopropyl Alcohol
IEO	-	International Energy Outlook
PV	-	Photovoltaic
Al	-	Aluminum
ITO	-	Indium doped Tin Oxide
AM	-	Air Mass
EHP	-	Electron Hole Pair
SRH	-	Shockley Read Hall
H_2O_2		Hydrogen peroxide
H_3PO_4		Phosphoric acid
NaOH	-	Sodium Hydroxide
H_2SO_4		Sulfuric acid
KOH	-	Potassium Hydroxide
HF	-	Hydrofluoric acid
HNO_3	-	Nitric acid
CH_3COOH		Acetic acid
DMSO		Dimethyl sulfoxide
N_2	-	Nitrogen
O_2	-	Oxygen
Ar	-	Argon
SF_6	-	Sulfur hexafluoride
He		Helium
KrF		Krypton fluoride
Cl_2		Chlorine
TMAH		Tetramethyl ammonium hydroxide

Nd:YAG	-	Neodymium-doped yttrium aluminium garnet
Nd:YVO_4	-	Neodymium-doped yttrium orthovanadate
SEM	-	Scanning Electron Microscopy
RPM	-	Rounds per minute
IR	-	Infrared
NIR		Near Infrared
UV	-	Ultraviolet
ANOVA	-	Analysis of Variance
SWR	-	Solar Weighted Reflectance
PECVD		Plasma Enhanced Chemical Vapor Deposition
NP	-	Nano Particle
FF	-	Fill Factor

List of Symbols

R_a	-	Average surface roughness
J_d	-	Dark current density
J_L	-	Photo current density
I_{sc}	-	Short circuit current
V_{oc}	-	Open circuit voltage
L	-	Diffusion length
P_{max}	-	Maximum output power
$\alpha(\lambda)$	-	Absorption coefficient
τ	-	Minority carrier lifetime
E_g	-	Band gap

CHAPTER 1. Introduction

1.1 General overview

Energy is reported as the number one problem that human is facing today. The world population is reported 7 billion while it is predicted to be around 9 billion by 2040, therefore people are demanding for more energy due to the increase in their population. It is forecasted by the International Energy Outlook (IEO) that energy consumption will grow by 56% in 2040 compared to 2010 [1]. As a result of global demand for energy, global warming has become a serious problem originated from fossil fuels which are accounted for a total of 86% of our energy consumption [1]. Furthermore, natural resources for providing energy such as gas and petroleum are finite therefore, if the energy consumption is further increased, the natural energy resources would be depleted. Sun, which is one of the largest and cleanest sources of energy, can provide 4.3×10^{20} J in one hour for the earth, which is almost equal to the amount of energy that is consumed in one year [2]. Therefore, solar electricity is becoming one of the alternatives to the fossil fuels and growing at a rate of 40-50% per year [3]. However, the huge potential of solar energy is not still used due to some challenges in the photovoltaic (PV) area, which are mainly due to the trade-off between cost and efficiency. That is, more expensive materials and more complicated fabrication techniques can lead to higher efficiency photovoltaics. Therefore, it is essential to establish new methods in which both factors are improved without scarifying the other.

Scientists around the world are conducting researches in the field of renewable energy in order to reduce the material and fabrication costs while increasing the efficiency so that PV devices can compete with the traditional sources of energy. Silicon (Si), which is the second abundant element on the earth, is one of the promising semiconductors used in PV modules due to its lower price and easy fabrication techniques compared to other semiconductor materials. Based on solar energy utilization report, currently 90% of the PV modules are based on crystalline silicon (c-Si) where 60% are based on multicrystalline silicon (mc-Si) and 30% are based single crystalline silicon (sc-Si) [3]. Multicrystalline silicon, which is a low-cost alternative to the sc-Si, has a lower quality therefore, many researches are being conducted in order to make it efficient enough so that it can replace the expensive sc-Si. Texturing is a method to increase the efficiency by enhancing the light absorption. This technique reduces the optical losses due to high reflection from the surface by

increasing light trapping and optical path length of the light. Alkaline chemical etching, which is an anisotropic texturing method, is a typical technique in sc-Si texturing, and is not appropriate for texturing mc-Si wafers due to their random crystallographic orientation. Laser texturing which is independent of the crystallographic orientation is a beneficial method for texturing mc-Si wafers. For instance, the efficiency of a solar cell has increased from 5-6% (for bulk sc-Si solar cell) to 25% (for mc-Si solar cell textured with laser) [4] that is close to the theoretical limit for a single junction solar cell, which is 31% [5].

1.2 Literature review

Texturization of the silicon is one of the major techniques in decreasing the reflection loses. This is achieved by various methods such as mechanical techniques, alkaline chemical etching, acidic etching and laser texturing.

In many reports, Solar Weighted Reflectance (SWR) is calculated in order to compare the optical properties of the textured an untextured surfaces. SWR is defined as the integration of reflectance over the range of wavelengths times air mass (AM) 1.5 photon density divided by the total number of photons at that range of wavelengths. The importance of calculating SWR relies on the fact that, most of the times comparing the reflectivity of different surfaces is more important than knowing the reflectivity of each surface at a selected range of wavelengths. For such investigations, it is complicated to compare the reflectivity response of each surface at each wavelength. By integrating the reflectivity over any desired range of wavelengths, we can attribute to each surface a single value, which is called SWR calculated using Equation 1.1.

$$SWR = \frac{\int_{300}^{1100} R(\lambda) I(\lambda) d\lambda}{\int_{300}^{1100} I(\lambda) d\lambda} \tag{1.1}$$

where R is the reflectance, I is solar irradiance for AM1.5 [6] and d is the wavelength range considered for the integration. For silicon based solar cell applications.

1.2.1 Mechanical texturing

Nakaya et al. [7] have used the dicing machine with beveled blades for creating 70 μm V-shaped groves on the surface of the p-type mc-Si. An alkaline chemical etching process was used to remove the damage caused during the dicing. They investigated the effect of etching time (5 min,

10 min and 20 min) on the surface reflectance and concluded that, reflectivity increases as etching time goes further than 5 min. It was found that, after 5 min etching in NaOH (3%) not only the damage layer was removed but also the best surface reflectance was achieved. However, this technique is not considered as an efficient texturing method because it is not suitable for mass production [8].

Machida et al. [9] implemented mechanical grooving technique, for texturing mc-Si as the basis of solar cell. In order to achieve the maximum light trapping, they investigated the grooving angle and showed that, a grooving angle of 40° to 55º results in a better solar cell performance. By implementing a multi-blade wheel grinding method (Figure 1.1), they tried to make their technique more suitable for mass production. In this technique, process time of grooving was reduced by increasing the table speed to 6 m/min and implementing a diamond wheel with a diameter of 200 mm and thickness of 28 mm at 9000 rpm.

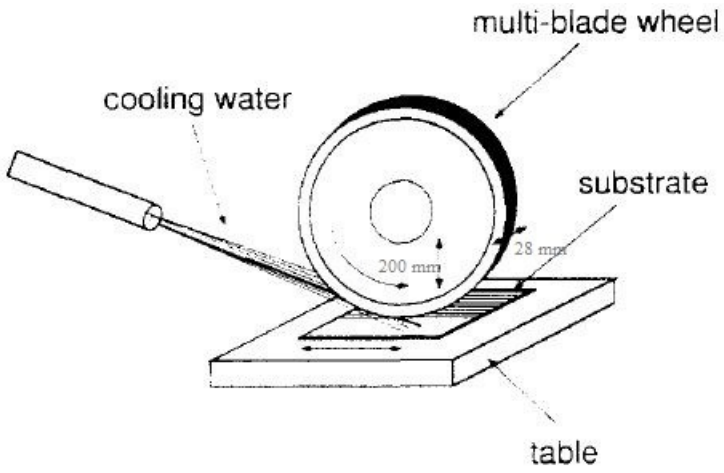

Figure 1.1 Schematic of the multi-blade wheel grinding [9].

The pattern formed by multi-blade technique had pitch and depth of 70 μm, which highly took the advantage of light trapping effect. In order to remove the damage, they etched the textured samples in acid or alkaline solution and it was shown that the conversion efficiency of a cell based on etched samples in acid solution for only 10 s is almost equal to that of a cell etched in alkaline solution for 5 min.

1.2.2 Alkaline chemical etching

Singh et al. [10] implemented inorganic alkaline chemical etching for creating pyramids on the Boron-doped (100) sc-Si in order to reduce the reflection loses by increasing the light trapping. In their work, etching was carried out on Czochralski grown sc-Si wafers with resistivity of 1-2 Ωcm. The etchant was a combination of NaOH and KOH diluted in 18 MΩ deionized (DI) water. They did the texturing in two steps including removing the saw damage for 20 min where the temperature and etchants concentration were high (>80ºC, >20wt %) and the texturing step where the etchants concentration was low (<5wt %) and temperature was 70-80 °C. Figure 1.2 shows the effect of etching time on the surface topography of sc-Si wafers etched with 2 wt% NaOH and 20 wt% isopropyl alcohol (IPA) at 80 °C. Results show that size and density of pyramids increase as etching time increases up to 35 min and further increasing the etching time results into formation of smaller pyramids on top of the existing ones and alters their uniform distribution. Figure 1.3 shows that reflectivity decreases by increasing the etching time and it is evident that further increase in etching time beyond 35 min does not dramatically reduce the reflectivity. The formation of pyramids is because, in anisotropic etching techniques, etch rate of (111) surface is 35 times lower than that of (100) plane and etching is preferential. This dependency of the etch rate on the crystal orientation, leads to formation of pyramids at (100) planes of the silicon wafer. However, if this technique is applied on mc-Si wafers, it will not give a uniform texturing pattern due to the anisotropic crystal orientation of the wafer and the preference of the alkaline chemicals etchants to the (100) facades.

Papet et al. [11] implemented tetramethyl ammonium hydroxide (TMAH) for texturing the front surface of sc-Si to improve the light trapping for the application of solar cell. They carried out their experiments on p-doped (100) sc-Si wafers with resistivity of 1-10 Ωcm. In order to remove the native oxide layer, they etched their samples in 5% HF for 10 s and rinsed them in DI water before each texturization process. They investigated the effect of different parameters such as temperature, concentration and duration on texturization of as cut, etched and polished Si. By implementing TMAH, which has a good compatibility with solar cell devices, they solved the problem of contamination that is one of the issues in KOH and NaOH wet etchings. Since the etching rate is highly dependent on the concentration of the etchants, they minimized the amount of TMAH by using IPA and agitation. In this work, the minimum SWR they could achieve was

13% by applying 2% TMAH and 8% IPA at 80 °C for 30 min. As shown in Figure 1.4, increasing the concentration of TMAH up to 2% decreases the reflectivity while further increasing its concentration increases the reflectivity.

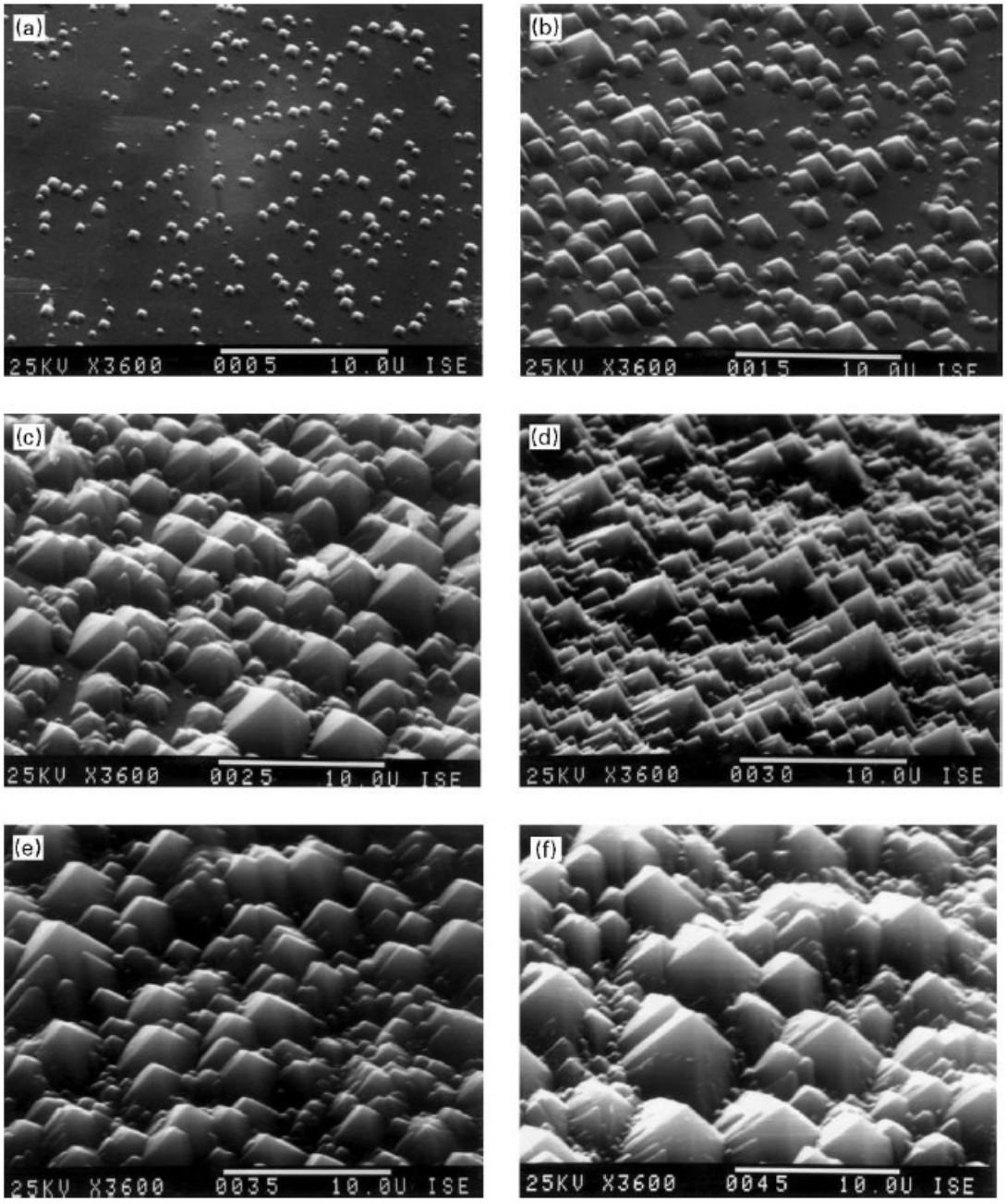

Figure 1.2 SEM image of the sc-Si after etching in 2wt% NaOH and 20% IPA at 80 °C for; a) 5 min, b) 15 min, c) 25 min, d) 30 min, e) 35 min, f) 45 min [10].

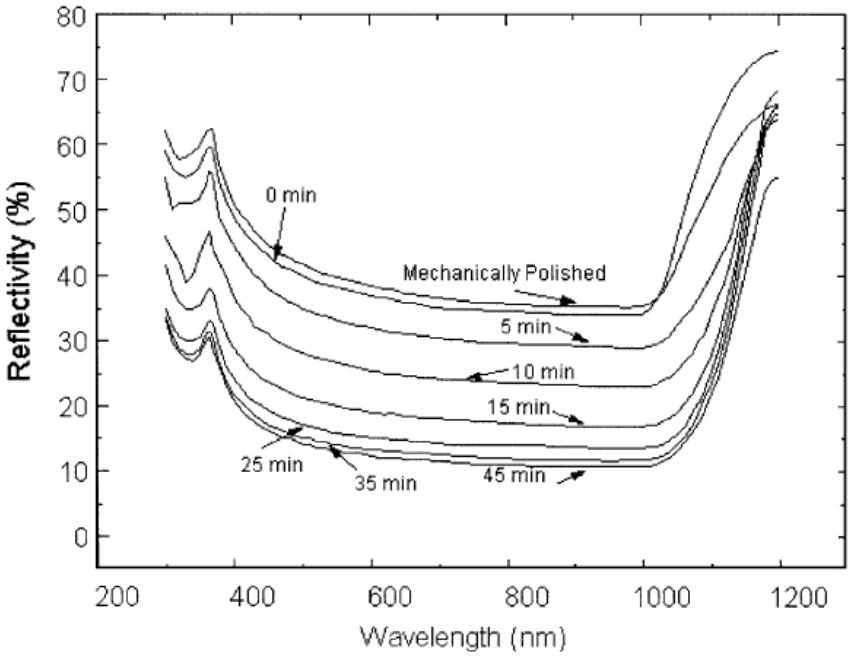

Figure 1.3 Reflectivity of textured sc-Si wafers at different etching durations [10].

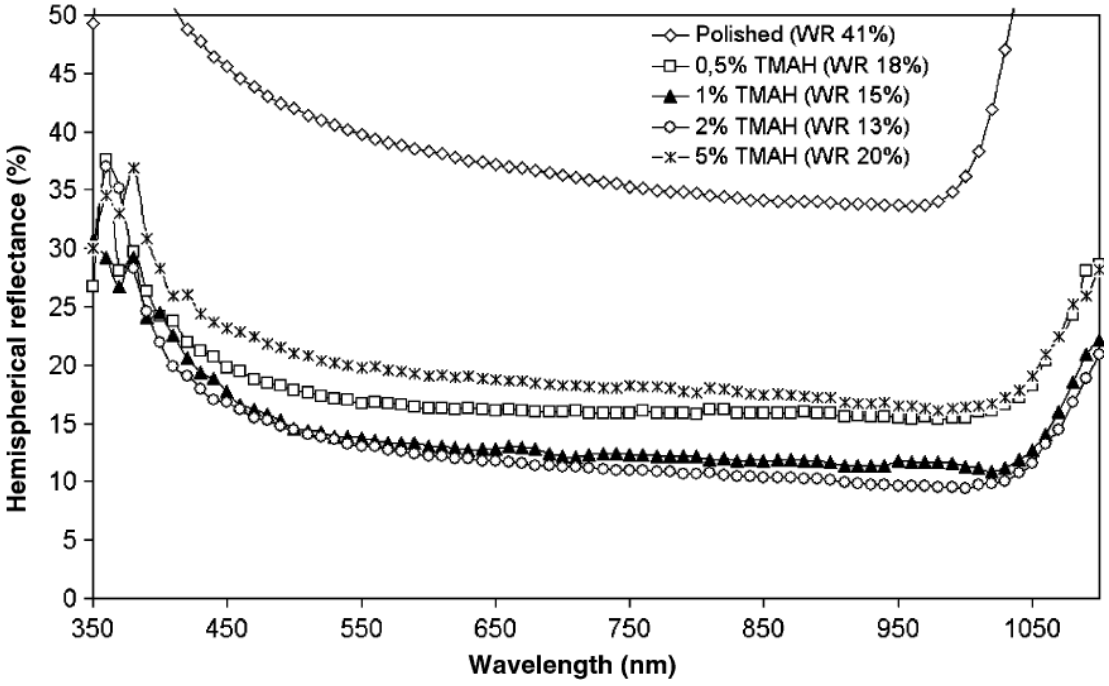

Figure 1.4 Effect of TMAH concentration on reflectivity [11].

1.2.3 Acid texturing

Cheng et al. [12] used acidic texturing which is an isotropic etching approach for texturing mc-Si. They implemented HF and HNO_3 to create hemisphere like patterns (Figure 1.5) on the wafer, which result in uniform texturing. By investigating the effect of acid concentration and etching-time duration, it is understood that at room temperature, the minimum reflectivity is achieved at etching ratio of $HF:HNO_3:H_2O$ (15:1:2.5) and etching time of 60 s. In the acidic texturing, due to its isotropic nature, if the etching is deep a smooth roughness will be achieved and if the etching is not deep, the saw damage will not be removed which results in low short-circuit current (I_{sc}) and open-circuit voltage (V_{oc}), respectively. Therefore, this technique has some deficiencies including, incapability to form a rough surface compared to the alkaline etched wafers as well as hazardous nature of the chemicals such as HF.

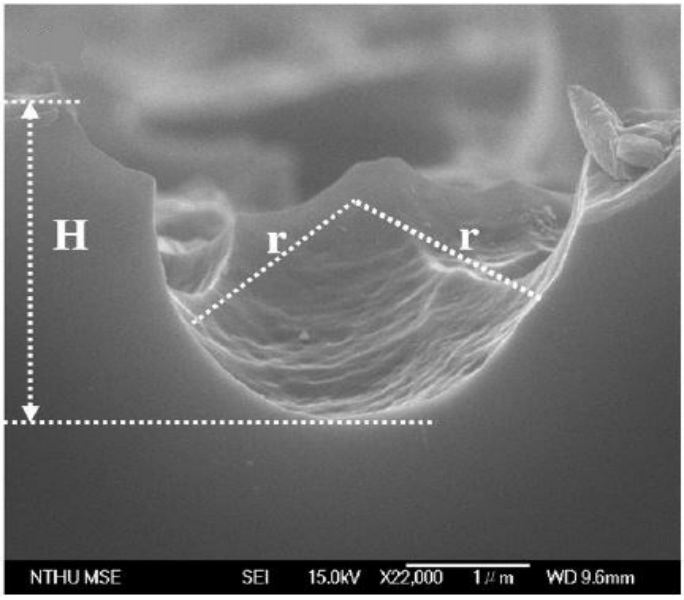

Figure 1.5 SEM image of hemispherical pattern due to acid texturing [12].

Marstein et al. [13] implemented acid solutions for texturing mc-Si wafers used for optoelectronic devises. They conducted their experiments on Boron-doped as-cut mc-Si and polished (100) sc-Si with resistivity of 0.5-2 Ωcm and 10-15 Ωcm, respectively. These wafers having thicknesses of 330 μm for mc-Si and 525 μm for sc-Si were textured in HF and HNO_3 diluted with H_2O, H_3PO_4 or H_2SO_4. The wafers were then rinsed in DI water and blown dry. They showed that the textured surface was covered with a porous Si layer that has detrimental effects on electrical properties of

solar cell devices due to its high resistivity and recombination rate [14]. Therefore, they removed this layer with 1% aqueous solution of NaOH for a few seconds. By investigating the optical properties of polished and textured mc-Si, they found that, reflectivity of a polished wafer is 25%-30% while it is improved to 15% by acid etching. However, the minimum reflectivity of 15% is achieved for a crack-dominated wafer. They also showed that, although cracks gradually diminish if etching-time duration extends, but the reflectance exceeds that of a polished wafer. Therefore, one of the main limitations of acid texturing is that, the minimum reflectance is achieved when a weak etching is applied with a crack-dominated texture where electrical properties are not favorable. On the other hand, if texturing goes beyond the damage layer in order to improve recombination issues, reflectivity becomes dramatically high. Therefore, in this method there is a tradeoff between light absorption and carrier collection, which in turns affects I_{sc} and V_{oc}, respectively.

Volk et al. [15] implemented a dielectric layer to create a honeycomb structure on p-type mc-Si with a thickness of 200 μm and resistivity of 3 Ωcm. A picosecond laser with wavelength of 355 nm and pulse repetition rate of 50 KHz was used to create openings on the dielectric masking layer, which covered the whole surface of the mc-Si wafers. The dielectric layer was a Plasma Enhanced Chemical Vapor Deposition (PECVD) Si_3N_4 with a thickness of 200 nm. After making hexagonal openings on the PECVD Si_3N_4 layer, isotropic etching was applied by spraying the wafers with an acid solution of 1:4 HF (40% (w/w)) and HNO_3 (69% (w/w)). After etching process, wafers were immersed in a buffered HF solution for 10 min in order to remove the masking layer. Morphology characteristics of the etched wafers has been characterized with confocal microscopy. Results show that, the spacing between the spots is equal to 34.3 ± 1.5 μm and that there is a homogenous triangular alignment between the holes with a diameter of 8 μm. It reported in [16] that aspect ratio is an important factor in the SWR of the structures with spherical segments, therefore in this work aspect ratio has been analyzed to investigate SWR. These investigations suggest that, aspect ratio of 0.5 has the minimum SWR. That is, a surface reflectance of 15% for a 600 nm wavelength light. Furthermore, their results validated the correlation of higher aspect ratio with increased SWR. The maximum aspect ratio was achieved after 78 s of etching where holes of depth of 15 μm and width 31.5 μm were featured (Figure 1.6 (a)). Further etching the structures had a reverse effect on aspect ratio and SWR that is, a lower aspect ratio of 0.2 and SWR of 29% were achieved upon etching time of 144s. The reduced aspect ratio due to increased etching

time from a certain limit is reported to be due to overlapping of the neighboring holes (Figure 1.6 (b)).

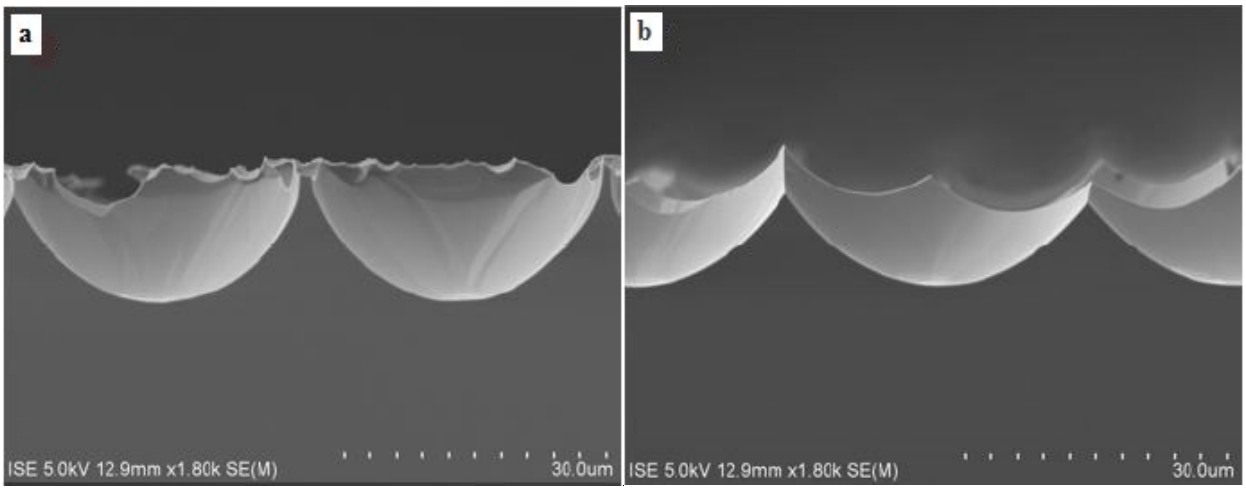

Figure 1.6 SEM image of the honeycomb structure after 2 different etching-time durations; a) 78 s and b) 144 s [15].

Gangopadhyay et al. [17] investigated different approaches of mc-Si texturing. In this work, they textured p-type (Boron-doped) mc-Si wafers with resistivity in the range of 0.5-2 Ωcm. In the first stage, all samples were etched for 3 min in an acid solution of HF (49%), HNO_3 (69%) and DI water (14:1:5). This step created a mesoporous layer on the mc-Si samples. Then all samples were categorized into 3 groups under which different etching treatments were applied. In the first treatment, samples were immersed in 1.5% diluted NaOH for 15 s. Samples in the second group were baked in conveyor IR belt furnace at 450 ºC for 5 min. This step was followed by 10 s etching in HF. In the third treatment stage, samples were dipped in HNO_3 and HF (98:2) for 2 and 5 min. Note that, all steps were followed by rinsing in DI water and drying. Optical investigations show that, the samples underwent the third treatment ($HF:HNO_3:H_2O$ (14:1:5) followed by HNO_3:HF (98:2)) have the least reflectance compared to others. They attributed this to the fact that, these samples are more roughened and have taller microstructures created on their substrates.

- Based on section 1.2.1, mechanical grooving is not a suitable technique to be used in mass production of textured mc-Si.
- Based on section 1.2.2, alkaline chemical etching, is not an appropriate method for texturing mc-Si since it is an anisotropic etching technique.
- Based on section 1.2.3, although acid texturing is a more suitable technique for texturing mc-Si wafers due to its isotropic nature, the texture pattern does not revel fine optical properties if etching is performed in a way that surface damages are removed. Therefore, if better absorbance property is desired the wafer would be dominated with cracks, which are considered as defect centers where recombination occurs; and electrical properties of the final solar cell device are degraded.

As a conclusion, none of the above approaches is technically efficient for texturization of mc-Si wafers. As such, laser texturing which is known as a method independent to the crystallographic orientation of the wafer and has a high throughput, is explained in the following sections:

1.2.4 Laser texturing

Laser texturing of Si is categorized based on different factors including:

- Texturing ambient
- Wavelength of laser
- Pulse duration of laser

Investigations on the laser texturing of Si show that, morphology and optical properties of laser-induced Si structures depend on the texturing ambient. For instance, as shown in Figure 1.7 [18] microstructures formed in the presence of SF_6 or Cl_2 have sharper tips compared to those created in air and N_2. Furthermore, it is shown that surface roughness and number density of the conical structures made in SF_6 are more substantial than other ambients. Furthermore, based on Figure 1.8, in the range of $\lambda < 1$ μm the reflactance of the textured sampels is less than that of a flat surface and in the wavelength range of 1.2-2.5 μm SF_6-prepared samples have the lowest reflectanse.

As shown in Figure 1.9 Si has a higher absorption coefficient, which is inversely proportional to reflectance, at lower wavelengths and its absorption coefficient sharply reduces to zero when the energy of the laser goes bellow its band gap energy. Therefore, based on the application, it is important to choose the best laser that provides the desired energy for that particular experiment.

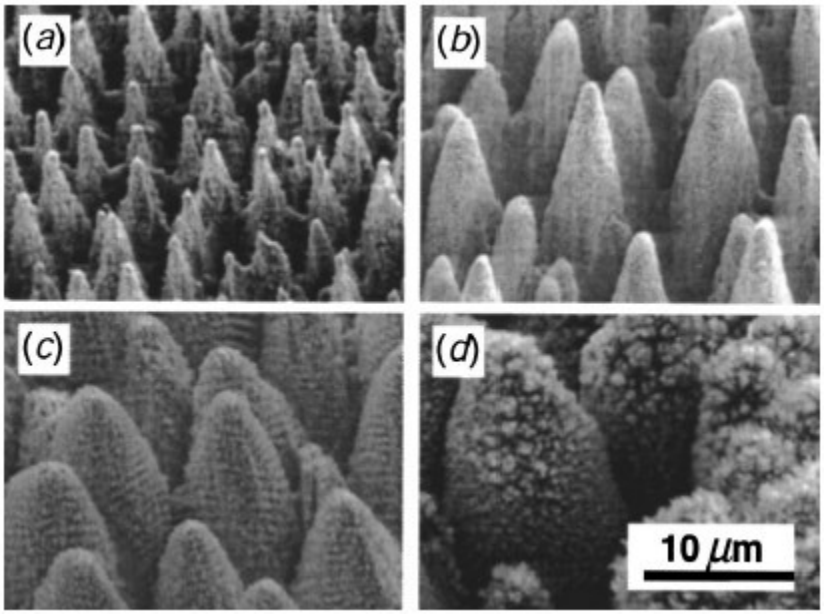

Figure 1.7 SEM image of the fs-formed microstructures in different ambients; a) SF_6, b) Cl_2, c) N_2 and d) air [18].

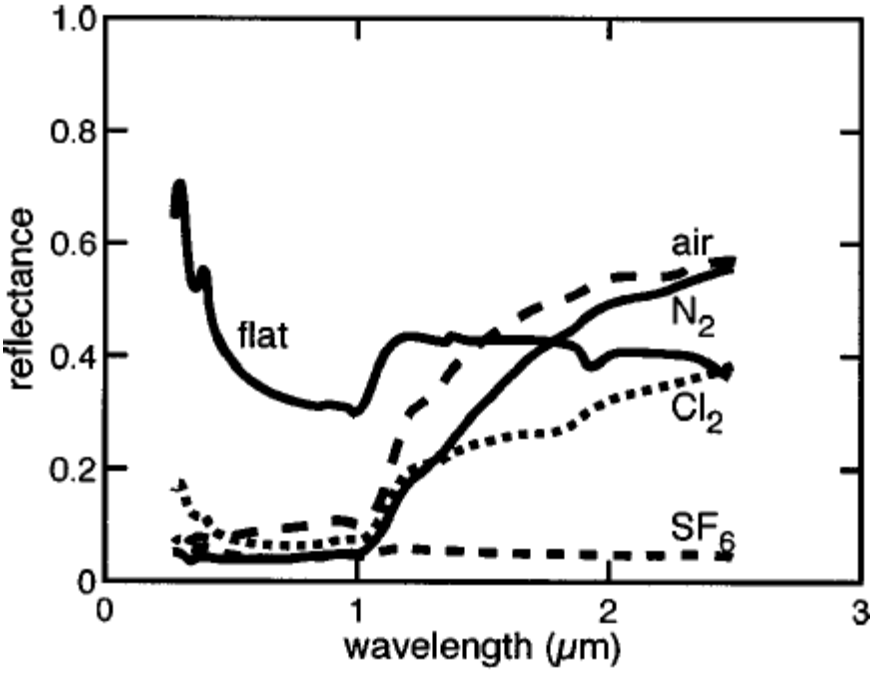

Figure 1.8 Reflectance of Si textured in different ambients (SF_6, Cl_2, N_2 and air) [18].

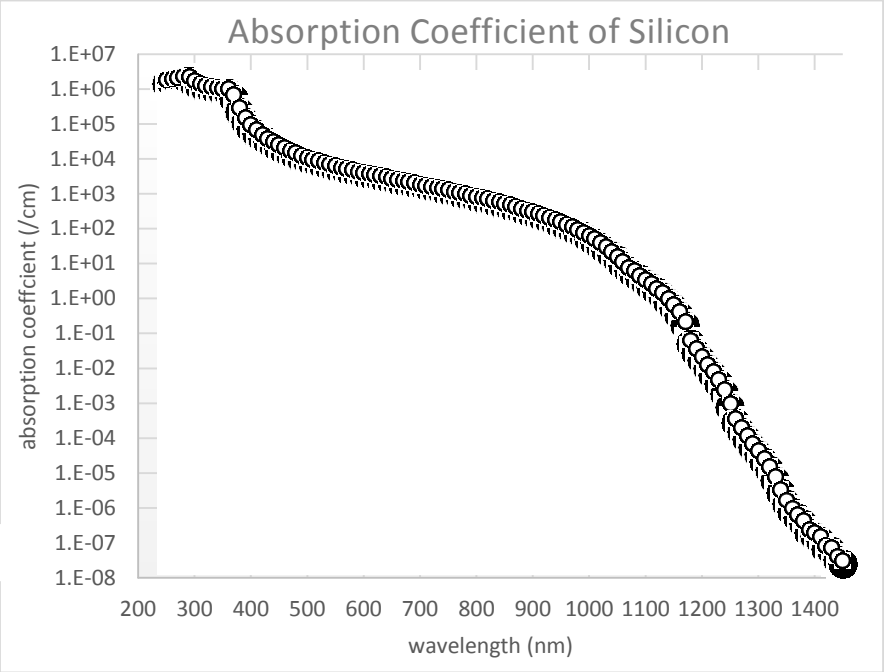

Figure 1.9 Absorption coefficient of Si as a function of wavelength [19].

When the laser is set in the pulsed mode, pulse width, which is the time duration that the pulse laser is being emitted, becomes as an important factor since it influences the heat affected zone in the laser processing experiments. In Figure 1.10 ‘t’ is the pulse duration that in ultrashort lasers is in the range of femtosecond to picosecond and is in the range of nanosecond for the short pulse lasers. ‘R’ is the repetition rate of the laser that affects the peak power that is, increasing the repetition rate of the laser reduces the peak power.

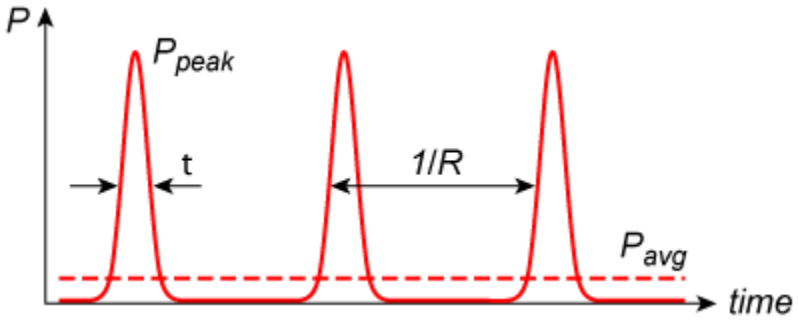

Figure 1.10 Temporal mode of laser power.

1.2.4.1 Laser texturing in air

Dobrzañski et al. [20] used laser texturing method for increasing the light absorption of mc-Si wafers. The material used in this work was p-type (Boron-doped) mc-Si with the thickness of 330 µm and resistivity of 1 Ωcm. The operating laser in this work was an Nd: YAG laser with wavelength of 1064 nm and pulse repetition rate of 15 KHz, max output power 50 W and spot diameter of 10 µm. After the process of laser texturing, samples were etched in 20% KOH at 80ºC for removing the laser-induced damage. By investigating the optical properties of the produced textures, a significant reduction in the effective surface reflectance from 34.08 to 12.44% was observed.

Fu et al. [21] investigated nanosecond laser multi-pulse effect on ablation of Si in air ambient. Schematic of the experimental setup is shown in Figure 1.11. Experiments were performed on undoped, (100) sc-Si with a thickness 680 µm and irradiations were done with a fiber laser with wavelength of 1064 nm and pulse duration of 200 ns. The spot diameter of the laser beam was reduced to 30 µm by a 100 mm focal length lens. Investigations on the morphology of the textured structures has been done with optical microscope and scanning electron microscope (SEM) and for measuring the *ablation rate*, which is defined as the *ablation depth divided by number of pulses*, phase-shift white-light interferometer has been used. Results show that, at pulse repetition rate of 25 KHz, ablation rate of a hole irradiated by 10 pulses increases from 1 µm/pulse to 4.5 µm/pulse when laser fluence increases from 20 J/cm^2 to 100 J/cm^2. Besides, by investigating the effect of number of pulses on the ablation rate, they found that at laser fluence of 70 J/cm^2 and pulse repetition rate of 25 KHz, increasing the number of pulses from 4 to 7 results in a 1.8 µm/pulse increase in the ablation rate. Furthermore, by investigating the effect of pulse duration on the ablation rate, they understood that beyond 5 KHz, increasing this parameter enhances the ablation rate since the temporal distance between the pulses is decreased. Therefore, it is concluded that ablation rate is improved by increasing the number of pulses and reducing the pulse-to-pulse temporal distance. On the other hand, they demonstrated that when the spatial distance between the neighboring holes decreases ablation depth from the second hole increases. In broad terms, they showed that ablation depth of holes with the same laser parameters is the same only for the first ablated holes and it increases as the spacing between the holes reduces while there is no

overlap between the pulses (Figure 1.12). They found that this phenomenon occurs only when the spatial distance between the pulses is less than 300 μm. They explained this multi-pulse enhancement effect by the fact that, the residual heat at the specimen induced by previous pulses increases the absorption coefficient of Si, when the temporal and spatial distance of the pulses is very short.

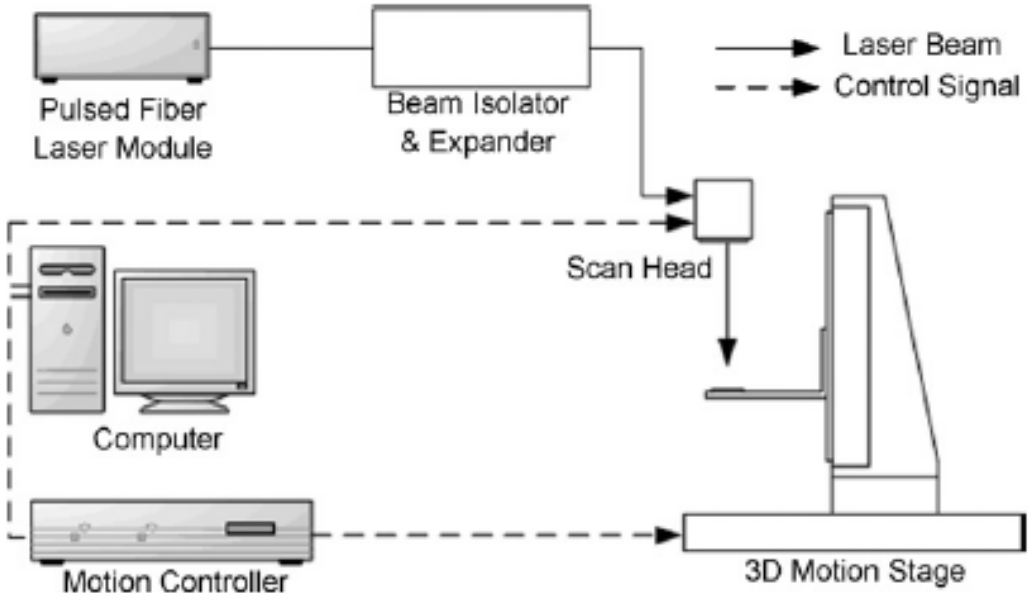

Figure 1.11 Schematic of the experimental setup of Si laser texturing in air ambient. [21].

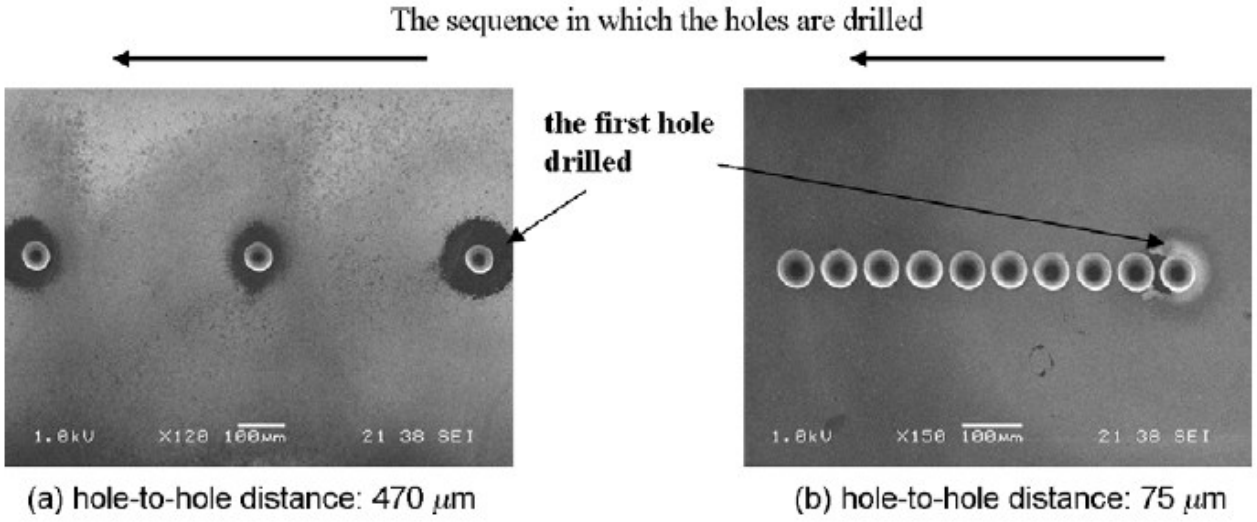

Figure 1.12 SEM image of the laser-drilled holes on Si with different spacing; a) 470 μm and b) 75 μm [21].

1.2.4.2 Laser texturing in gas ambient

In order to investigate the effect of background gas on morphology and optical properties of the laser-induced Si structures, some reports on laser texturing in different ambient such as O_2 [22], SF_6 [23], or other gases [24][25] are reviewed in this section. Figure 1.13 is a schematic of a laser texturing experimental setup in gas ambient.

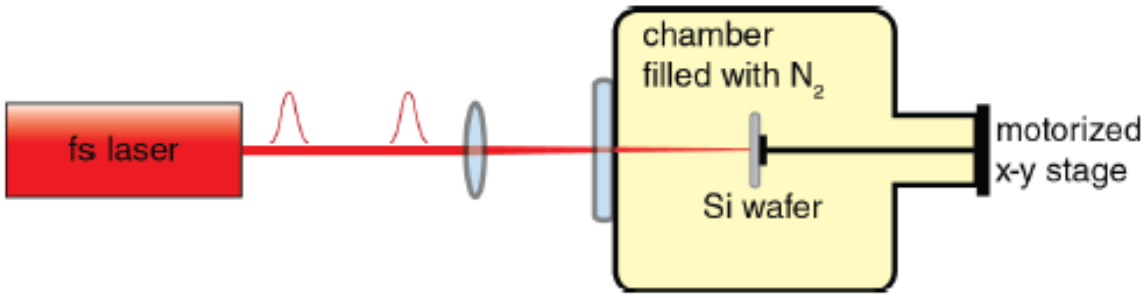

Figure 1.13 Schematic of Si laser texturing in N_2 ambient [28].

Pedraza et al. [24] investigated the effect of laser beam polarization on the morphology of Si nanostructures. They conducted all laser texturing experiments on Boron-doped Si wafers in 99.999% pure He atmosphere. Irradiations were done with Excimer laser with wavelength of 284 nm and pulse duration of 25 ns. Some of the samples were first irradiated in SF_6 atmosphere prior to laser texturing in He. Samples were immersed in 10:1 HF aqueous solution for 5 min to remove the native oxide layer and after being rinsed and dried, they were kept in vacuum chamber of pressure 1×10^{-7} Torr. They investigated formation of periodic nanometer structures on the Si substrates and found a relation between the wavelength of the periodic structures and the irradiating laser wavelength as well as incident angle. Furthermore, it is shown that upon polarized beam irradiation, linear arrays of Si NPs protrude the Si substrate while such alignment was not observed when the laser light was not polarized.

Crouch et al. [25] compared the effect of pulse duration on optical properties, chemical composition and crystallinity of microstructures formed on Si substrates by laser texturing in SF_6 ambient. They conducted their experiments in a vacuum chamber of SF_6 with a pressure of 0.67 bar for femtosecond experiments and 1 bar for nanosecond experiments. The femtosecond laser used in this work, was a Ti:sapphire with wavelength of 800 nm and pulse duration of 100 fs. The average laser fluence of this femtosecond laser that has a Gaussian profile was 8 KJ/m^2. The KrF

Excimer laser with a wavelength of 284 nm and pulse duration of 30 ns was operating at fluence of 30 KJ/m^2 and had a flat-top profile. An average of 500 and 1500 pulses were delivered to each part of the samples in fs and ns experiments, respectively. Results from SEM images show that, the height and spacing between the microstructures formed with nanosecond laser are 5 times more than those of femtosecond laser are. Furthermore, it is demonstrated that particles in the order of 10-50 nm cover the microstructures formed with fs laser while, the surface of the ns-formed structures have a smother surface. In order to study the wavelength dependence profile of the structured and unstructured substrates, they calculated the absorbance by measuring the total reflectance and transmittance. Results show that in the range of 1.1-2.5 μm, the absorbance of the ns-formed microstructures is higher than that of fs-formed microstructures (Figure 1.14). By annealing the ns and fs-formed microstructures at 875 K for 45 min, they investigated that the bellow band-gap absorbance is affected more in the case of fs than ns-formed microstructures.

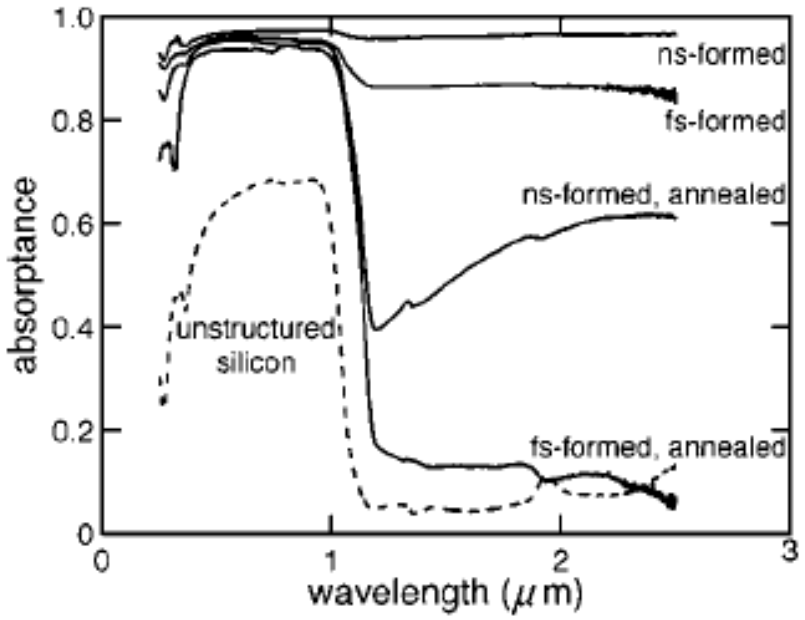

Figure 1.14 Absorbance of fs/ns formed microstructures and unstructured Si [25].

Li et al. [23] investigated the effect of scanning speed and pulse energy on laser structuring of silicon. They conducted their experiments using Nd:YAG laser with a Gaussian profile and wavelength of 532 nm and pulse duration and pulse repetition rate of 10 ns and 10 Hz, respectively. The thickness of the n-type (Arsenic–doped) (100) sc-Si wafer was 525 μm and had a resistivity

of 2-4 Ωcm. Wafers were cleaned with acetone, methanol and DI water and they were immersed in HF in order to remove the native oxide layer and after being dried with N_2 gas, they were kept in vacuum chamber of 1 atm SF_6. Results from SEM investigations reveal that, decreasing the scanning speed results in more deposition and solidification of the ablated material on the Si substrates. Furthermore, optical measurements demonstrate an increase in the absorbance of the samples that underwent slower scanning speeds. Furthermore, they studied the effect of laser energy on the morphology of the Si substrate with SEM. It is shown that, by increasing the laser energy from 173 mJ to 425 mJ the height of the microstructures first increases and then reduces since further increasing the laser energy from a certain limit degrades the surface roughness and consequently absorbance.

Sheehy at al. [26] investigated the effect of background gas in the morphology and optical properties of Si substrates irradiated with femtosecond laser. They kept the samples in vacuum chamber of 50 mTorr. Experiments were carried out on n-type (111) Si with resistivity of 800-1200 Ωcm. The irradiating laser was a 100 fs laser with wavelength of 800 nm and pulse repetition rate of 1 KHz. The laser was operating at a fluence of 10 KJ/m^2 and the spot size on the specimen was 150 μm. The pressure of the chamber filed with any of the pure gasses including H_2S, SF_6, SiH_4, H_2 or a mixture of Ar and SF_6, was 500 Torr. The horizontal scanning speed was 250 μm/s and the laser was stepped 75 μm in the vertical direction after each row was completely scanned. This scanning speed, results in almost 600 spots at each part of the target and it is clear from the spot size and vertical step size (75 μm) that there is 50% overlap in the vertical direction. Samples irradiated in H_2S ambient were annealed in a 2×10^{-6} Torr stainless steel chamber in order to study the effect of annealing temperature on the morphology and optical properties of the microstructures. The annealing duration was 30 s and the chamber pressure was always kept bellow 5×10^{-4} Torr. They conducted reflectance and morphology measurements and found that, presence of Sulfur in the background ambient has a crucial effect in creating sharp microstructures. A shown in Figure 1.15, the microstructures formed in the presence of Sulfur were taller and had smaller tip areas, which result into their higher aspect ratio compared to resultant microstructures of other gaseous ambient. Furthermore, they concluded that the bellow band-gap absorbance is not probably due to morphology or lattice damage alone. This is because, microstructures formed in H_2S or SF_6 ambient with different morphologies have similar absorbance values. In addition,

lattice damage in all microstructures was almost the same since the laser fluence was unchanged during all experiments. They related this phenomenon to the Sulfur incorporation in the high-density defect areas of Si where Sulfur stabilizes. Observations show that, for samples annealed to 900 K, absorbance in the NIR region drops from 90% to 70%. They suggested, that this might be due to the thermally induced relaxation of the S-Si network and a reversion of the electronic states to that of the sc-Si.

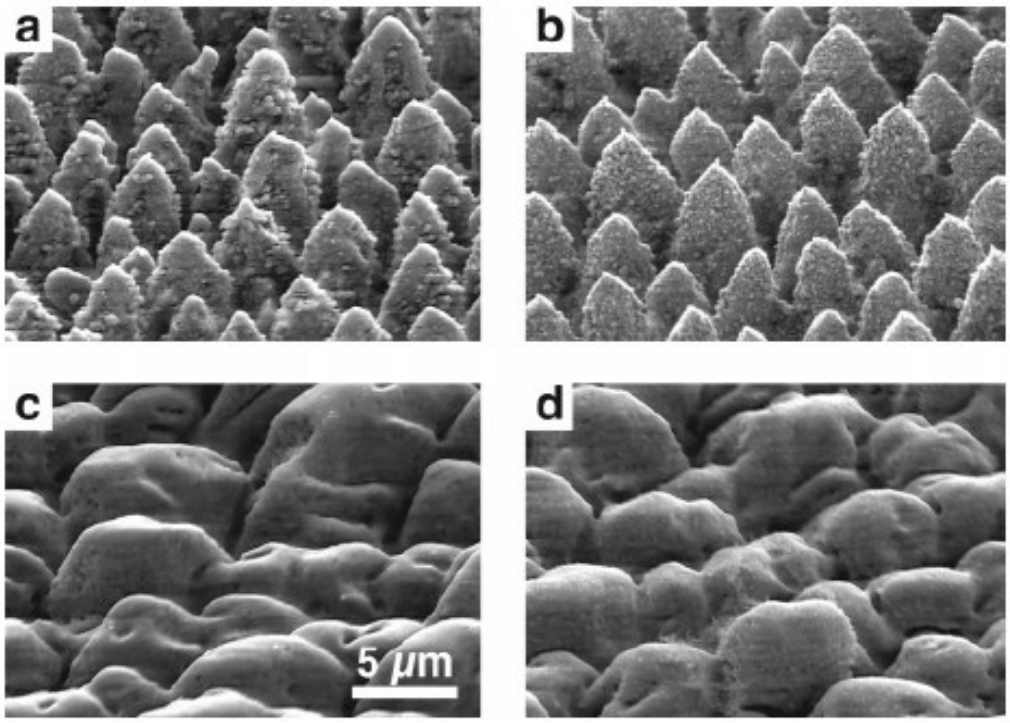

Figure 1.15 SEM image of sc-Si textured in different gas ambient; a) H_2S, b) SF_6, c) SiH_4 and d) H_2 [26].

Iyengar et al. [27] investigated the effect of ultrafast laser texturing of Si in vacuum chamber of 800 mbar SF_6 ambient. They used 1 mJ pulses of Ti:Sapphire laser with wavelength of 800 nm, pulse duration of 130 fs and pulse repetition rate of 1 KHz. In order to remove the laser-induced damage, they etched textured samples in a solution of 15% NaOH for 30 s at 40º C and 5 s in (30:10:4) HNO_3, CH_3COOH and HF. The etching step was followed by cleaning the samples in H_2SO_4 and H_2O_2 (3:1) at 70 °C and then annealing them in a furnace of O_2 for 60 min at 1050 °C for fabrication of a defect free device. In order to investigate the morphology of the self-organized microstructures, SEM images have been investigated. Results demonstrate the presence of uniformly formed conical structures with height of 15μm and cone angle of 20º and 30º that

provides a perfect light trapping. By investigating the effect of fs laser in SF_6 ambient, they concluded that, SF_6 disassociates into radical upon intense laser irradiation, which in turn acts as a supplementary element in etching Si during laser texturing procedure where sharper microstructures are achieved compared to laser texturing experiments conducted in non-reactive gasses such as Ar and N_2.

Jimenez-Jarquin et al. [22] employed their experiments on n-type (Arsenic-doped) (100) Si with resistivity of $< 7\times 10^{-5}$ Ωm. They rinsed their samples in ultrasonic bath of acetone and then immersed them in aqueous solution of 5% HF. In this work, texturing was done in 100 Torr O_2 ambient using Nd:YAG laser with pulse repetition rate of 10 Hz, pulse duration of 10 ns and energy density of 6 J/cm^2. Si wafers were irradiated at both fundamental (1064 nm) and third harmonic (355 nm) wavelengths of the Nd:YAG laser. A comparison has been made between the morphology of the created structures and results show that a conical and mountain-like structure forms in the case of IR and UV, respectively. However, in both cases, results validate the correlation between higher number of pulses with increased grooves depth and craters height.

1.2.4.3 Laser texturing in liquid ambient

Zhu et al. [28] investigated the optimal water thickness that results in the maximum ablation rate when laser texturing is conducted in water. As shown in Figure 1.16 they used a wide-band microphone to detect the audible acoustic wave that generates during the ablation of Si with 23nm KrF laser with a wavelength of 248nm. They showed that the amplitude of the first peak-to-peak acoustic wave is strongest when the water layer above the Si is 1.1 mm, which is the same amount of water that results in the maximum ablation rate. That is, the pressure induced by the plasma is maximum when the thickness of the water layer is 1.1 mm. By means of detecting the audible acoustic wave, they also concluded that the ablation rate in water is more than the ablation rate in air [29].

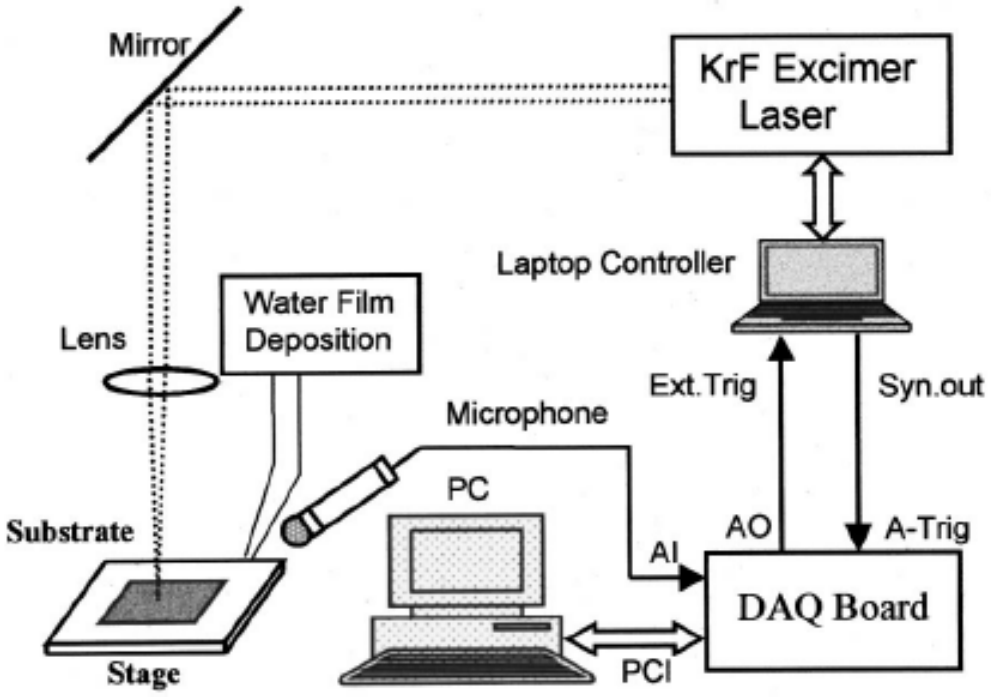

Figure 1.16 Schematic of the experimental setup of Si laser texturing in water ambient [28].

Ren et al. [30] used 5 ns Nd:YAG laser with wavelength of 355nm for texturing Si in water ambient. They demonstrated that the ablation rate of Si in water is twice the ablation rate of Si in air, which is due to the laser energy coupling that occurs within the cavity-confinement geometry. Furthermore, they found that at higher laser irradiances, laser ablation rate diminishes due to the plasma formation at water-air interface. This layer of plasma acts like an opaque layer to the laser beam and hampers its energy.

Sobhani et al. [31] investigated a method of laser texturing conducted in distilled water. The optical and topographic properties of the sc-Si has been assessed and an improvement in the absorption and cluster height and density has been observed. In this work p-type (100) sc-Si wafers were irradiated with 532 nm Nd:YAG laser with the repetition rate of 10Hz and pulse duration of about 9 ns. The irradiation ambient was DI water, which was changed after each irradiation stage. In this study different pulse numbers and laser fluences have been applied in order to investigate their influence on the formation of the micro/nano structures and optical properties of the textured surface. Results show that, by increasing the number of pulses, surface cluster density increases to a maximum and it reduces or remains the same if further pulses are applied. It was concluded by

the same work that due to the higher cooling rate of water compared to air, higher clusters are featured when texturing is conducted in DI water rather than air. Furthermore, they showed that optical properties of the textured wafers are highly dependent to the clusters density and cluster height.

Karimzadeh et al. [32] investigated the effect of nanosecond laser texturing in dimethyl sulfoxide (DMSO) and water. They irradiated their n-type (100) sc-Si samples with 15 ns Nd:YAG laser with wavelength of 532 nm and pulse repetition rate of 1Hz. Laser beam diameter was reduced to 150 μm with a 500 mm focal length lens and laser fluence was in the range of 4-11 J/cm^2. Their results show cavity sites on the surface of silicon, which is a consequence of the bubble nucleation (Figure 1.17). It is also found that by increasing the laser fluence, bubble nucleation sites increase. Results show a smaller ablated area in Si samples irradiated in DMSO compared to water, which is due to the different plasma pressures at different liquid ambients. Furthermore, they found that the ablation threshold of Si is lower in DMSO compared to water. They concluded that the melt explosion is the dominant procedure in nanosecond laser ablation in liquids, which is due to confined plasma-induced shock wave.

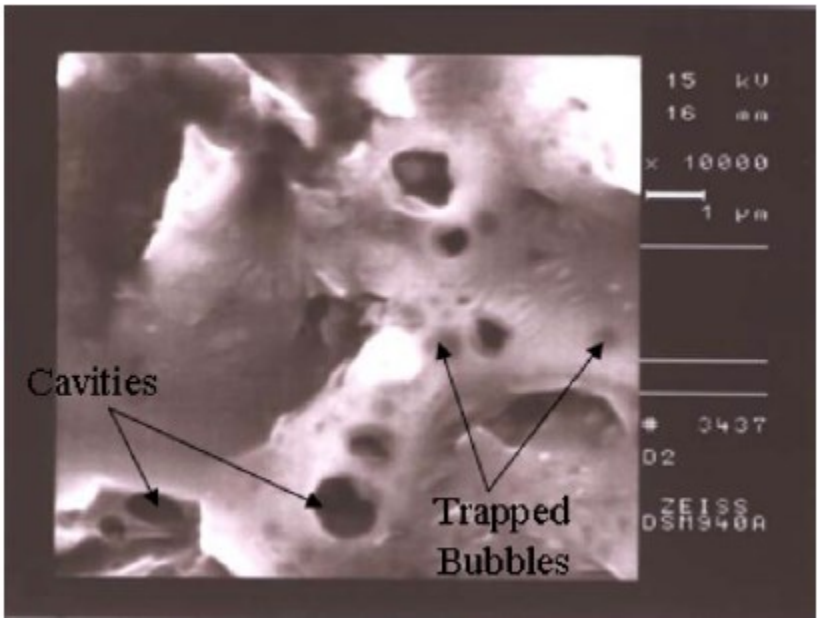

Figure 1.17 SEM image of irradiated Si under DMSO [32].

1.2.5 Laser-assisted chemical etching

It is mentioned earlier that laser texturing is an appropriate alternative to alkaline chemical etching for texturing mc-Si however, it is interesting to investigate whether the combination of laser and chemical etching in texturing mc-Si is beneficial or not. To this aim, we have reviewed the limited literatures on laser assisted chemical etching.

Zhao et al. [33] investigated the effect of femtosecond laser texturing of n-type (111) sc-Si in KOH ambient. They used Ti:Sapphire with wavelength of 800 nm, pulse duration of 120 fs and pulse repetition rate of 1 KHz. The average output of the laser was 1 W, which is equal to the pulse energy of 1 mJ. The laser beam diameter was reduced from 5 mm to 260 μm by a 600 mm focal length lens. Samples were all cleaned in ultrasonic bath of acetone for 10 min as well as 10 min in ultrasonic bath of ethanol and they were rinsed with water. Laser texturing experiments were conducted in KOH solution (0.1 g/ml) at room temperature. Schematic of the experimental setup is shown in Figure 1.18.

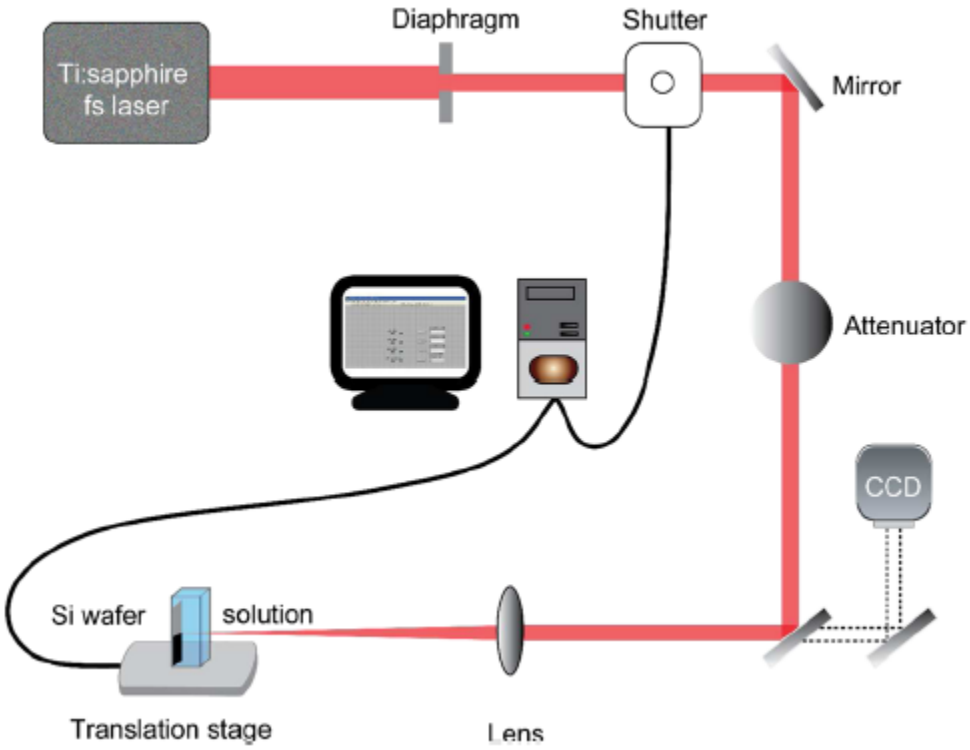

Figure 1.18 Schematic of the experimental setup of laser-assisted chemical etching of Si [33].

In order to investigate the morphology of the textured samples, SEM has been used. Results show that, upon low laser fluence (0.63 KJ/m^2), micrometer-scale triangle pit structures are formed while, for the case of higher laser fluences (1.88 KJ/m^2, 2.83 KJ/m^2, 3.77 KJ/m^2) triangle stack structures are featured. It is known that KOH is a good etchant of Si in temperatures above 80 °C however, if laser was not assisting the etching process, it was difficult that 0.1 g/ml KOH react Si at room temperature. In fact, due to the increased temperature of the surface to 1850 K by laser energy at the threshold fluence, KOH reaction with Si was initiated. In the process of the laser-assisted chemical etching, energy of the laser plays an important role in the average surface roughness (R_a) of the textured surface. As shown in Figure 1.19, size and number of stack layers are increased with increasing the laser fluence.

Fule at al. [34] compared the effect of Si laser texturing in air, water and KOH (20 wt%) at room temperature. They used polarized beam of Ti:Sapphire laser with wavelength of 800 nm, pulse duration of 22 fs and pulse repetition rate of 200 Hz. Laser fluence during experiments in KOH was 330 μJ. Prior to texturing experiments, (100) sc-Si wafers were cleaned in ultrasonic bath of acetone and then ethanol. The volume of the KOH solution and water was 11545 μl and the liquid layer above the samples was 6 mm$\pm$ 5 μm. In air and water experiments, increasing the number of pulses enhanced the created holes depths. However, in case of laser texturing in KOH ambient, samples were not etched when they were irradiated with fs laser. Etching was neither detected, when laser fluence was increased from 0.2 J/cm^2 to 1 J/cm^2. Therefore, they leaved the samples in KOH solution for about 20 min after laser processing was done. Results show an increase in the etching rate at those areas affected with more number of pulses where native oxide layer was removed. Nevertheless, when samples were kept in KOH solution for 20 min, holes depths were much smaller compared to those created in air and water ambient. They concluded that laser texturing in KOH was not improved but inhibited and attributed this to the presence of high temperature plasma ambient where new redox reactions occur and potassium oxide forms due to lower electronegativity of K compared to Si.

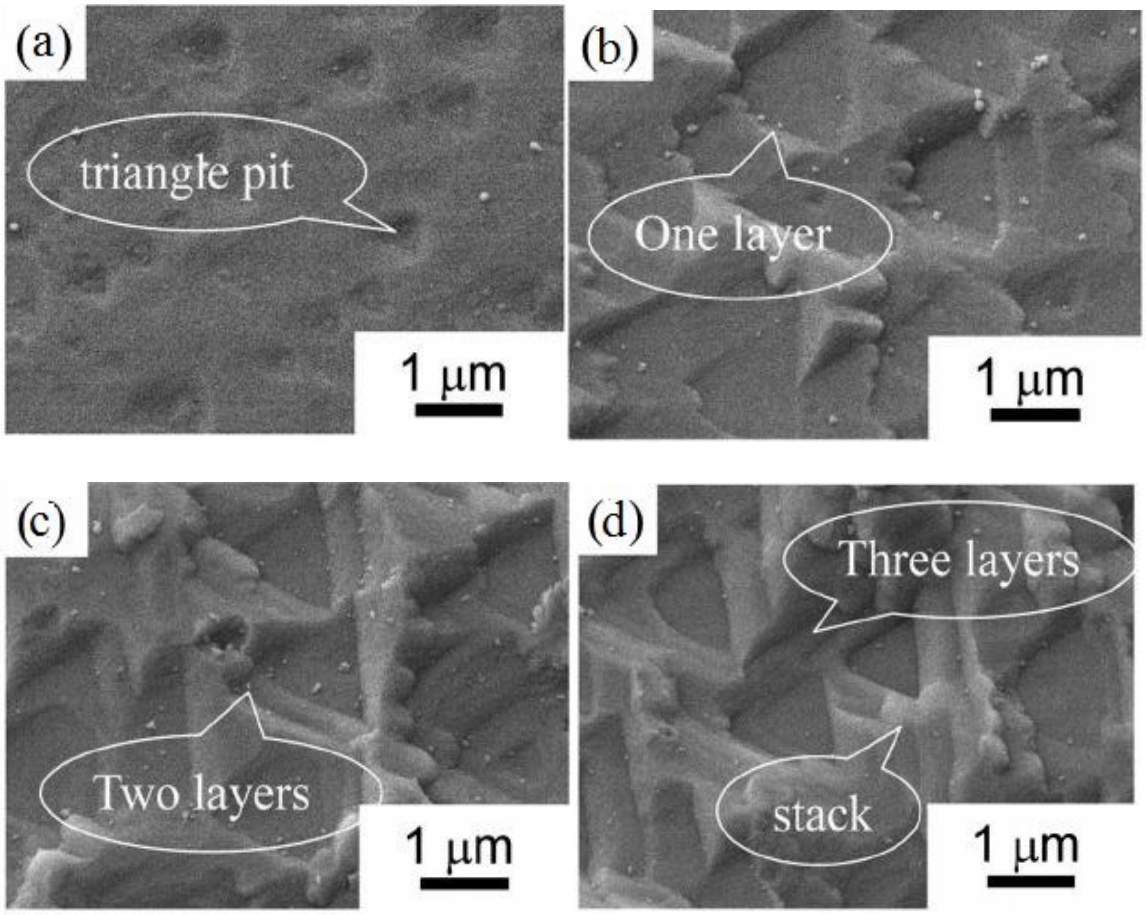

Figure 1.19 SEM image of the triangle structures etched in KOH and irradiated by different laser fluence; a) 0.63 KJ/m^2, b) 1.88 KJ/m^2, c) 2.83 KJ/m^2, d) 3.77 KJ/m^2 [34].

1.3 Motivation for the work

In the existing literatures on mc-Si texturing, different techniques have been studied and among all, laser texturing has shown to be the most appropriate method to give the best textured pattern where optical losses are minimized. Furthermore, many investigations have been made to understand the effect of different parameters, which are involved in laser texturing such as, texturing ambient, laser wavelength, laser energy, laser pulse repetition rate, laser pulse duration, laser scanning speed etc. However, to the best of the knowledge of the author, there are no concerted efforts to analyze statistically the effect of laser parameters and to identify the most efficient method to reduce SWR on mc-Si wafers that are to be used for solar cell applications. In this work, we implemented analysis of variance (ANOVA) and regression analysis to investigate the significance level of the laser texturing parameters on the morphology and optical properties

of textured mc-Si. To this aim, p-values were tested to investigate the significance of the input parameters such as laser fluence, overlap and number of irradiations, on the output parameters including R_a, depth and SWR and F values were compared to find the significance level of the tested parameters. In statistics, p-value is used to test the statistical hypothesis, which states that, within group variation is larger than between group variation. Therefore, if the significance level is chosen to be 0.05 and p-value is equal or less than 0.05 the null hypothesis is rejected which means that the between group variation is more significant and the factor which is being assessed in term of significance, is statistically significant. F value on the other hand, defines the significance level of the tested parameters. That is, a factor is statistically of more significance level if it has a higher F-value compared to others.

1.4 Objective and scope of the work

In this research nanosecond laser, which takes the advantage of less fabrication costs, is implemented for creating micro/nanostructures on mc-Si as a basis of potentially higher efficiency solar cells. This research is mainly concerned with:

1. Increasing R_a and depth
2. Reducing SWR
3. Minimizing the laser energy consumption

The scope of the work includes investigating the optimum condition for factors involved in nanosecond laser texturing that improve the morphological properties of mc-Si in a way that not only better optical properties are attained but also minimum time and energy is consumed. The variable parameters in this study are:

- laser fluence
- pulse overlap
- number of irradiations
- texturing ambient

The effect of each variable on the morphology and optical properties are measured with interferometer microscope along with SEM and spectrophotometer, respectively. By means of ANOVA, we have provided statistical tests for evaluating the significance of the mentioned variables in laser texturing of mc-Si samples that result in saving the energy and time by

minimizing the huge amount of experiments. Regression test is also implemented to investigate the significance level of depth and R_a in SWR reduction.

Though solar cell fabrication is not the focus in this study, an attempt was made to build solar cell devices based on textured and non-textured wafers and their electrical properties were measured.

1.5 Organization of the thesis in manuscript-based format

This manuscript-based thesis is organized in six chapters. In the present chapter, we discussed the main reasons for demanding the solar cells and explained their benefits compared to other sources of energy like fossil fuels. Furthermore, we explained how their expenses and efficiency could improve in order for them to become as an alternative to the existing energy resources. Texturing is explained as a practical technique for decreasing the optical loses and laser texturing is described as an efficient method for texturing the mc-Si that has a lower price compared to sc-Si. In Chapter 2 we explained the experimental setup in addition to detailed information about the optical configuration and the controlling software. Chapter 3 and Chapter 4 are duplicated from published and submitted journal articles. These chapters are organized in a cohesive manner to address the objectives of the thesis defined in Section 1.3 and formatted according to "Thesis Preparation and Thesis Examination Regulations (version-2013)" of the School of Graduate Studies at Concordia University. In the duplicated articles, sections, figures, equations, and tables are numbered according to the thesis preparation regulations. A single comprehensive reference list rather than individual papers reference list is presented in Reference section. Conclusions of the thesis and the future recommendations are presented in Chapter 6.

Chapter 3 is based on the following article published in Journal of Laser applications [35].

Mehrnegar Aghayan and Sivakumar Narayanswamy, "Morphology based statistical analysis of nanosecond pulsed laser texturing of the multicrystalline silicon" J. Laser Appl., vol. 27, no. 3, 2015.

In this work, we investigate the surface morphology of the textured multicrystalline silicon with nanosecond (ns) Nd: YVO4 laser (wavelength 1064 nm, repetition rate 10 KHz, pulse duration of 14ns). Various surface topographies have been achieved with different laser as well as irradiation parameters. The textured area average roughness and depth have been statistically analyzed

through ANOVA test, which could evaluate the significance and effectiveness of the adopted design of experiment. This research work is based on three control factors: Laser fluence, laser pulse overlap percentage and number of irradiations. The statistical assessments were conducted based on roughness and depth values measured by optical interferometry. The effect of roughness and depth on Solar Weighted Reflectance (SWR) was analyzed and significant reduction in SWR with increase in R_a was observed. In addition, time an energy consumption which are highly significant in the industrial applications, have been investigated.

Chapter 4 presents the following article submitted to the Journal of Materials Research Express.

Mehrnegar Aghayan and Sivakumar Narayanswamy, "Nanosecond laser interaction with multicrystalline silicon under acetone confinement", Manuscript ID- MRX-101806 (under review).

Nanosecond Nd:YVO_4 laser (wavelength of 1064 nm, repetition rate of 10 KHz and pulse duration of 14 ns) interaction with multicrystalline silicon in acetone and air has been investigated. In contrast to experiments in air, debris free microstructures are featured in the acetone environment, resulting from ejection of the ablated material into the surrounding ambient. At higher number of pulses, laser ablation depth and reflectivity of the samples are found to be improved when texturing was done under the acetone film. Experiments in acetone show an improvement in average surface roughness (Ra), depth and solar weighted reflectance (SWR) by increasing the number of pulses while, increasing the laser fluence reduced the depth and R_a and degraded the SWR due to the shielding effect, which occurs at high laser fluences. Statistical analysis show that while both R_a and depth affect the SWR, depth plays a more significant role especially at SWR values below 2.44%.

In Chapter 5, physics and principal parameters of solar cells are studied. In addition, we explained the procedure that we followed to fabricate the P-N junction and the electrodes. Chapter 6 is the conclusion of the work along with some suggestions for the future work.

CHAPTER 2. Experimental Setup

2.1 Introduction

As described in section 1.3, the objective of this work is to create micro/nano structures on the surface of mc-Si by means of laser texturing technique, for improving the optical properties of mc-Si wafers. In order to assess the effect of different laser parameters and texturing ambient on R_a, depth and consequently SWR, we adopted laser fluence, irradiation numbers, pulse overlap and texturing ambient as the variable factors. As such, in each experimental stage, at least one of the mentioned factors was changed. In the following experiments, optical setup and LabVIEW program was modified only when the texturing ambient and pulse overlap was changed, respectively.

2.2 Laser and sample description

The laser used in this work was PRISMA Nd:YVO_4 1064-16V (Neodymium Doped Yttrium Orthvanadate) provided by Coherent Inc. This solid-state Q-switched laser having wavelength of 1064 nm and pulse duration of 14ns has a Gaussian profile (TEM00 mode). This laser has continues and pulsed output. The pulsed mode has a repetition rate in the range of 10-100 KHz and the output current is tuned with the diode current, which is in the range of 13-34 Amp. As shown in Figure 2.3, peak power varies with pulse repetition rate of the laser. That is, the maximum peak power is achieved when pulse repetition rate is put at its minimum values, which is 10 KHz. In Figure 2.3't' is the pulse width, which is the duration that the pulse laser is being emitted and 'R' is the pulse repetition rate of the laser. In this work, we have adjusted the pulse repetition rate at 10 KHz and this value was fixed during all experiments.

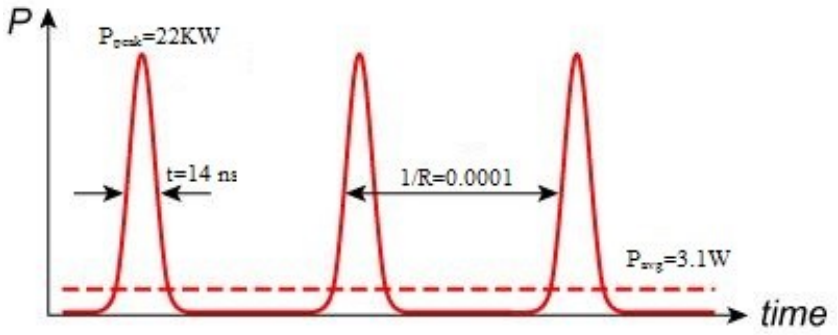

Figure 2.3 Temporal profile of the laser power [36].

The samples used in this work were p-type (Boron-doped) multicrystalline silicon (mc-Si) wafers with resistivity of 0.02 Ω-cm and thickness of 700 μm. These wafers were cut into 20mm ×30mm rectangular pieces and were cleaned in ultrasonic bath of acetone for 10 min and then kept in DI water before being used in the texturing experiments.

2.3 Optical setup

Alignment of the optical setup was in a way that the laser beam coming from the telescopic lens, hit the center of the galvoscanner and central part of the converging lens. Therefore, all of the mentioned optical elements were set at the same height and lateral position.

2.3.1 Air experiments

As shown in Figure 2.4 and Figure 2.5 in air experiments, optical setup consists of the laser telescopic lens, galvoscanner mirrors, a converging lens and mc-Si sample, which is mounted on a three-axis translation stage and fixed with a sample holder.

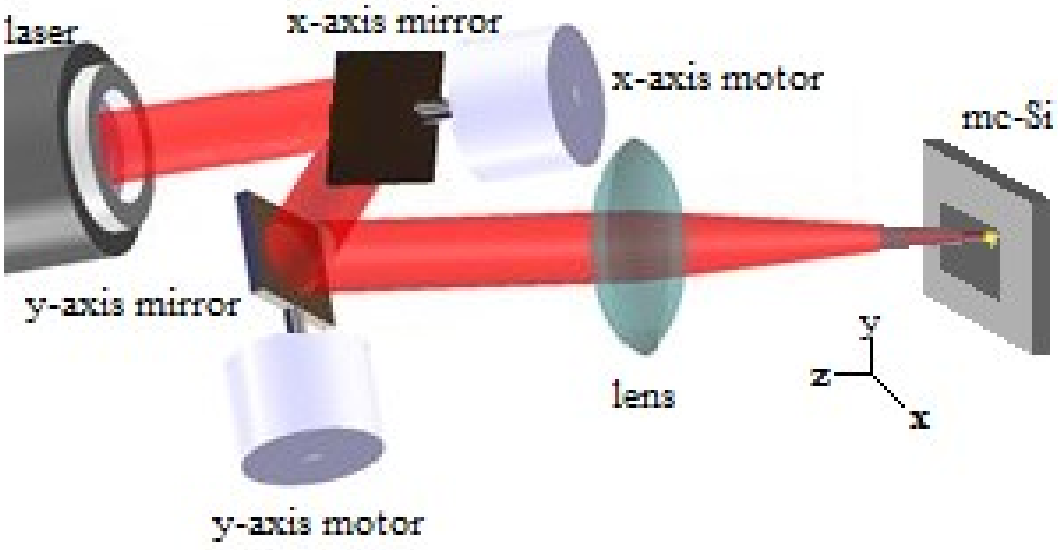

Figure 2.4 Schematic of the laser texturing experiments in air ambient.

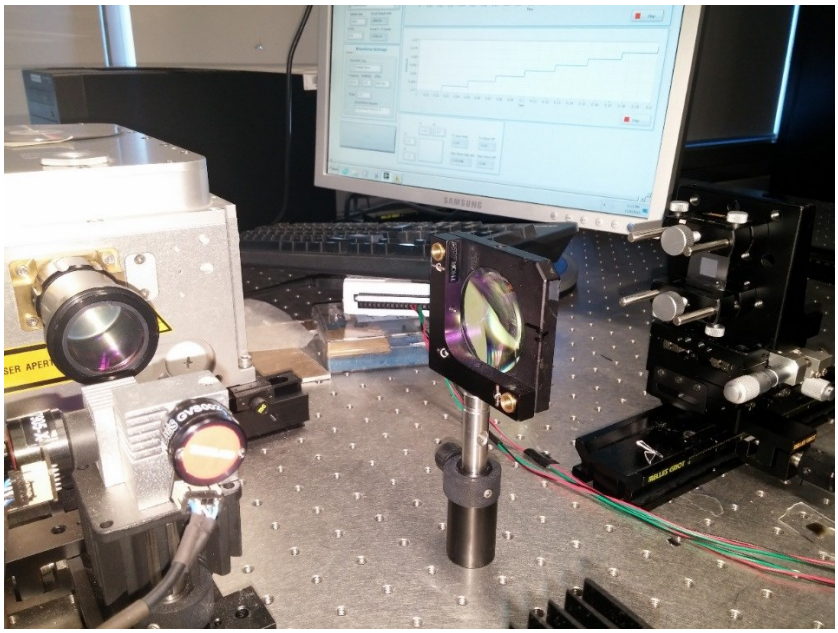

Figure 2.5 optical setup of the laser texturing experiments in air ambient.

Diameter of the laser beam coming out from the telescopic lens, can change from 0.8 mm to 5 mm with a beam expander. Based on Equation 2.1, in order to achieve the minimum spot diameter, the diameter of the laser beam coming from the telescopic lens, should be maximum (5 mm). Therefore, using a 150 mm focal length lens the diameter of the laser beam was reduced from 5 mm to 40 μm.

$$d = 1.27 \times f\lambda/D \tag{2.1}$$

Where 'd' is the spot diameter, 'f' is the lens focal length,'λ'is the laser wavelength and 'D' is the initial diameter of the laser beam.

Galvo mirrors control the scanning speed in addition to the size and location of the texturing area. A converging lens with diameter of 50 mm is placed 150 mm away from the galvo scanner mirrors so that the beam hit normal to the scanning plane. In order to make sure that the laser beam hit the lens at its central parts, we used an IR card to trace the invisible laser light. The 20×30 mm^2 rectangular pieces of mc-Si were mounted on a three-axis translation stage 150 mm away from the lens so that the minimum possible spot size is provided on the specimen and in order to fix the scanning plane at the focal point of the lens, we manipulated the stage in the z-axis.

2.3.2 Acetone experiments

As shown in Figure 2.6 and Figure 2.7, in acetone experiments, optical setup consists of the laser telescopic lens, galvoscanner mirrors, a converging lens, a 45° mirror and mc-Si sample covered with a 1 mm layer of acetone which is placed on a three-axis translation stage.

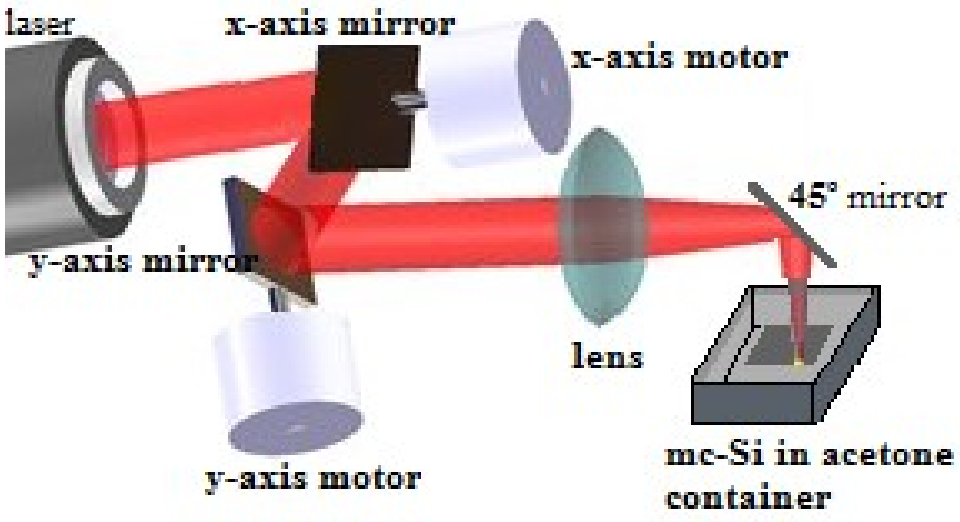

Figure 2.6 Schematic of the laser texturing experiments in acetone ambient.

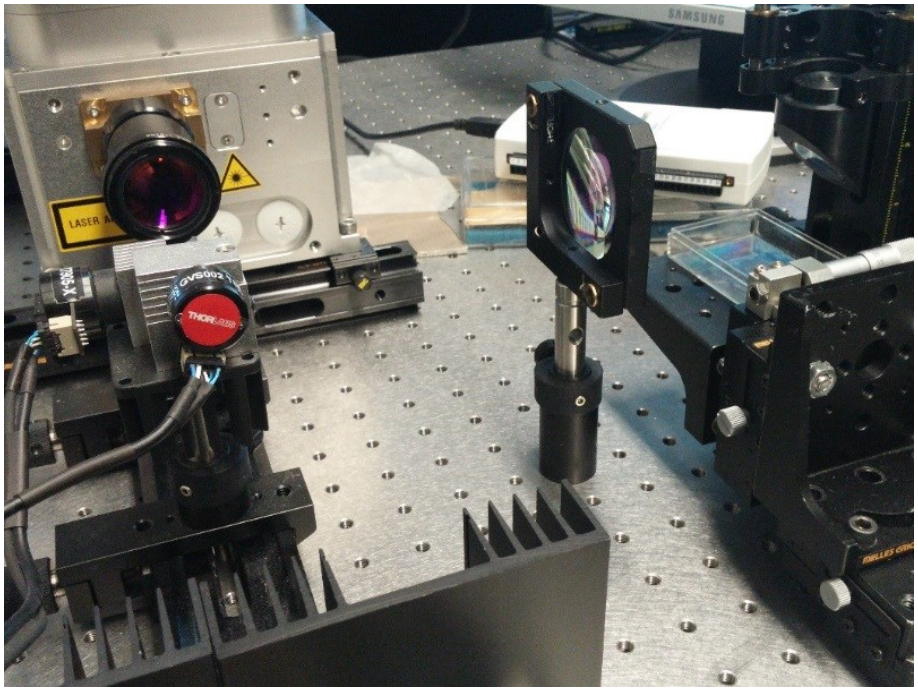

Figure 2.7 Optical setup of the laser texturing experiments in acetone ambient.

In the acetone-assisted experiments, the optical setup was changed from horizontal to vertical since the samples had to be placed in a liquid environment. To this aim, we placed a 45º reflecting mirror after the converging lens so that the beam refract 90º and hit the samples placed bellow the mirror. As shown in Figure 2.8 the horizontal distance between the lens and the 45° mirror plus the vertical distance between the mirror and the sample should be almost equal to the focal length of the lens. In the acetone experiments, due to different refractive index of acetone compared to air, the focal point was modified from dry experiments and it was slightly more than 150 mm from the lens.

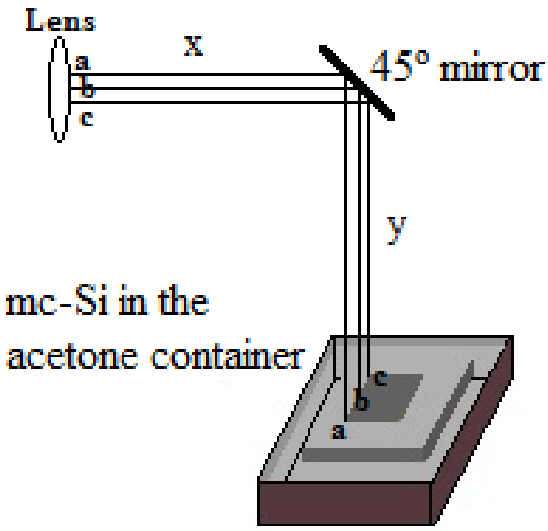

Figure 2.8 Schematic of the horizontal beam converted to vertical.

2.4 Software for control

A LabVIEW program was developed to control the movement of the galvoscanner mirrors model THORLABS GVS002. Each galvo mirror was attached to a servo DC motor and the motor was controlled with a NI6211 USB DAQ board. The rotation angle of the mirrors was proportional to the applied voltage to the servo motor from the board. This voltage was in the range of ± 10 volt and the corresponding angle limit for the galvoscanner mirrors was $\pm 12°$. That is, 1 volt is equal

to 1.2º rotation of the mirrors therefore, based on the desired rotation angle of the mirrors the corresponding value was modified in the LabVIEW program in terms of volt.

As mentioned earlier, pulse overlap is one of the variables in this work. For controlling this factor, we had to find the scanning speed that provides the certain overlap percentage. Scanning speed is calculated using Equation 2.2 and Equation 2.3 calculates the pulse pitch.

$$\text{Scanning speed } (\mu m/s) = \text{ Pulse pitch} \times \text{pulse repetition rate of the laser} \quad (2.2)$$

$$\text{Pulse pitch } (\mu m) = \text{Spot diameter} \times (1\text{-overlap percentage}) \quad (2.3)$$

Table 2.1 Pulse pitch, pulse numbers and scanning speed associated with 3 different overlap percentages.

Overlap percentage	0	30	60
Laser pulse pitch (μm)	40	28	16
Number of pulses per row	250	357	624
Scanning speed (μm/s)	4×10^5	2.8×10^5	1.6×10^5

As mentioned earlier, the input values in the LabVIEW program should be in terms of voltage. For instance, as shown in Table 2.1, for a texture with 30% overlap, scanning speed should be 2.8×10^5 μm/s. However, in order for the program to perform scanning speed of 2.8×10^5μm/s, all parameters that define the scanning speed such as pulse pitch should be converted into their degree equivalent. That means one should define to the program that how much voltage should be applied to the galvoscanner mirrors so that they rotate with a speed that the desired overlapping pattern is achieved. In order to find the rotation speed of the galvoscanner, Equation 2.4 is used. By using this equation, the degree equivalent of the pulse pitch, which in turn defines the scanning speed, is calculated.

$$L = 2d.\tan\varphi \quad (2.4)$$

As shown in Figure 2.9 ‘L’ is the scanning length, ‘d’ is the distance between the galvoscanner and the lens and ‘φ’ is the rotation angle of the galvo mirrors.

From Equation 2.4, φ = Arctan (L/2d) Where d =1.5×10^5μm therefore, φ = Arctan ($L/3\times 10^5$).

For example, for a 0% overlap the pulse pitch is calculated from Equation 2.3 to be 40 μm therefore, degree equivalent of 40 μm is:

φ = Arctan $(40/3\times 10^{5})$ =$7.6\times 10^{-3^{\circ}}$ and voltage = 6.3×10^{-3} volt

Therefore, in order to obtain a texture pattern with 0% overlap, the corresponding value for the pulse pitch in the LabVIEW program is 6.3×10^{-3} volt. From this proportionality, we can find that:

1 μm ~ 1.6×10^{-4} volt (2.5)

In this work, we aimed to have a square texturing pattern of area 10×10 mm^2 for the air experiments and 12×12 mm^2 for acetone experiments therefore, using equation 2.6, the number of cycles that provided the desired texturing area, was defined to the program.

Number of cycles = width of the texturing area (μm)/pulse pitch (μm) (2.6)

Since the scanning was uniform, the overlap percentage was the same in both x and y directions. As mentioned earlier, the overlap in the horizontal direction (x-axis) and the width of the square was defined with the pulse pitch and number of cycles, respectively. However, in order to have the same overlapping percentage in the vertical direction (y-axis) by using Equation 2.7 the frequency of y-axis mirror is calculated and entered in the program.

$$\text{Frequency of the y axis galvo mirror} = \frac{\text{Pulse repletion rate of laser}}{(2\times\text{number of cycles})} \quad (2.7)$$

In this program the length of the square, is not dependent to the scanning speed and it is calculated regardless of the frequency of the y-axis galvo mirror. As such, the voltage equivalent of half-length of the desired square, which is called amplitude in the program, is calculated using Equation 2.5. For instance, the amplitude, which maintains a length of 10 mm, is:

$10\times 10^{3}\times 1.6\times 10^{-4}$= 1.6 volt

The final position box in Figure 2.10 , defines the location where the laser stops scanning. It is important, that this point does not lie on the textured square otherwise, it would damage that area.

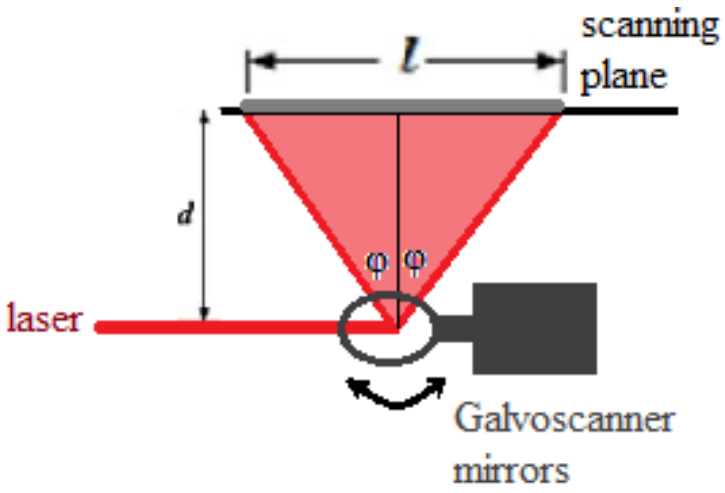

Figure 2.9 Schematic of the scanning length associated with the galvomirror rotation.

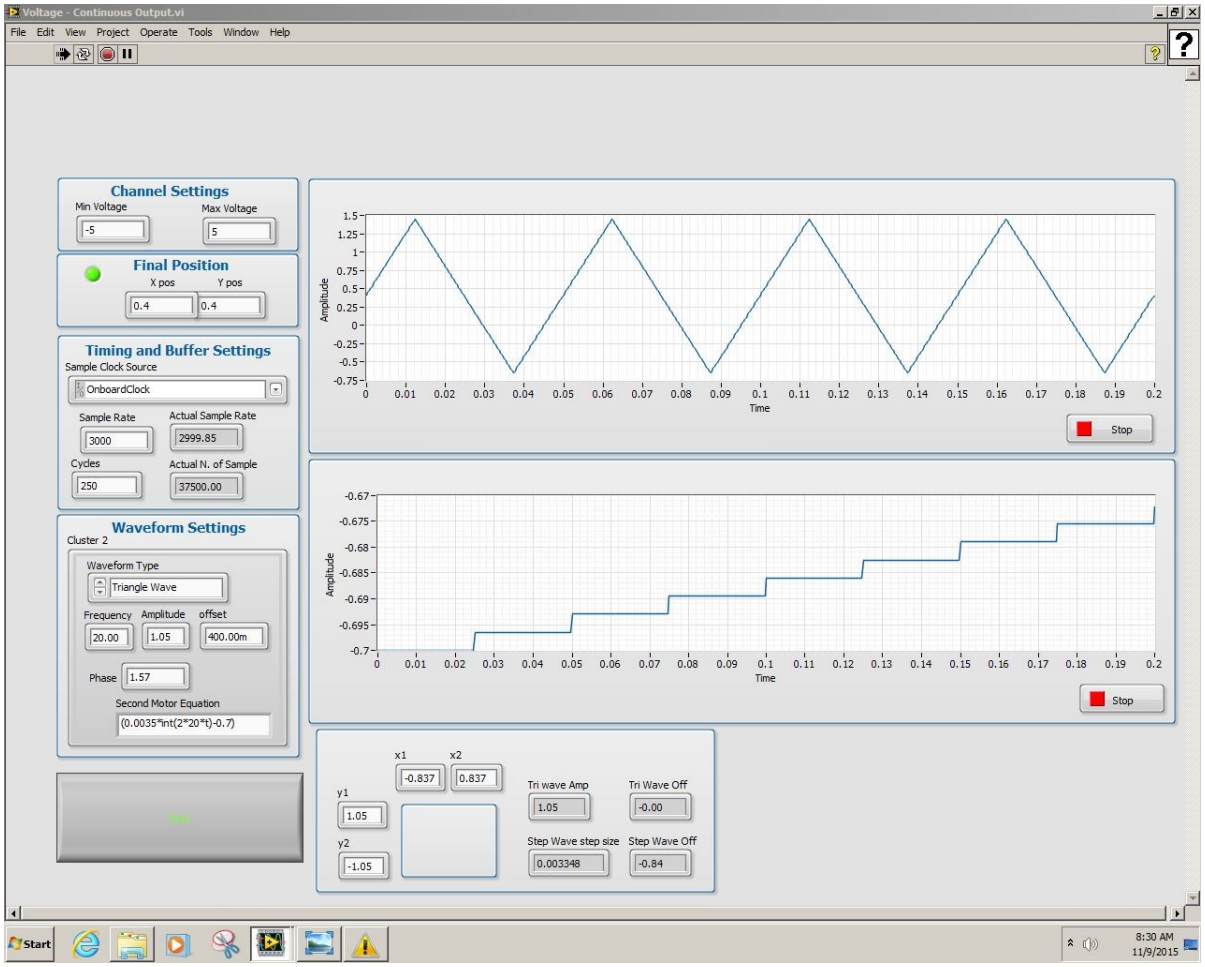

Figure 2.10 Screenshot of the LabVIEW program.

2.5 Measurement of R_a and depth

We used Veeco nt1100 white light interferometer to investigate the surface profile of the textured samples. In order to calculate the average surface roughness we measured R_a, which is defined by the *arithmetic mean deviation of surface height from mean value,* at 5 different points of the textured area (including the four corners and the center) and attributed the average of these values to each sample as their R_a. We measured the depth by measuring the holes on each surface and with the same approach and calculated the average depth for each textured surface.

2.6 Spectroscopic measurement of reflectance

In order to measure the optical properties of the textured mc-Si samples under different laser texturing parameters, we used Varian Cary 5000 UV-Vis-NIR spectrophotometer (Figure 2.11) equipped with integrating sphere. With the Cary, we directly measured the total hemispherical reflectance and transmittance of each sample in the range of 300 nm to 1100 nm. We used the plain area of each sample as the baseline. A shown in Figure 2.12 plain wafer with true reflectivity of about 19% (blue line) was shown to be 100% reflective (orange line), after applying the baseline correction and sample 2 is shown to be almost 15% reflective after the baseline correction (yellow line).

Figure 2.11 Varian Cary 5000 spectrophotometer.

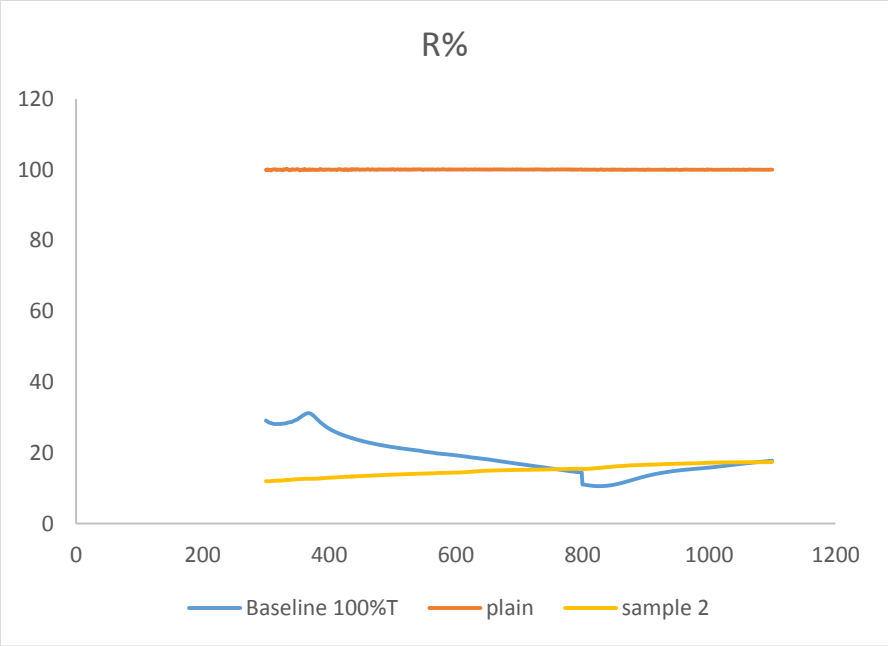

Figure 2.12 Reflection from polished and textured mc-Si.

2.7 Design of experiment

In this work, statistical investigations on the effect of laser fluence, pulse overlap and number of irradiations on R_a, depth and SWR of mc-Si has been made. We implemented, ANOVA and regression for evaluating our results. Our measurements were carried out using SEM, optical interferometry and spectrophotometer.

2.7.1 Laser fluence

We measured the power of the laser beam at the surface of the samples with laser meter. These measured values, which were in units of Watts, were converted to fluence (F) by using Equation 2.8.

$$F = \frac{P}{f\left(\frac{d}{2}\right)^2 \pi} \tag{2.8}$$

Where, F is the laser fluence, P is the laser power, f is the repetition rate of the laser and d is the laser spot diameter.

The values for laser fluence used in this work were 12.7 J/cm^2 17.5 J/cm^2 and 18.6 J/cm^2 when texturing was conducted in air and 18 J/cm^2 and 22 J/cm^2 when it was performed in acetone environment. In air experiments, each laser fluence was used at 6 different experiments where

overlap or number of irradiations was changed. In acetone experiments, at each laser fluence we performed 4 different experiments where number of pulse was varying.

2.7.2 Overlap

Another variable parameter in our studies was the overlap percentage between the pulses. Based on Equation 2.2 overlap in x direction is controlled by the pulse pitch and it is controlled by the speed of y-axis mirror by using Equation 2.7. In air experiments, we did 6 different experiments at each overlap percentage including 0%, 30% and 60%. Figure 2.13 is the schematic of 0%, 30% and 60% overlap percentages.

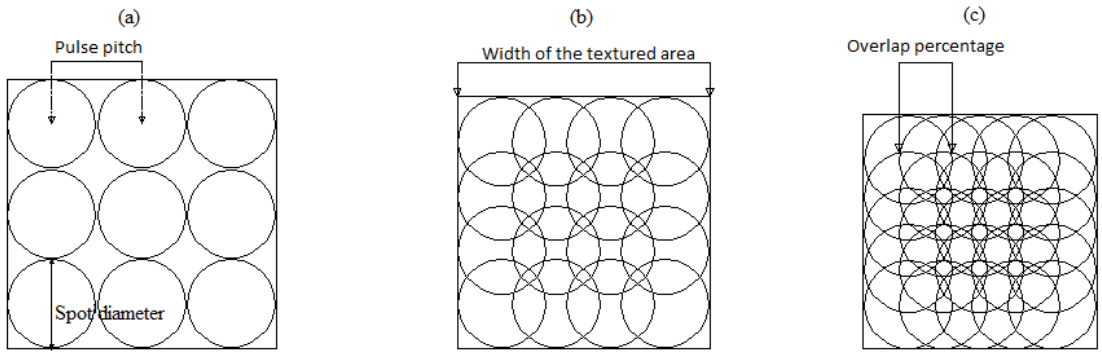

Figure 2.13 Schematic of the mc-Si samples textured under three different overlap values, (a) 0%; (b) 30%; and (c) 60%.

2.7.3 Number of irradiations and number of pulses

Number of irradiations refers to the number of times that we did laser texturing over the whole texturing area with the same laser fluence and overlap values. In this work, we did the texturing on the same sample for 1, 2 and 4 times when texturing was done in air.

In acetone experiments, instead of having overlap and number of irradiations as our variables, we used a combination of both called number of pulses.

Based on Taguchi design of experiment method, we conducted 27 set of experiments in air and 8 set of experiments in acetone. Table 2.2 and Table 2.3 represent the detail of the laser and scanning parameters in air and acetone experiments, respectively.

Table 2.2 Number of experiments in air.

Sample number	Laser fluence (J/cm^2)	Overlap	Number of irradiations
1	12.7	0%	1
2	12.7	0%	2
3	12.7	0%	4
4	12.7	30%	1
5	12.7	30%	2
6	12.7	30%	4
7	12.7	60%	1
8	12.7	60%	2
9	12.7	60%	4
10	17.5	0%	1
11	17.5	0%	2
12	17.5	0%	4
13	17.5	30%	1
14	17.5	30%	2
15	17.5	30%	4
16	17.5	60%	1
17	17.5	60%	2
18	17.5	60%	4
19	18.6	0%	1
20	18.6	0%	2
21	18.6	0%	4
22	18.6	30%	1
23	18.6	30%	2
24	18.6	30%	4
25	18.6	60%	1
26	18.6	60%	2
27	18.6	60%	4

Table 2.3 Number of experiments in acetone.

Sample number	Laser fluence (J/cm^2)	Number of pulses
1	18	62500
2	18	125000
3	18	255000
4	18	510000
5	22	62500
6	22	125000
7	22	255000
8	22	510000

2.8 Summary

The setup was designed to align the laser beam so that it hit the galvoscanner mirrors that are controlled by LabVIEW program and then pass through the convex lens before it hits the specimen. The LabVIEW software, mainly controls the overlap percentage, which is referred to scanning speed in the equations. Although the final result from the LabVIEW program is an angular variation of Galvo mirrors, all input values in this program are in volts since the required voltage that has to be applied to the servo DC motor should be defined to the program.

CHAPTER 3. Morphology based statistical analysis of nanosecond pulsed laser texturing of the multicrystalline silicon

This chapter is based on the manuscript published in the Journal of Laser applications, where statistical analysis is implemented to not only improve R_a, depth and SWR but also minimize the energy and time consumption.

3.1 Introduction

Due to increase in the world population and consequently energy consumption, global warming has become a serious problem originated from fossil fuels, which are finite energy recourses. As a result, researchers have proposed solar cells as an alternative for solving the energy demand and global warming issues. As of today, solar energy has a share of only about 1% of the total energy consumption, however the electricity supplied by solar cells is predicted to be double by 2018 [1][37]. Silicon, which is the second abundant element on the earth, has been used in the solar cells structure. By replacing the single-crystalline silicon (sc-Si) with the low-cost multicrystalline silicon (mc-Si), solar cell fabrication expenses can further be decreased. On the other hand, due to lower quality of mc-Si compared to sc-Si, research on methods to improve the efficiency of low-cost mc-Si solar cells is being conducted. Increasing the efficiency throughout minimizing the reflection of incident light from the surface can be achieved by using antireflection coatings [38]. Surface texturing is another method for decreasing losses due to high reflection [18]. This technique enhances the efficiency by increasing light trapping [39-41]. When a surface is textured, formation of pyramids and grooves scatters or re-reflects light back to other facades of the conical structure. This phenomenon traps light between the structures on the surface and thus reduces reflection. Along with lowering the reflection, light trapping increases the absorption by increasing the effective path length of the incident light [41][42].

Silicon surface texturing has been achieved by various methods such as: alkaline chemical etching [43], mechanical techniques [7], pulsed laser deposition [44] and laser texturing [45] in which the first is known to be historically the major method in surface texturing. Furthermore, it has been reported that pulsed laser ablation leads to deposition of some nanoparticles (NPs) on the target surface. As per Wang et al. [44] Si NPs were deposited on the Si substrate by nanosecond laser ablation in high-purity Ar gas.

Although mechanical techniques and alkaline chemical etching are more cost effective, mc-Si wafers, which are more favorable in terms of cost, cannot be textured through the same processes due to their poorer crystallographic quality. Therefore, alkaline chemical etching is an ineffective approach for texturing mc-Si wafers. Furthermore, these high-temperature etching processes might deteriorate the crystallographic quality of the mc-Si wafers [46]. On the other hand, due to fragility of the Si thin films, mechanical techniques are also incapable for texturing them [47]. Therefore, laser texturing, which is independent of crystal grain orientations, can become beneficial in texturing mc-Si wafers for improving their optical properties. This method enables a high extent of control over the shape and size of the formed structure on the surface [48].

Currently laser application in solar cells is not restricted to only the surface texturing, but also it is applicable in other stages of the solar cell fabrication such as, doping, transparent conductive oxide layer deposition, contact creation etc. [49-53]. In addition, several reports have been documented on the dependency of the surface topography to the properties of the irradiating laser and scanning conditions as well as variety in the morphologies that form on the textured area [20][26][54-57].

Laser texturing is multifactorial, including laser fluence, pulse repetition rate, pulse duration, laser wavelength, etc. along with several variable factors in the irradiation system such as number of irradiations, overlap between the laser pulses, in addition to lots of options for the ambient where the texturing is performed. Various surface topographies can be achieved under different texturing conditions. As a result, it is vital to exploit a designed experiment to minimize the huge amount of variables at a fixed number of experiments. In this work, texturing has been executed using nanosecond laser and a comparison between the morphology, average roughness (R_a) and depth of the structures formed on the silicon surface via different laser and scanning parameters has been made. ANOVA (analysis of variance) test was adopted for evaluating the significance and investigating the effect of input factors on the output parameters, respectively. In addition,

investigations on the reflectivity of textured silicon samples as well as time and energy consumption, has been conducted. To the best of our knowledge, this is the first report of implementing statistical based analysis for investigating the significance and effect of the process parameters including, laser fluence, overlap between the pulses and number of irradiations, in achieving the desired microstructure pattern on mc-Si where the probability of light absorbance is increased.

3.2 Experimental setup

Experiments have been carried out in ambient air on polished p-type (Boron doped) multicrystalline silicon surface with a thickness of 700μm and resistivity of 0.02 Ω-cm. The laser used for irradiations was the Nd: YVO_4 (Neodymium-doped yttrium orthovanadate) from Coherent Inc. This laser was operating at TEM_{00} mode with Gaussian profile at a wavelength of λ=1064 nm, pulse repetition rate of 10 KHz and pulse duration of about 14 ns. Wafers were cut into 20 mm×30 mm rectangular pieces and mounted on a three axis translation stage. They were cleaned before the texturing procedure for 10 min in the ultrasonic bath of acetone in order to reduce the effect of native oxide layer and were kept in deionized water before being used. Laser beam was irradiated normal to the target surface and the textured area was 10 mm by 10 mm.

As shown in Figure 3.1, the laser beam passes through the Galvoscanner mirrors, which produce the desired pattern on the surface. The initial diameter of the beam coming from the telescopic lens was 5 mm, which was reduced to 40 μm by a 150 mm focal length lens. This lens was placed 150 mm away from the Galvoscanner mirrors so that the focused laser spots hit normal to the target, which was also placed 150 mm away from the lens. In order to produce a 10mm by 10mm textured area, mirrors rotation angle was calculated to be ±1.909° and the overlap between the pulses was controlled by the Galvoscanner mirror oscillation frequency as calculated by Equation 3.1. Irradiation parameters and laser fluence values are shown in Table 3.1 and Table 3.2, where the presented data are calculated by Equations 3.2 and 3.3.

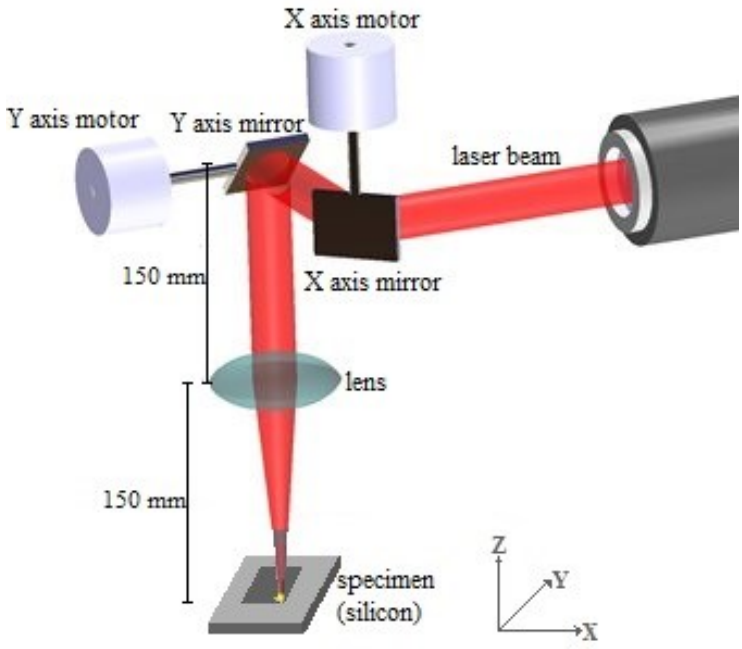

Figure 3.1 Schematic of the experimental setup.

$$\text{Scanning speed} = \text{Pulse pitch} \times \text{pulse repetition rate of the laser} \quad (3.1)$$

$$\text{Pulse pitch} = \text{Spot diameter} \times (1 - \text{overlap percentage}) \quad (3.2)$$

(Where, spot diameter = 40μm)

$$\text{Pulses per row} = [(\text{width of the textured square} - \text{Spot diameter})/(\text{pulse pitch}) + 1] \quad (3.3)$$

Table 3.1 Properties of the laser and irradiation parameters.

Laser fluence (J/cm^2)	Overlap percentage	Number of irradiations
12.7	0,30,60	1,2,4
17.5	0,30,60	1,2,4
18.6	0,30,60	1,2,4

Table 3.2 Pulse pitch and pulse numbers associated with spot overlap.

Overlap percentage	0	30	60
Laser pulse pitch (μm)	40	28	16
Number of pulses per row	250	357	624
Scanning speed (μm/s)	4×10^5	2.8×10^5	1.6×10^5

As mentioned earlier, three parameters including laser fluence, overlap between the pulses and number of irradiations were the varying factors in this experimental research work. As such, laser was irradiating with different fluences including 12.7 J/cm^2, 17.5 J/cm^2, 18.6 J/cm^2 and for each laser fluence three different overlaps and number of irradiations including 0%, 30%, 60% and 1,2,4 were applied, respectively. Figure 3.2 schematically illustrates the three overlap percentage values

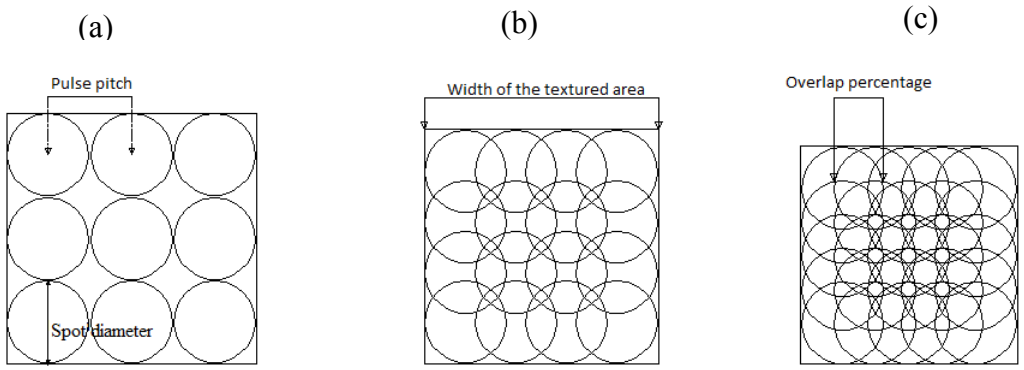

Figure 3.2 Schematic of the mc-Si samples textured under three different overlap values. (a) 0%; (b) 30%; (c) 60%.

Table 3.1 represents the arrangement of experiments based on the mentioned variable parameters. 27 set of experiments were performed in order to study the effect of laser fluence, overlap percentage and number of irradiations on mc-Si morphology, depth and reflectivity. Furthermore, time and energy consumption in achieving the best microstructure pattern, in terms of SWR and depth, has been assessed. Note that, number of irradiations refers to the number of times that the laser was used to scan over the whole textured area with the same laser scanning parameters such as fluence and overlap percentage.

To this aim, textured samples were studied under optical interferometry (Veeco nt1100 white light interferometer) for investigating the structural characterization including their depth, average

roughness and overall profile. Furthermore, scanning electron microscopy (SEM) analysis were performed in order to have a clearer view about the shape of the textured area and validating the measurements throughout the optical interferometry tool.

3.3 Results and discussion

In order to investigate the significance and compare the effectiveness of the variable factors with respect to each other, ANOVA test has been conducted based on the R_a and depth data obtained from optical interferometry.

3.3.1 Effect of surface texturing under three different laser fluences:

ANOVA was employed in order to investigate if there is any significant difference in R_a and depth by varying the laser fluence. Since the mc-Si samples were textured under three different laser fluences, we classified them into three groups where they were having the same laser fluence properties. Based on the ANOVA test initial hypothesis, if p-values is less than 0.05, mean value of the groups statistically differ from one another. Therefore, in assessing the significance of the laser fluence in terms of R_a and depth, p-Values of 0.44 and 0.11 (Table 3.3), respectively suggest that there is no statistically significant difference between the groups. In other words, the range of laser fluence from 12.7 J/cm^2 to 18.6 J/cm^2 could not statistically alter R_a and depth. Note that, F in this table represents the degree of importance of the source of variation, which in this assessment is the laser fluence. This value is later compared with its counterparts at the end of the report.

Table 3.3 ANOVA results - effect of laser fluence on R_a and depth.

Source of variation	F (R_a)	P-value (R_a)	F (depth)	P-value (depth)
Laser fluence	0.84	0.44	2.36	0.11

Figure 3.3 shows that at one and two times irradiation, increase in the laser fluence has resulted in increase in R_a, whereas at four times irradiation, decrease in R_a resulted when the laser fluence is increased from 12.7 J/cm^2 to 17.5 J/cm^2 and on further increase in fluence to 18.6 J/cm^2, R_a increased. This is because, at lower number of irradiations including one and two times, increasing the laser fluence creates higher craters in addition to deeper holes. However, when the surface is irradiated for the fourth time, increasing the laser fluence from 12.7 J/cm^2 to 17.5 J/cm^2, results in

melting and destroying the previously formed protrusions, which is due to the higher number of irradiations. Whereas, by further increasing the laser fluence to 18.6 J/cm^2, creation of larger size clusters on the surface is more significant than melting the previously formed craters. This is probably why at four times irradiation, by increasing the laser fluence R_a reaches a minimum value and then increases by further increasing the fluence. This result is also evident in the SEM images presented in Figure 3.4 where the density of the clusters on the surface is highest in Figure 3.4 (c) and (a) compared to Figure 3.4 (b).

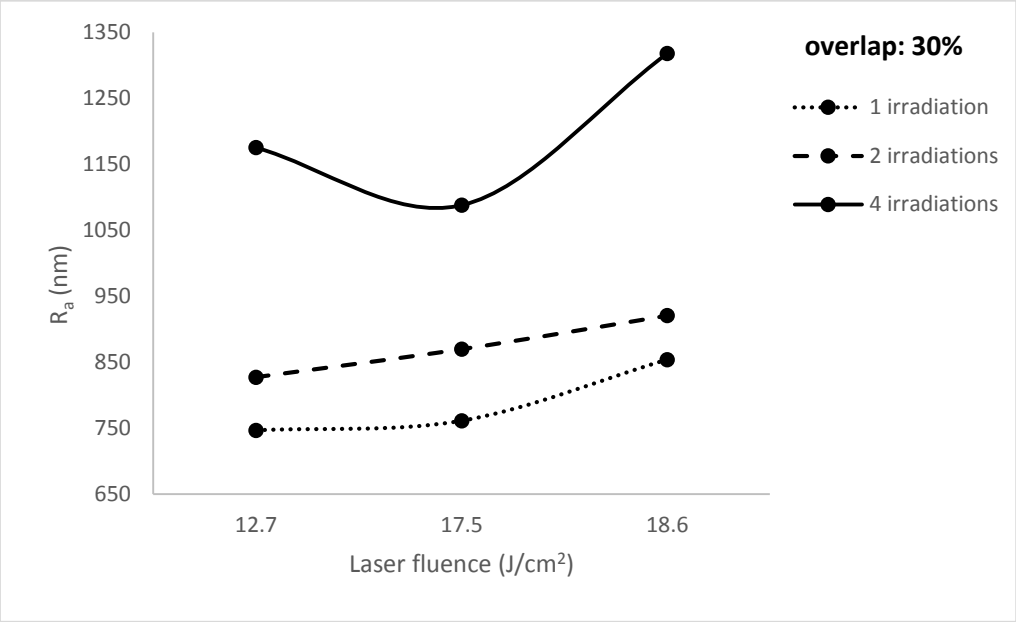

Figure 3.3 R_a versus laser fluence at 30% overlap and one, two and four times irradiation of the sample.

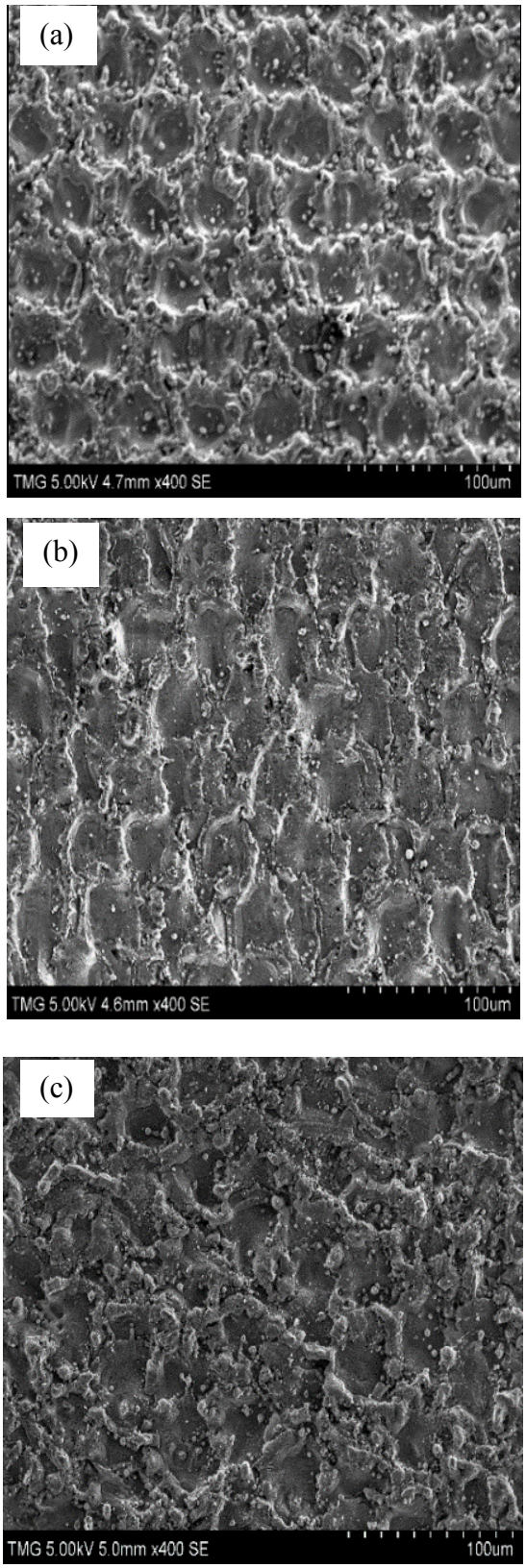

Figure 3.4 SEM images of the mc-Si textured under four times irradiation, 30% overlap and different laser fluences. (a) 12.7 J/cm^2; (b) 17.5 J/cm^2; (c) 18.6 J/cm^2.

In addition, depth information of the surface has been investigated. As shown in Figure 3.5 by increasing the laser fluence at a fixed number of irradiations and overlap percentage, deeper holes are featured. This is because, pulses with higher fluence values, are more powerful to get into the deeper parts of the sample where they destroy the crystallographic structure and melt the material which in turn leads to creation of deeper holes. There are also other works documented on the dependency of the depth to the laser fluence. As per Abbott et al. [58] deeper pits were achieved upon higher energy of the laser pulses.

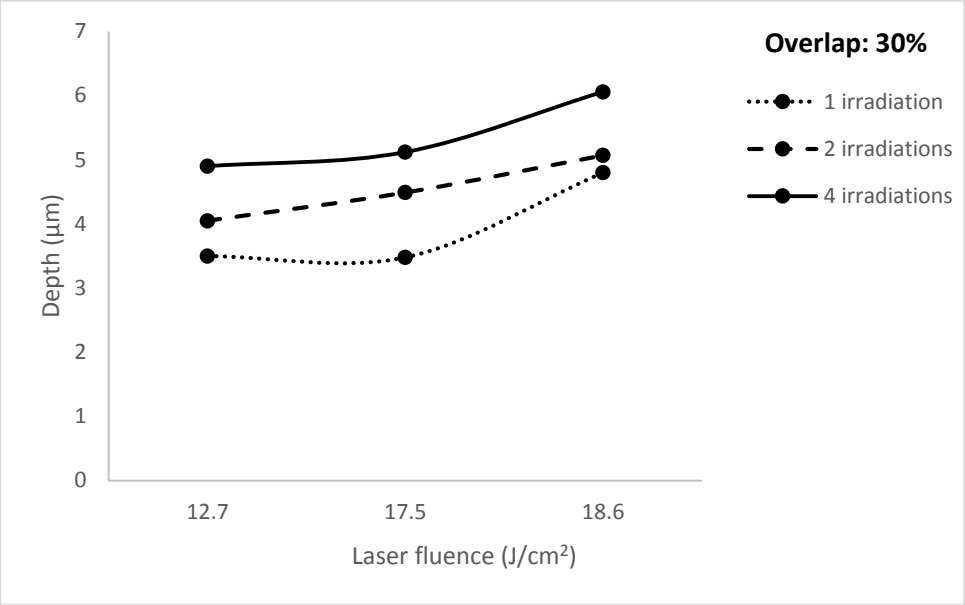

Figure 3.5 Average depth of the holes versus laser fluence at 30% overlap and one, two and four times irradiation of the sample.

3.3.2 Effect of surface texturing under three different overlaps:

Overlap percentage between the laser spots has been assessed in terms of R_a and depth. As such, irradiation has been conducted under three different overlap percentages of the laser spot diameter, including 0%, 30% and 60%. ANOVA results (Table 3.4) show that this factor having P-value of 0.0005 and 0.0003 is of significant importance both from the R_a and depth points of view, respectively. In other words, R_a and depth are statistically affected by the overlap percentage of the pulses. Later when it comes to comparison between the F value of parameters, it is shown that overlap has the highest impact (larger F) on both R_a and depth.

Table 3.4 ANOVA results - effect of overlap on R_a and depth.

Source of variation	F (R_a)	P-value (R_a)	F (depth)	P-value (depth)
Overlap	10.30	0.0005	11.11	0.0003

The R_a and depth information of the created holes on the surface of three samples textured under the same laser fluence and irradiation number but different overlap percentages, has been characterized. Based on Figure 3.6, increasing the overlap has resulted in a surface with a higher R_a. This is because, at the higher overlap conditions, the melting of the material from the surface increases, as such when the molten material re-solidifies on the surface, creates a rougher structure compared to that of the lowest overlap. This effect is also evident in Figure 3.7, which represents the SEM images of three samples with the same laser fluence and irradiation properties, but different overlap conditions. By comparing Figure 3.7 (a), (b) and (c), where overlap between the pulses is 0%, 30% and 60%, respectively, it is understood that the density of the clusters becomes higher as the overlap percentage increases. That is, in the 0% overlap case, the spacing between the protrusions is larger compared to that of 30% and 60% overlap.

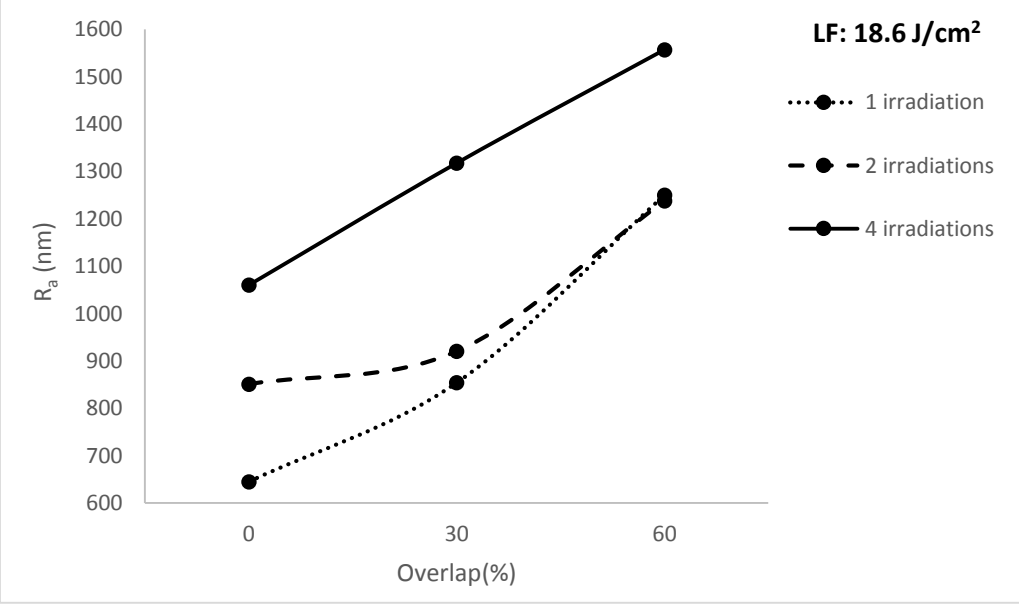

Figure 3.6 R_a versus overlap percentage at laser fluence of 18.6 J/cm^2 and one, two and four times irradiations.

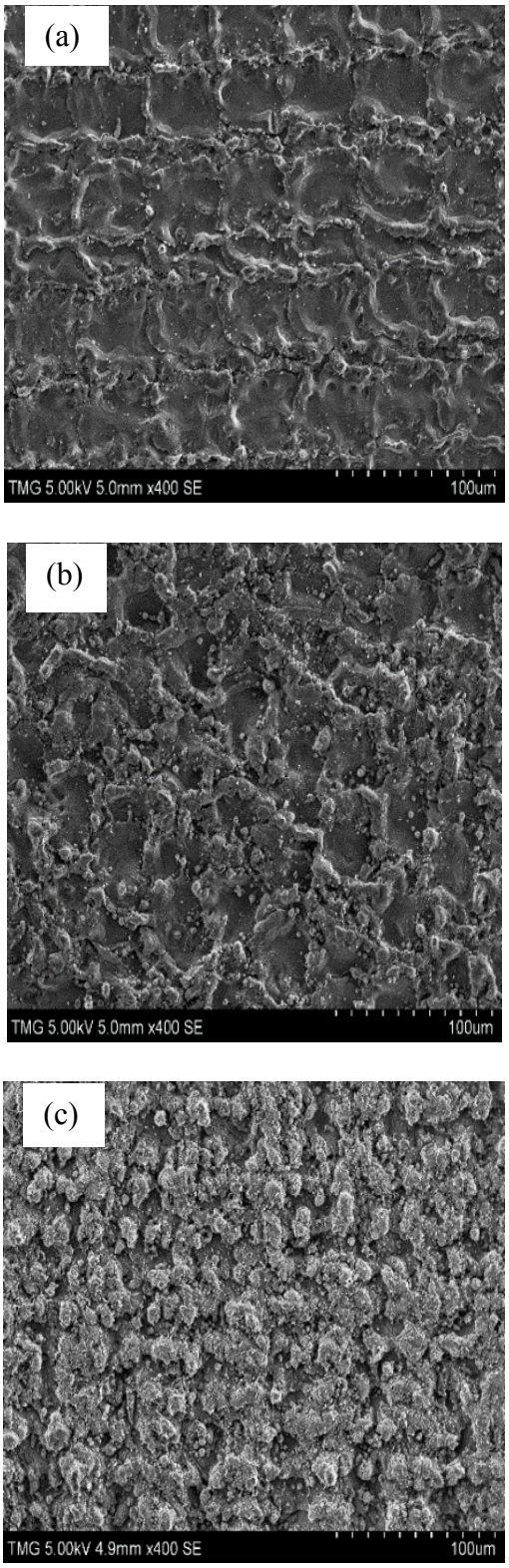

Figure 3.7 SEM images of the mc-Si samples textured under laser fluence of 18.6 J/cm^2, four times irradiation and different overlap percentages. (a) 0% overlap; (b) 30% overlap; (c) 60% overlap.

From Figure 3.8, it is evident that the average depth for a single hole has a higher value for the 60% overlapped sample with respect to a sample in which the laser pulses did not have any overlap with respect to each other. At areas where the pulses have overlap with each other, depth of penetration increases because those parts are actually affected by the laser pulse more than once. As can be seen in this Figure 3.8, the average depth for a single hole at 0% overlap, laser fluence of 18.6 J/cm^2, which is equal to 2.3 watts, is about 3.74 μm. Tao et al. [59] have reported ablation depth of about 1 μm for a single pulse upon a laser power of 3.5 watts, pulse duration of 200 ns and the same wavelength as the current work. This shows that, despite the fact that the laser has a higher power in [59], it could produce shallower holes compared to our work, which is due to its higher pulse duration of 200 ns compared to this work where the pulse duration was 14ns.

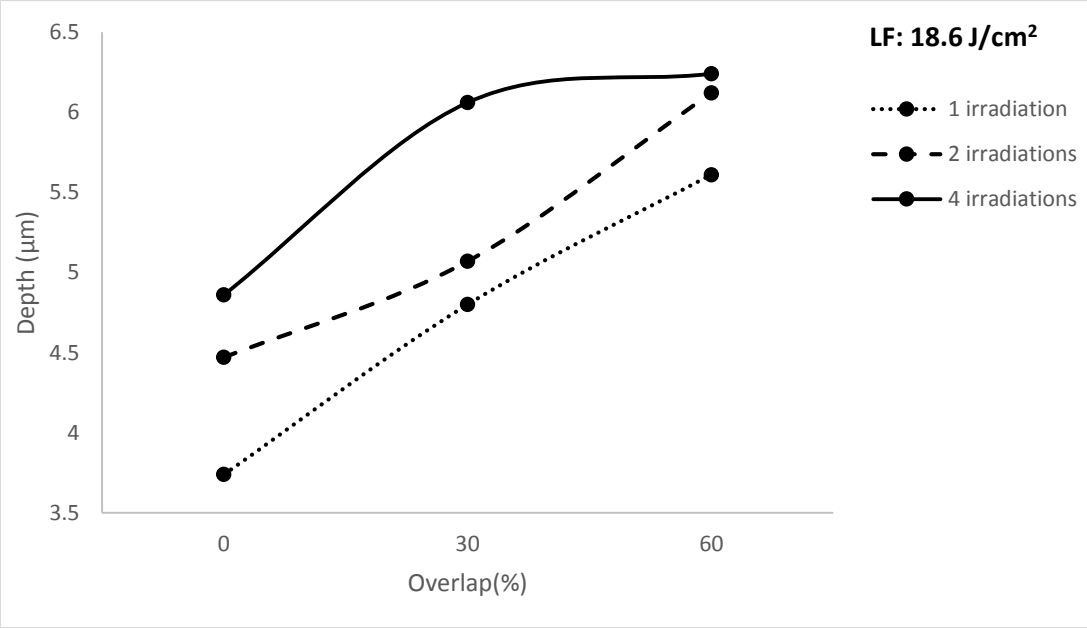

Figure 3.8 Average depth of the holes versus overlap percentage at laser fluence of 18.6 J/cm^2 and one, two and four times irradiations.

3.3.3 Effect of surface texturing under three different number of irradiations:

As for the case of laser fluence and overlap, number of irradiations has been assessed. In this step, all samples that were textured under the same number of irradiations were put in one group. ANOVA has been applied on three groups in order to investigate the impact of number of irradiations, on R_a and depth. This factor having a p-value of 0.001 and 0.02 (Table 3.5) proposes

to be an ideal factor in enhancing the R_a and depth, respectively. Considering the importance of this factor (number of irradiations) in affecting R_a and depth, it is important to find out how this factor modifies them.

Table 3.5 ANOVA results - effect of number of irradiations on R_a and depth.

Source of variation	F (R_a)	P-value (R_a)	F (depth)	P-value (depth)
Number of irradiations	8.40	0.001	4.49	0.02

From Figure 3.6 and Figure 3.8 it is clear that, when laser has irradiated the specimen more than once, R_a and depth increased, respectively. This effect is also visualized in Figure 3.9 where the SEM images corresponding to different number of irradiations, are presented. The reason of increase in the R_a and depth due to increase in the number of irradiations is attributed to the fact that, pulses in the second step of irradiation ablate an area that has previously been melted. When irradiating a sample for the second time, although the overall depth increases, the increment in the depth is lower than that of the first time irradiation, and even much lower when it comes to four times irradiation. This is probably due to re-solidified silicon after first set of irradiation that may have different properties compared to that of unablated silicon surface. In Figure 3.8, there are three points that have almost the same depth values, 30% overlap 4 times irradiation, 60% overlap 2 times irradiation and 60% overlap 4 times irradiation. While Figure 3.8 belongs to laser fluence of 18.6 J/cm^2, similar trend is observed for other fluences as well. In order to increase the depth, one should increase the overlap to 60% and keep the number of irradiations at two times or increase the irradiation times to four and maintain the overlap at 30%. Increasing both number of irradiations to 4 times and overlap to 60% do not show appreciable increase in depth, whereas it has an effect on the R_a.

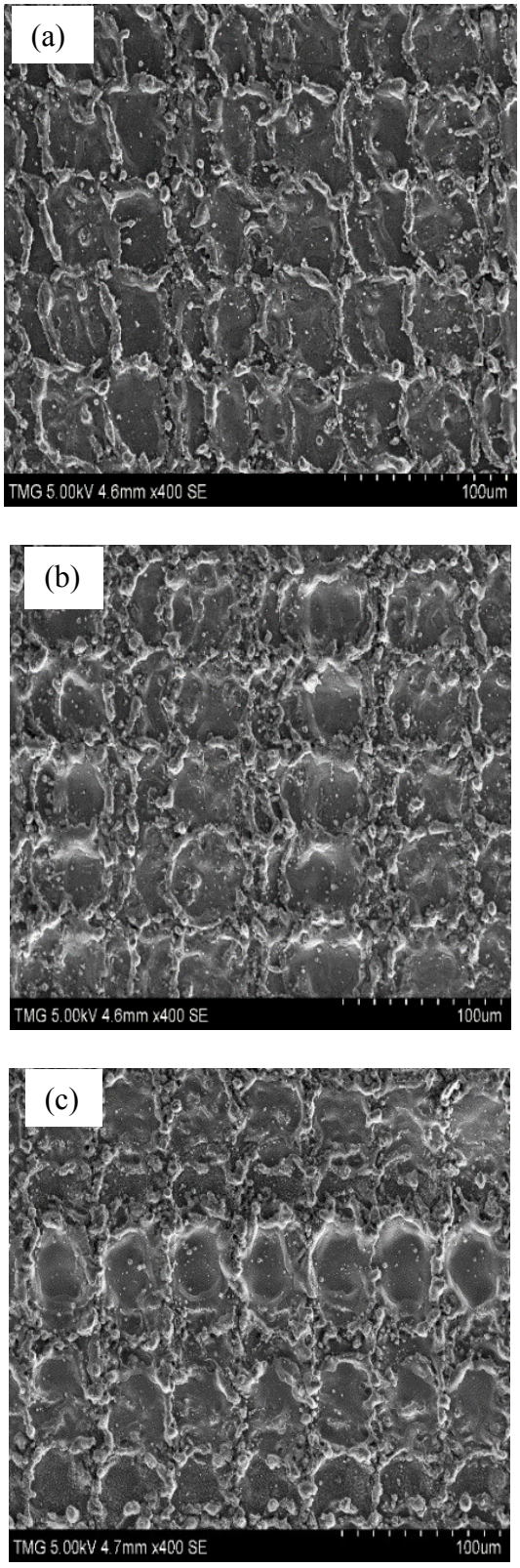

Figure 3.9 SEM images of the mc-Si samples textured under laser fluence of 18.6 J/cm^2, 0% overlap and different number of laser irradiations. (a) One time irradiation; (b) Two times irradiation; (c) Four times irradiation.

Although it was found that, the laser fluence modification did not statistically affect the surface morphology while irradiation numbers and overlapping did, it is still necessary to investigate the importance degree of the two effecting factors, overlap and number of irradiations. In broad terms, since now each of the variable parameters were individually evaluated whereas the correlation between them should also be studied. In this regard, F should be taken into account in order to distinguish between the variable factors in terms of significance. As such, overlap factor with the highest F value of 10.30 and 11.11 suggested to have the most impact on the average roughness and depth, respectively. Number of irradiations is the second effective parameter with F values of 8.40 and 4.49 for R_a and depth, respectively. Finally, laser fluence having the lowest F value of 0.84 and 2.36 is the least effective parameter on R_a and depth, respectively, among the factors we evaluated in laser texturing of mc-Si throughout the described laser.

3.4 Effect of R_a and depth on SWR

In order to calculate Solar Weighted Reflectance (SWR), reflectivity of the samples was measured by Varian Cary 5000 spectrophotometer with baseline correction. In reflectivity measurements, the plain area of each sample was considered as the baseline. Therefore, the plain area with R_a of 6.67 nm and true reflectivity of about 19% was shown to be 100% reflective, after applying the baseline correction. SWR of the textured surfaces has been characterized, in order to investigate the correlation between the morphology and optical properties of the samples. SWR, which is defined as the amount of solar energy reflected from a surface is shown in Equation 3.4.

$$\%SWR = \frac{\int(\%R \times I \times d)}{\int I \times d} \times 100 \tag{3.4}$$

Where, '%R' is the percent reflectance, 'I' is solar irradiance for AM1.5 [6] and 'd' is the wavelength interval of the integration which was over the range of 300 nm to 1100 nm of the solar spectrum.

As shown in Figure 3.10 by increasing R_a from 601 nm to 1100 nm, SWR reduced from 10% to less than 1% where it remained almost constant regardless of R_a or depth enhancement. This shows 99% reduction in the reflectance with enhancement of the R_a up to 1100 nm whereas, further increasing the R_a from 1100 nm did not reduce the reflectivity. On the other hand, there are other factors, such as time and energy consumption that have been taken into account in our study. In

this regard, 4 samples having the minimum SWR and within the range of 1100 nm to 1200 nm of R_a, have been investigated in terms of time and energy consumption. Table 3.6 demonstrates the texturing parameters along with R_a, depth and SWR as well as time and energy consumption of 4 samples with R_a above 1100 nm and SWR below 1%. Heat and time are referred to energy per pulse times number of pulses per cm^2 and number of pulses per cm^2 times number of irradiations divided by the pulse repetition rate of the laser, respectively. Based on Table 3.6, among these 4 samples, the minimum SWR and least time requirement for texturing a 10mm by 10mm square, was about 0.41% and 38 s, respectively which belongs to sample 1 textured under laser fluence of 18.6 J/cm^2, 60% overlap and 1 time irradiation. Sample 2 which was textured under laser fluence of 12.7 J/cm^2, 30% overlap and 4 time irradiation, has the least energy consumption while medium time requirement and maximum SWR. Sample 3 has almost the same SWR, as sample 1 while, the required time and energy for texturing this sample are maximum. Sample 4 has the same time requirement as sample 3, medium energy consumption and medium SWR value. Therefore, either of the first two samples can be used based on the application and the experimental conditions that is, the required SWR and available time and energy, respectively.

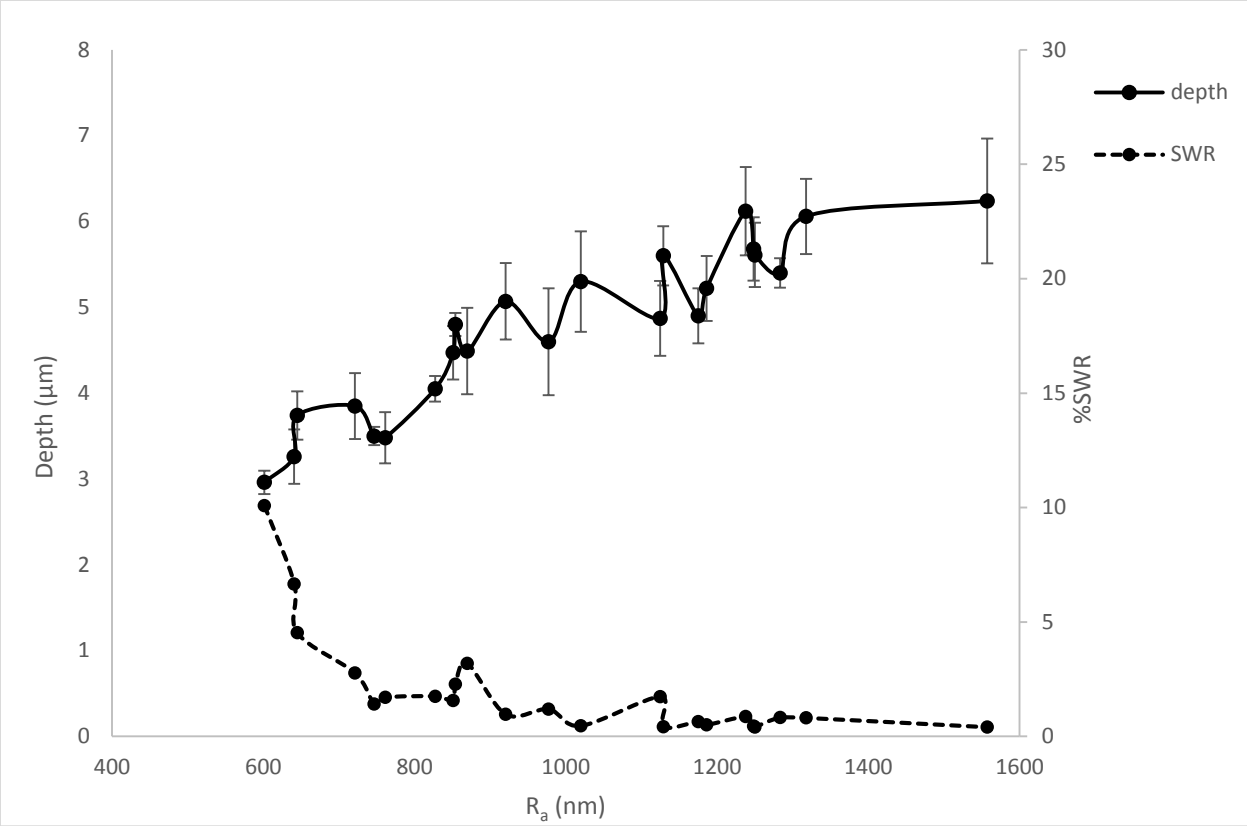

Figure 3.10 Depth and SWR versus R_a.

Table 3.6 Texturing parameters, R_a, depth, SWR, time and heat corresponding to 4 samples with SWR below 1%.

Sample	Fluence (J/cm^2)	Overlap %	Number of irradiations	R_a (nm)	Depth (µm)	SWR%	Time (s)	Heat (J)
1	18.6	60	1	1250	5.61	0.41	38.93	93.65
2	12.7	30	4	1175.3	4.9	0.65	50.97	81.05
3	17.5	60	2	1128.84	5.6	0.42	77.87	176.05
4	12.7	60	2	1186.3	5.22	0.50	77.87	127.82

3.5 Conclusion

In conclusion, the evolution of the nanosecond laser induced morphology on mc-Si has been demonstrated. The results have been analyzed through statistical tests for assessing the significance of the design of experiment. It is concluded that laser fluence does not statistically alter the average roughness and depth of the mc-Si and there is a maximum value at 18.6 J/cm^2 where the maximum R_a and depth is achieved. Overlap percentage was found to have the most impact on both the average roughness and depth. SEM images showed the advanced cluster density in samples being textured under the highest percentage of overlap.

The optimum value of laser fluence, overlap and number of irradiations was found to be 18.6 J/cm^2, 60% and 1 respectively, if SWR was to be minimal within shortest time duration. The optimum values are 12.7 J/cm^2, 30% and 4, if minimizing the laser energy is important while minimizing SWR. The significance of this work, lies not only in reduction of the variables through ANOVA, but also in identifying the parameters that result in lower surface reflectivity of silicon while minimizing time and energy consumption which are extremely important in the mass production.

CHAPTER 4. Nanosecond laser interaction with multicrystalline silicon under acetone confinement

This chapter is based on the manuscript submitted in the Journal of Materials Research Express, where the effect of texturing ambient is statistically evaluated with ANOVA and the effect of depth and R_a on SWR is assessed with regression test.

4.1 Introduction

Silicon photovoltaic (PV) has served as the major solar cell technology, which is evident from its great market share of about 90% in 2014 [37]. Furthermore, the resolute efforts in improving the expenses of silicon PV modules, has resulted in price reduction of 20% during the past 30 years, mainly controlled by the material costs [60]. Solar cell manufacturers are not only concerned about the costs but also they are challenged by the PV cells efficiency. In this regard, laser structuring has been introduced as an efficient technique in texturing the low cost multicrystalline silicon (mc-Si) wafers that cannot be textured through conventional alkaline chemical etching and mechanical techniques due to their anisotropic crystallographic orientation and poor quality, respectively [46][47]. On the other hand, the textured pattern formed by acid texturing, is not desirable in terms of reducing the optical losses [8]. That is, if soft etching is performed the saw damage, which is accounted as recombination sites, is not removed and electrical properties of the wafer will be degraded. On the other hand, due to the isotropic nature of the acid etching, if deep etching is employed to completely remove the saw damage, an almost non-textured surface is achieved. Furthermore, Laser texturing, improves the solar cell efficiency by creating pyramids and grooves on the surface of the mc-Si where the probability of light absorption is increased due to light trapping [39-41][61]. Low-cost and low-energy consumption infrared (IR) nanosecond (ns) lasers have shown to be efficient enough in silicon texturing because, their pulse duration is short enough to maintain a high processing accuracy and at the same time they have much lower equipment costs compared to the same UV/visible laser average power output [21]. On the other hand, laser structuring of different materials in liquids has proven to be one of the major approaches in debris-free microfabrication for optoelectronic devices [62] and a method to generate nanoparticles that appear as a colloidal solution in the liquid [63]. In the aqueous laser treatment of silicon, the molten material is removed from the target by the bubble motion. In other words, ablated debris is carried away due to the liquid thermal convection or bubble-induced liquid motion [64][65]. Laser

processing assisted with liquids such as water not only enables fabrication of cleaner and debris-free microstructures but also reduces the length of the heat-affected zone due to the high cooling rate of the water compared to air and results in better tolerances and more precise laser texturing [66]. In this work, effect of nanosecond laser fluence and number of pulses on the average surface roughness (R_a), depth and solar weighted reflectance (SWR) of mc-Si under acetone and in air has been investigated through analyzing the experimental results acquired by optical interferometry, scanning electron microscopy (SEM) and spectrophotometry. Furthermore, significance level of depth and R_a in SWR improvement of the textured mc-Si has been statistically evaluated.

4.2 Experimental

Figure 4.1 is the schematic of the experimental setup. Nanosecond laser texturing was carried out in acetone with 14 ns laser pulses at 1064 nm wavelength and pulse frequency of 10 KHz. The Nd: YVO_4 (Neodymium-doped yttrium orthovanadate) laser from Coherent Inc. was operating at TEM_{00} mode (Gaussian profile). The polished p-type (boron-doped) mc-Si wafers with thickness of 700 μm and resistivity of 0.02 Ω-cm were placed in a metal container covered with 1mm layer of acetone. The samples were located on a three–axis translation stage and the texturing area was a 10mm by 10mm square. The desired pattern on the target was controlled by the frequency of the galvoscanner mirrors that are shown in Figure 3.1. A 150 mm focal length lens was placed at a distance of 150mm from the galvoscanner to not only reduce the beam diameter to a 40 μm spot, but also make sure that the laser strikes perpendicular to the target surface within the texturing area. Due to different refractive index of acetone compared to air, the focal point was modified from dry experiments and it was slightly more than 150 mm from the lens. Detailed description of the experimental setup can be found in our earlier work done in air ambient [35].

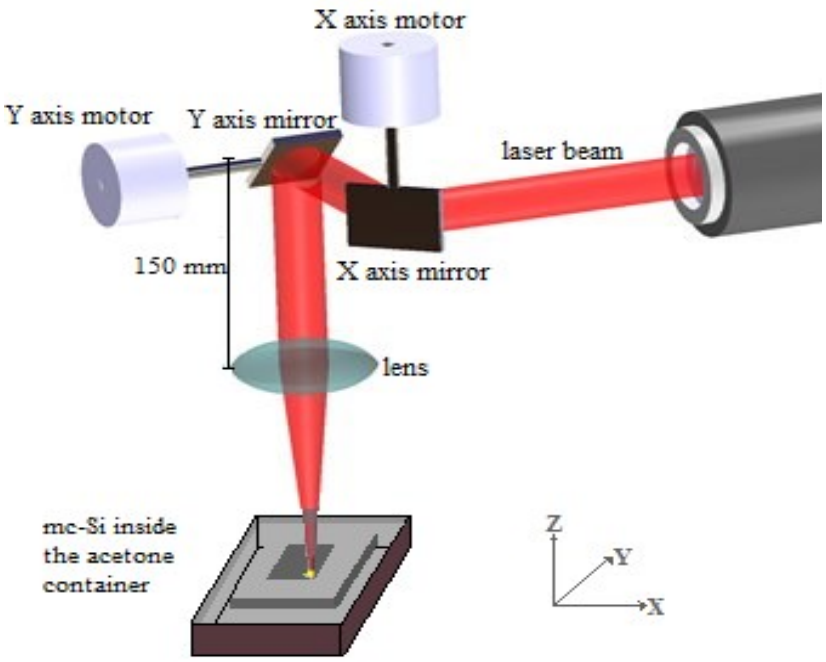

Figure 4.1 Schematic of the experimental setup.

4.3 Results and discussion

Experiments were done at two different laser fluences and four different pulse numbers. At the highest laser fluence, bubble generation in acetone, was accompanied with a loud sound and at the lower laser fluence ablation was initiated. Scattering from the bubbles inside the acetone confinement was increased by increasing the laser fluence. Figure 4.2 shows the effect of number of pulse on the R_a at laser fluence of 18 J/cm^2 and 22 J/cm^2 in acetone confinement. At both laser fluences, increasing the number of pulses from 62500 #pulses/cm^2 to 510000 #pulses/cm^2 has enhanced the R_a. Furthermore, Figure 4.2 demonstrates lower values for R_a at laser fluence of 22 J/cm^2 compared to 18 J/cm^2. As reported in [67-69], this is probably because, in most liquids when the laser fluence exceeds a certain value the delivery energy at the target dramatically drops due to the shielding effect which is a consequence of optically dense plasma above the target which hinder further improvement in the ablation rate.

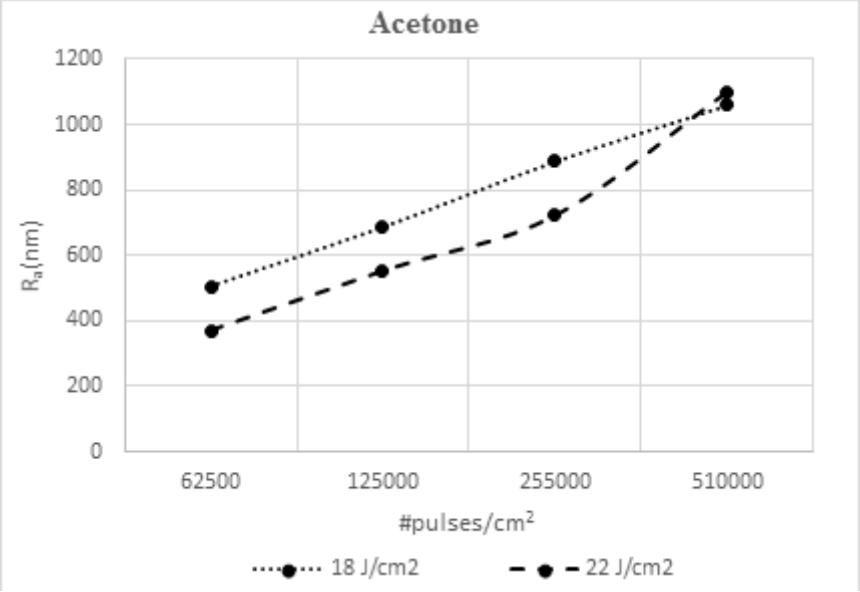

Figure 4.2 R_a vs number of pulses for laser fluences of 18 J/cm^2 & 22 J/cm^2 in acetone.

Figure 4.3 compares the effect of number of pulses on the R_a of the samples textured in air and acetone at the laser fluence of 22 J/cm^2. This figure clearly shows that unlike acetone, in air R_a does not continuously increase by increasing the number of pulses at the laser fluence of 22 J/cm^2. This is probably because, in the dry experiments increasing the number pulses to 125000 #pulses/cm^2 results in a large density of protrusions on the surface, which contribute to an increase in the R_a. While, further increasing the number of pulses re-ablate the mentioned protrusions and consequently reduces R_a and again more number of pulses improve the R_a by forming new depositions on the surface. Therefore, no particular trend is achieved for R_a when the texturing is conducted in air at the laser fluence of 22 J/cm^2. However, in case of acetone experiments, the surface is almost free of the ablated material and R_a is mainly due to depth. As such, increasing the number of pules results in deeper valleys and consequently higher R_a. Therefore, it might seem that in the dry experiments, ablated debris on the target mainly controls the R_a while in the acetone assisted experiments, R_a is mainly due to the deeper holes on the surface.

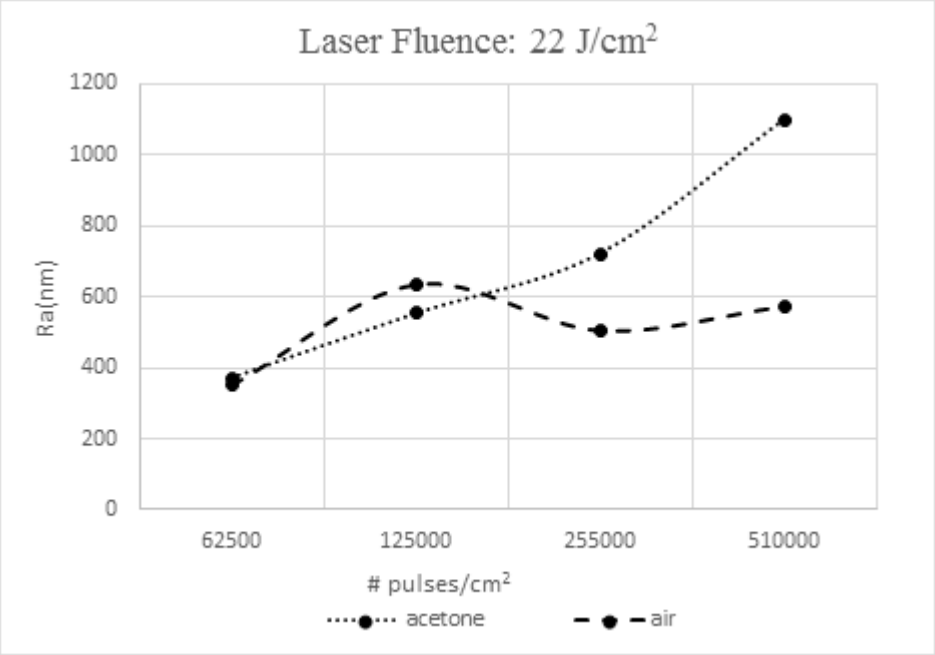

Figure 4.3 R_a vs number of pulses at laser fluence of 22 J/cm^2 in acetone and air.

Figure 4.4 shows the effect of number of pulse and laser fluence on depth of the holes formed on the targets in acetone at two laser fluences. From this figure, it is clear that at both laser fluences, increasing the number of pulses has enhanced the depth, which is similar to the results for the R_a while, depth values seem to be reduced by increasing the laser fluence. This might again be attributed to the shielding effect at the higher laser fluence, which hinders the laser beam to completely go through the medium and influence the target. The above results are better understood from the corresponding SEM images. Figure 4.5 shows the influence of the number of pulse on the morphology of the mc-Si at the same environmental conditions. As can be seen in Figure 4.5 (a) the holes created at 125000 #pulses/cm^2 are shallower compared to Figure 4.5(b) where the number of pulses is increased to 255000 #pulses/cm^2. In addition to depth, this figure, shows that the holes are formed closer to each other in (b) compared to (a) which in turn validates the results obtained for R_a. Figure 4.6 compares the morphology of the samples irradiated under the same ambient and pulse number conditions but at different fluences of the laser. Figure 4.6 (b) where the laser fluence is higher compared to that of (a) seems to be less modified. However, in Figure 4.6 (a) the surface is more roughened in addition to its deeper holes, which is consistent with the results obtained in Figure 4.2 and Figure 4.4.

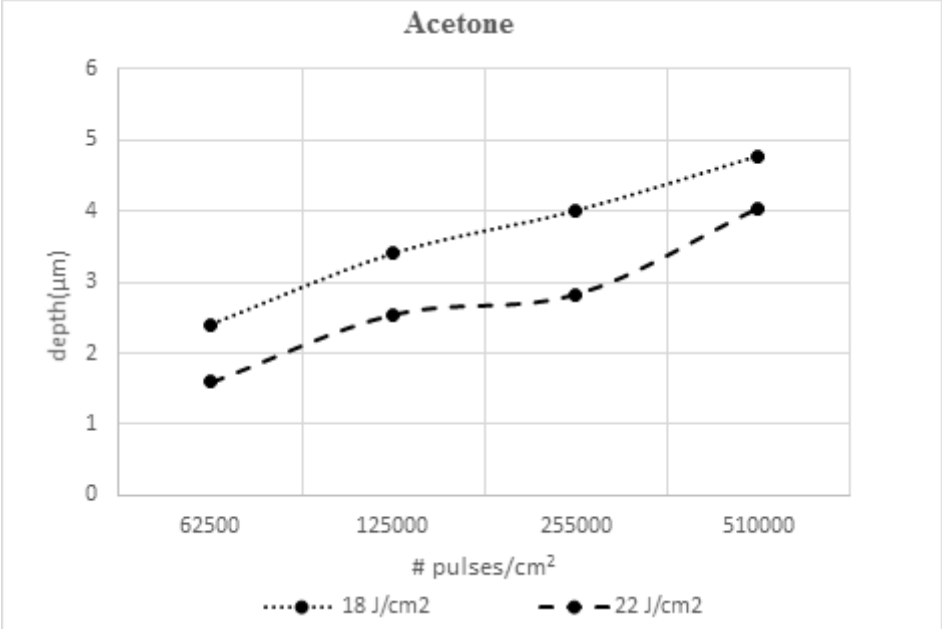

Figure 4.4 Depth vs number of pulses for laser fluences of 18 J/cm^2 & 22 J/cm^2 in acetone.

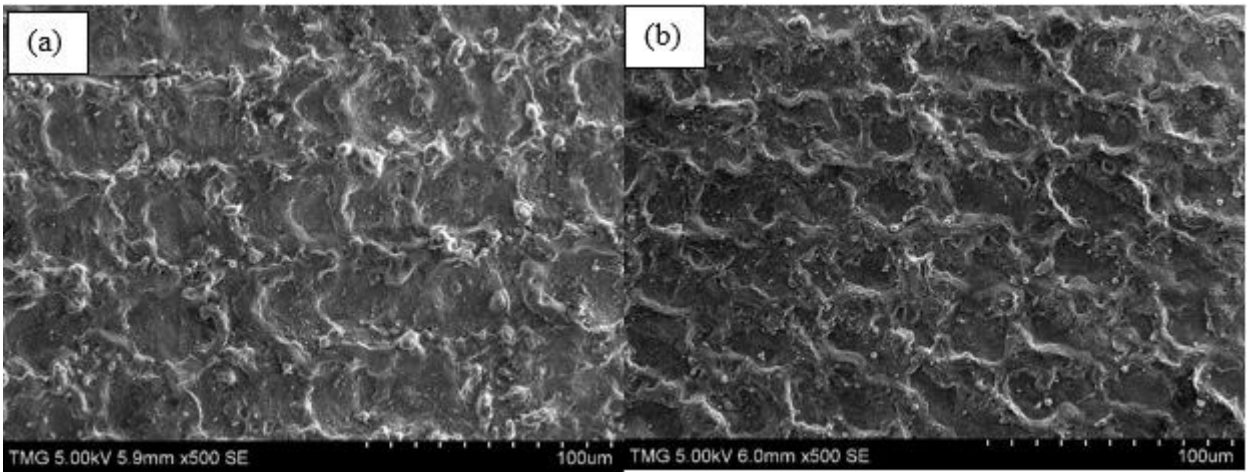

Figure 4.5 SEM images of the mc-Si samples textured under laser fluence of 18 J/cm^2 in acetone at different number of pulses, (a) 125000 #pulses/cm^2; (b) 255000 #pulses /cm^2.

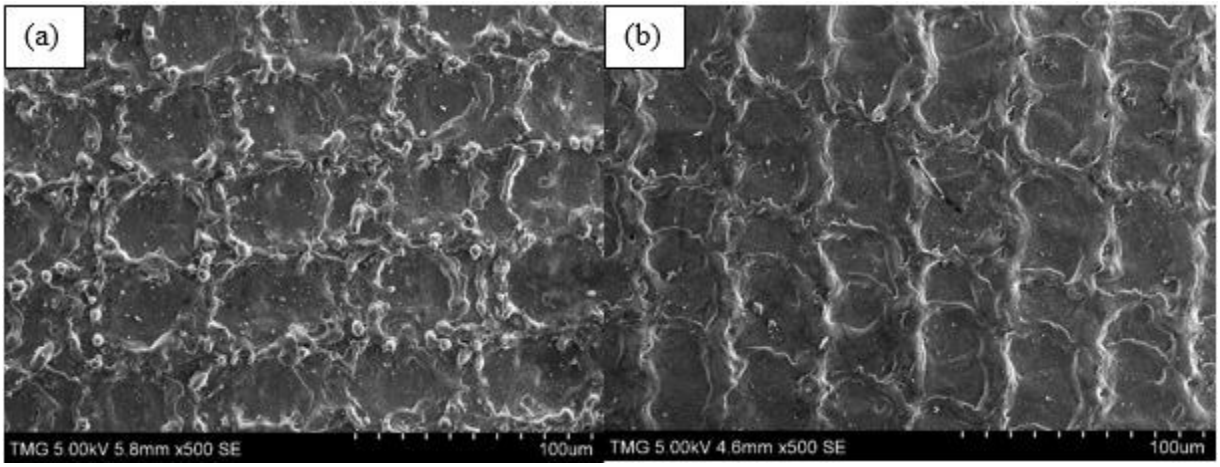

Figure 4.6 SEM images of the mc-Si textured under acetone at 62500 #pulses/cm^2 and different laser fluences. (a) 18 J/cm^2; (b) 22 J/cm^2.

Figure 4.7 which compares the effect of pulse number on the depth in air and acetone, shows the same values for the depth in acetone and air experiments at 62500 #pulses/cm^2 and 125000 #pulses/cm^2 while, deeper holes for the acetone experiments when the number of pulses is higher than 125000 #pulses/cm^2. In other words, acetone experiments seem to result in deeper holes compared to air when the pulse number is higher than 125000 #pulses/cm^2. This might be because, in case of ablation in air ambient, when the pulse number increases, the target is extremely ablated and a part of the ablated material re-solidify into the formed holes and consequently reduce their depth. However, at the lower number of pulses the target is not highly affected so neither the holes are so deep nor too much of the sample is ablated for filling the holes. As such, when the number of pulses is 125000 #pulses/cm^2 or lower, almost same holes, in terms of depth, are achieved in air and acetone at the laser fluence of 22 J/cm^2. Figure 4.8 compares the effect of the experimental ambient on the morphology of the mc-Si laser texturing. It is clear from Figure 4.8 that the presence of the re-deposition debris on the machined area is almost negligible in the acetone-assisted experiment Figure 4.8 (a). This is attributed to the heat convection in the acetone confinement compared to air where the ablated material is deposited on the target Figure 4.8 (b). It is also evident from Figure 4.8 (a) and (b) that deeper holes are achieved in acetone compared to air at the laser fluence of 18 J/cm^2 and 255000 #pulses/cm^2.

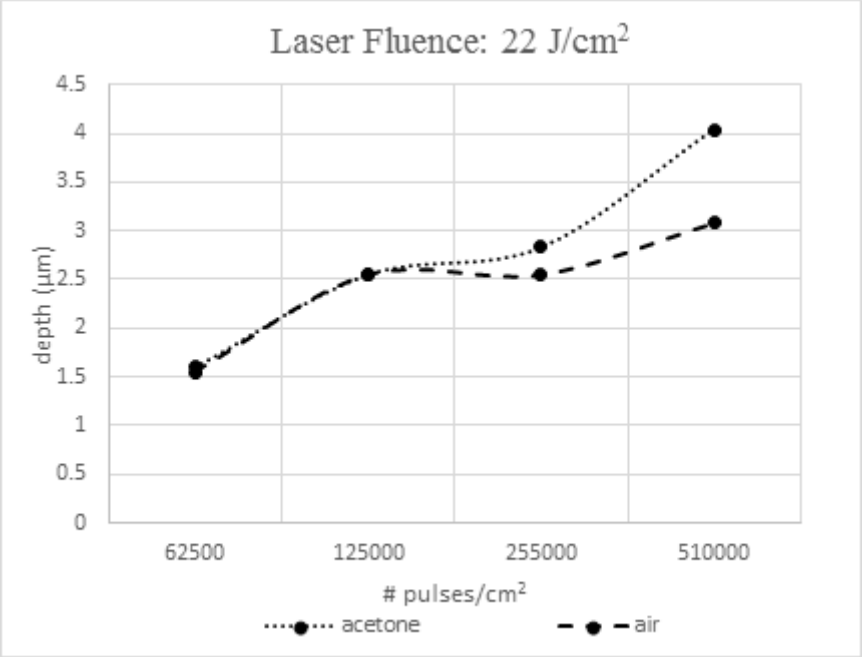

Figure 4.7 Depth vs number of pulses at laser fluence of 22 J/cm^2 in acetone and air.

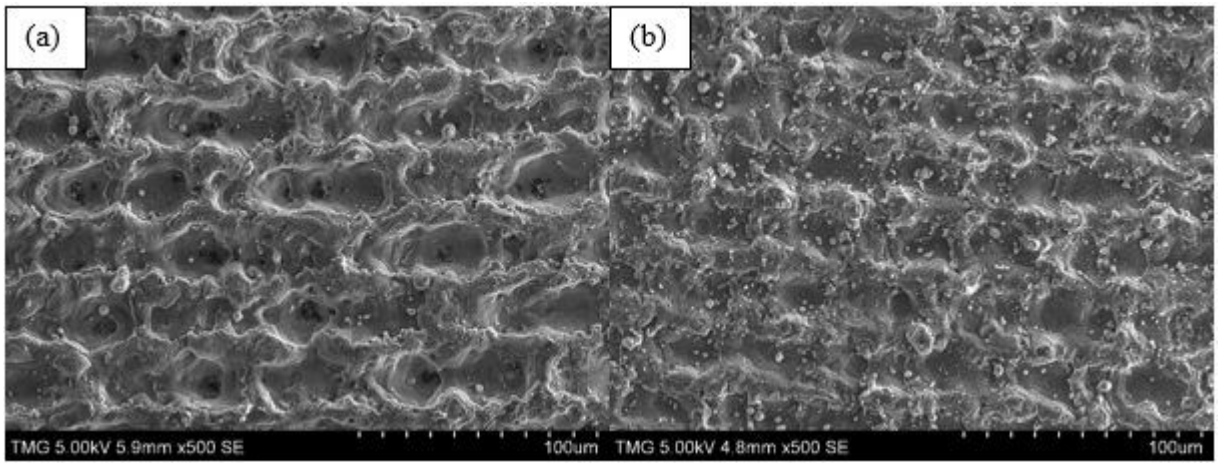

Figure 4.8 SEM images of the mc-Si textured by 255000 #pulses/cm^2, laser fluence of 18 J/cm^2 and at different ambient. (a) acetone; (b) air.

In addition to morphology, the reflectivity properties of the mc-Si wafer treated at different ambient, laser and irradiation parameters has been assessed in terms of SWR (Equation 4.1). As shown in Figure 4.9 samples affected by a higher number of pulses in acetone are less reflective, which is due to the improved R_a and/or depth. In addition, this figure shows an increase in the

reflectivity by increasing the energy of the laser, which is again due to the reduction in the delivery energy of the laser at the specimen, which was previously shown to degrade the R_a and depth. In order to examine which factor plays the major role in SWR improvement of the mc-Si samples textured in acetone, two approaches are adopted in this study. One approach is the prediction curve (Figure 4.10) which matches well with the R_a values only for samples with R_a below 722 nm or SWR above 2.44%. However, Figure 4.10 shows that SWR is predictable with depth even when the SWR is smaller than the mentioned limit. The second method is the statistical analysis of the SWR versus depth and R_a. From the regression tests, it is evident that depth is more significant than R_a in SWR improvement.

$$\%SWR = \frac{\int(\%R \times I \times d)}{\int I \times d} \times 100 \tag{4.1}$$

(%R is the percent reflectance, I is solar irradiance for AM1.5 [6] and d is the wavelength interval of the integration which was over the range of 300 nm to 1100 nm of the solar spectrum.)

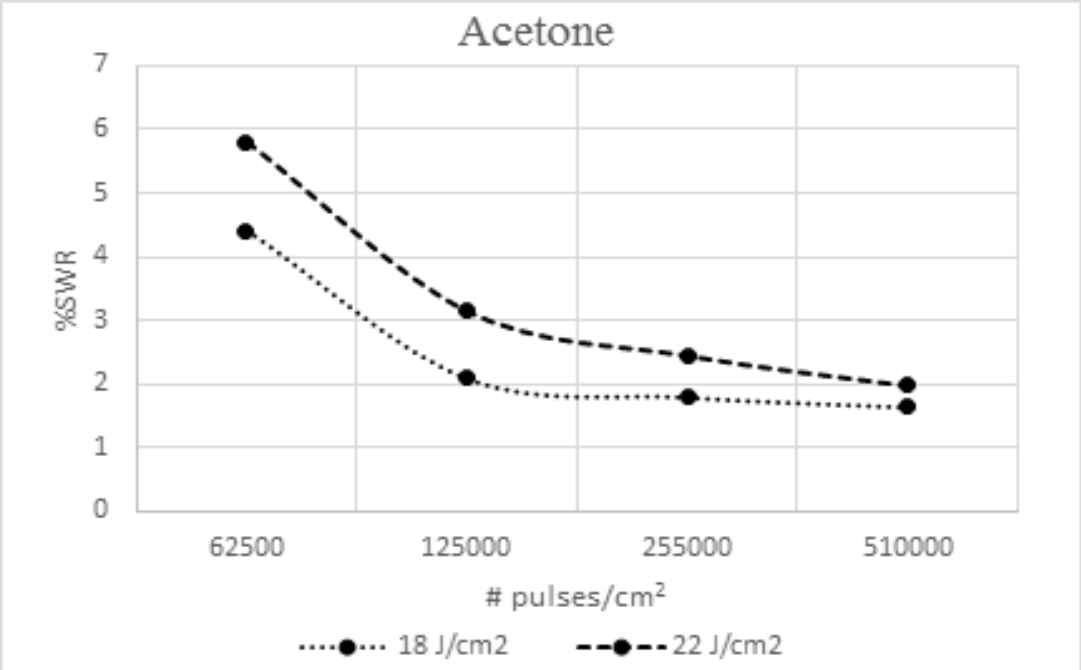

Figure 4.9 %SWR vs number of pulses for laser fluences of 18 J/cm^2 & 22 J/cm^2 in acetone.

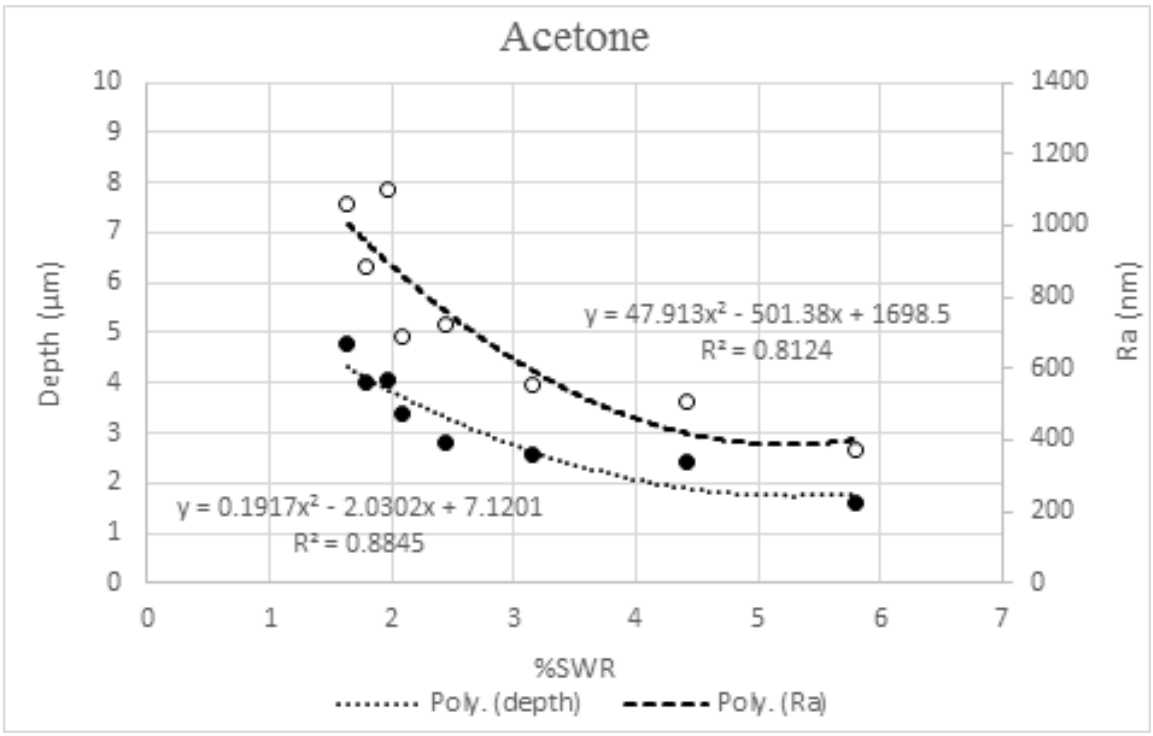

Figure 4.10 SWR prediction in acetone assisted experiments.

Table 4.1 Regression table for SWR of mc-Si laser texturing in acetone.

Source	P-value	F
R_a	0.0070	16.10
Depth	0.0027	23.89

Figure 4.10 is the trend of the SWR with respect to depth and R_a of mc-Si samples treated in acetone. As shown in this figure, SWR above 2.44% is dependent on both R_a and depth however, at lower SWR values, variation of depth plays a more significant role to control SWR compared to R_a. Therefore, lower SWR values are predicted by depth not the R_a. This result was also reported in [70][71] where a huge reduction in reflectivity was achieved by increasing the structures depth. Furthermore, the effect of depth and R_a on reflectivity has been statistically assessed. Based on Table 4.1, which presents the regression test results of the samples textured in acetone, both R_a and depth are statistically significant in SWR improvement since both have p-values less than 0.05. However, the significance level of depth is higher than R_a because depth has a higher F value. This

result is another translation of the prediction curves in Figure 4.10 where the R^2 is equal to 0.88 and 0.81 for depth and R_a curves, respectively.

Figure 4.11 compares the effect of texturing at different ambient on the SWR. As shown in this figure, experiments done in acetone resulted in lower reflective wafers compared to the ones textured in air. This result is probably because of the light scattering from the re-deposited material on the mc-Si textured in air as well as different R_a/depth properties of the samples in two different ambient. Furthermore, based on the Figure 4.3 and Figure 4.7 only depth improved with the number of pulses and R_a did not have a certain trend in air experiments. Therefore, based on Figure 4.11 where SWR improved by the number of pulses, it can be concluded that the reflectivity reduction is mainly controlled by depth, since SWR and depth trends are consistent.

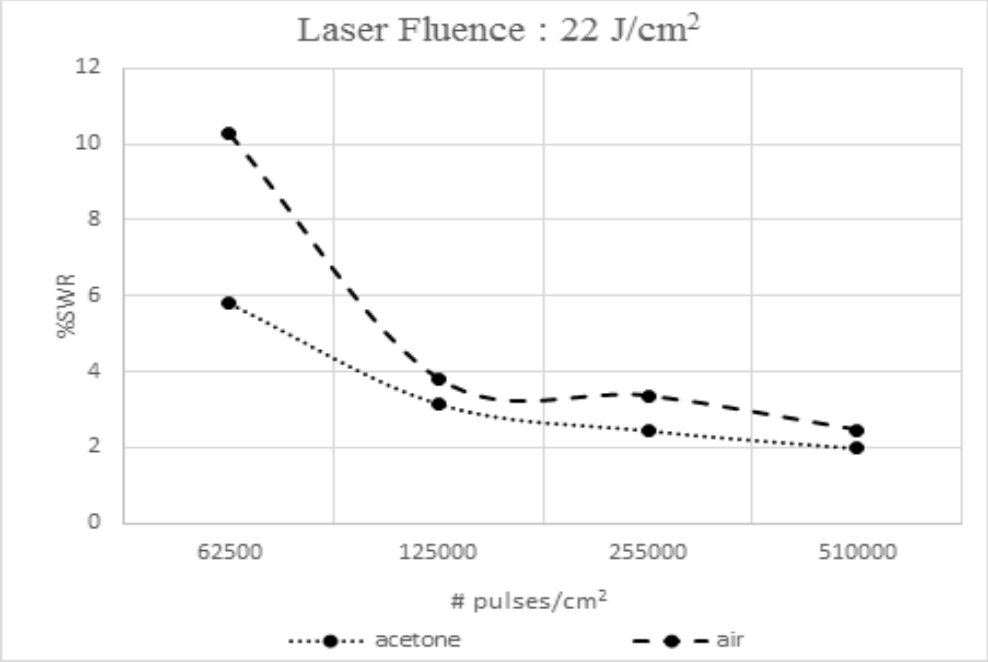

Figure 4.11 %SWR vs number of pulses at laser fluence of 22 J/cm^2 in acetone and air.

4.4 Conclusion

In conclusion, the effect of laser fluence and pulse numbers on the R_a, depth and SWR of the mc-Si in acetone and air, has been assessed. Results showed that presence of the acetone film helps in producing deeper holes and higher R_a compared to air, at pulse numbers higher than 125000 #pulses/cm^2. In addition, the increase in the laser fluence in the acetone experiments resulted in

lower R_a and depth, which is due to the shielding effect occurring at high laser fluences. On the other hand, increasing the depth of mc-Si treated in acetone from 1.6 μm to 4.7 μm, resulted in SWR reduction of 5%. However, R_a improved SWR only up to 722 nm and above this limit, R_a was not an effective parameter in SWR reduction. In addition, regression test validated that although both R_a and depth affect the SWR, depth is more significant in SWR improvement, when laser texturing is conducted under acetone. Finally, the preference of choosing acetone as the texturing medium instead of water is that, its absorption coefficient is almost half of the absorption coefficient of water in the range of infrared [72]. Therefore, the energy of the laser beam reaching the target in water is less than that of acetone. Note that, in order to use these textured wafers in the solar cells, we should etch them in alkaline chemical solutions for removing the laser-induced damage that has side effects on the electrical properties of the device.

CHAPTER 5. Electrical properties of the solar cells based on textured and untextured multicrystalline silicon

Laser texturing of mc-Si significantly reduces the light reflection from the surface, which can make the wafers potentially suitable for higher efficiency solar cells. We fabricated and characterized solar cells based on polished and textured mc-Si. Although laser texturing results in higher electron-hole pair (EHP) generation due to increased light absorption, it introduces damage to the wafer that acts as recombination centers for minority carriers. Therefore, it is essential to employ a chemical etching method to remove the laser-induced damage and make the textured wafers ready to be implemented as the basis of solar cells. Otherwise, solar cells based on textured wafers will not show better electrical properties than cells based on polished wafers. Furthermore, prior to fabrication of the front contact, passivation should be considered in order to tie up the dangling bonds, which are one of the main sources of surface recombination.

5.1 Introduction

One of the main approaches in lowering the reflectivity of the Si wafers is texturing. Alkaline chemical etching is historically and commercially the main technique for texturing sc-Si and it is not adoptable to mc-Si due to anisotropic nature of the etching and random crystallographic orientation of the wafer. Other chemical etching techniques that are not suffering from anisotropy properties, such as HF have other drawbacks like safety issues or incapability of performing a sufficiently rough surface comparable to that of the alkaline chemical etching. Laser texturing which is a method independent of crystallographic orientation of the wafer has proven to be a suitable alternative to wet etching for texturing mc-Si wafers. However, this technique should be followed by alkaline chemical etching in order to remove the laser-induced damage that is considered as recombination sites. For example, Dobrzanski et al. [20] applied a chemical solution including 20% of KOH at temperature of 80ºC to remove the laser damage and increasing the electrical performance of the solar cell device. Furthermore they validated that a non-textured wafer after saw damage removal demonstrates better electrical properties than a textured wafer which is not amended in chemical solutions [20]. In should be noted that, the thickness of the etched layer should be optimized in order to remove the laser-induced damage that has detrimental influence on the electrical properties and at the same time maintain the roughness that affects the reflectivity.

5.2 Background and theory

Solar energy can be converted into electricity in PV cells. The surface of sun emits light spectrum ranging from ultraviolet (UV) through visible into infrared (IR). Considering the particle-like behavior of the light, it consists of energy packets called, photons. The energy of the photons emitted from the sun is in the range of 3.5 eV to 0.5 eV. The peak power of the solar light is in the yellow region (2.5 eV) of the visible spectrum. Solar cells absorb light with energies only above a certain limit, called band-gap energy (E_g). Therefore, only photons with energies higher than the band gap are absorbed and others pass through the cell. The process of absorption is not only dependent to the energy of the incident photon, but also relies on the thickness and properties of the semiconductor material. Absorption depth (α^{-1}) which is the inverse of the absorption coefficient (α) is the distance that a light of particular wavelength travels before being absorbed. Based on Equation 4.1, for a particular material the absorption coefficient is not constant and depends on the wavelength of the incident photon. That is, photons with higher energies have lower absorption depths and photons with larger wavelengths need to travel more in the material in order to be absorbed. Therefore, for absorption to occur, the thickness or the optical path length of the material should maintain the absorption depth of the incident photon. However, increasing the physical thickness of a device is not the best solution for increasing the absorption and consequently improving the efficiency of a solar cell. First of all, if the light is absorbed out of the diffusion length of the junction, carriers will recombine before reaching the junction. Furthermore, solar cells based on thicker Si wafers, are more expensive since more material is implemented. Nevertheless, texturing not only takes the advantage of lowering the reflectivity, but also results in higher absorption by making the incident light hit the surface of the device with an oblique angle resulting in a larger optical path length than the physical thickness of the material.

$$\alpha = \frac{4\pi K}{\lambda} \qquad \text{or} \qquad \alpha^{-1} = \lambda/4\pi K \tag{5.1}$$

The building block of solar cells can be inorganic semiconductors, organic polymers, or even a combination of both. In semiconductors, when the energy of the light is absorbed by the cell, electrons transfer from the valance band (the highest band that is full at 0 kelvin) to the conduction band (the lowest band that is empty at 0 kelvin). Since there is no allowed energy states between the valence band and the conduction band, only photons with energies higher than the band gap can promote electrons to the conduction band. When electrons transfer to the conduction band,

they leave behind positive charges called, holes in the valance band. The process of EHP creation is called generation. In an intrinsic semiconductor, the concentration of the electrons in the conduction band is equal to the concentration of the holes in the valance band. Any electron in the conduction band is not stable and stabilizes to the valance band by giving off its energy as a photon. The process of removing a hole by an electron is called recombination. There are three types of recombination in the bulk of the single crystalline semiconductor, including radiative or band-to-band recombination, Shockley-Read-Hall (SRH) recombination and Auger recombination. In radiative recombination, which happens in direct band-gap material, an electron in the conduction band directly combines with a hole in the valance band and releases energy. Since this energy is equal to the E_g, it is more likely to exit the semiconductor rather than being absorbed. SRH recombination, which is a two-step process, occurs in semiconductors with defects that introduce energy states in the forbidden gap. In this process, recombination happens when an electron/hole transfers to the energy sates in the forbidden gap where a hole/electron has been trapped. In this type of recombination, energy levels close to the band edges are not considered as effective recombination states. Auger recombination is due to high carrier concentration under heavy doping or high-level injection under concentrated sunlight, which is the case for Si-based solar cells.

The time that excited electron-hole pairs spend and the distance they move before being recombined is called minority carrier lifetime (τ) and minority carrier diffusion length (L), respectively.

$$\tau = \Delta n/R \tag{5.2}$$

$$L = \sqrt{D\tau} \tag{5.3}$$

In Equation 5.2, Δn denotes the excess minority carriers concentration and R the recombination rate and in Equation 5.3, D denotes the diffusivity. Surface recombination, which is more probable in solar cells, is mainly due to the defects such as disruptions or impurities at the surface of the semiconductor. Dangling bonds at the surface of the textured semiconductors used in solar cells are one of the main sources of recombination. Surface passivation is the process of tying up these bonds by growing a layer such as CO_2, on top of the surface of the semiconductor.

By doping the intrinsic semiconductor with atoms that have one more/less valance electron than the intrinsic semiconductor, n-type/p-type semiconductor materials are produced. In n-type/p-type

semiconductors, electrons/holes are the majority carriers and holes/electrons are the minority caries. As mentioned earlier, minatory carriers are created upon illumination or thermal excitation. The number of majority carriers at equilibrium (when there is no external bias applied) is equal to the number of intrinsic carriers plus the number of free carriers added to the semiconductor with doping. When an n-type and p-type semiconductor are in contact, a P-N junction is formed. Due to the high concentration of electrons in the n-type region and high concentration of holes in the p-type region electrons and holes diffuse toward the p-type and n-type regions, respectively. When electrons/holes leave their crystal lattice and move to the other side of the junction, they leave behind positively/negatively charged ions in the n-type/p-type region. Therefore, an electric field is formed at the junction in which the direction is from the n-type material to the p-type material. Although this electric field hinders further diffusion of the majority carriers over the junction and depletes this region from the carriers, some carriers have enough energy to diffuse and cross the junction. On the other hand, minority carriers that are at the edge of the junction are swept to the other side of the junction by the drift current, which is due to the electric field. Since the electron/hole drift current is equal to electron/hole diffusion current and they balance each other the net current from the device at equilibrium is zero. As mentioned earlier, electron-hole pairs are created upon illumination of light and carriers are swept by the electric field at the junction and increase the number of electrons in the n-region and holes in the p-region thus creating a current in the external circuit. This current applies a voltage across the load in the circuit, which is connected to the p-n junction. Since this voltage is opposite to the built in potential at the p-n junction, the electrical field at the junction is reduced thus increasing the diffusion current. If the electrons diffuse to the p-type region and recombine with the existing holes at that region, a current flows from the n-type region to the p-type region, which is opposite to the light current and is called diode current (J_d). Diode current (Equation 5.4) is a measure of the recombination rate and is defined by the saturation current density (Js (Equation 5.5)).

$$J_d = \left[\frac{eD_p P_{n0}}{L_p} + \frac{eD_n n_{p0}}{L_n}\right]\left[\exp\left(\frac{eV_a}{nKT}\right) - 1\right] \tag{5.4}$$

$$J_S = \left[\frac{eD_p P_{n0}}{L_p} + \frac{eD_n n_{p0}}{L_n}\right] \tag{5.5}$$

As shown in Equation 5.6, the total current from a solar cell (J(v)) is the difference between the light current the photo current.

$$J(v) = J_s\left(\exp\left(\frac{qv}{nkT}\right) - 1\right) - J_L \quad (5.6)$$

Equation 5.6 shows that the total current from a solar cell is dependent to the photo generated carriers and the diode current or the recombination rate. When the photo current outweighs the diode or dark current, I or J(v) becomes negative resulting in a negative power, meaning the power has been generated by the solar cell.

The voltage at which the values of the diode current and photocurrent are equal is called the open circuit voltage (V_{oc}) and is the maximum voltage that is produced by a solar cell.

$$v_{oc} = \frac{nkT}{q}\ln\left(\frac{J_l}{J_s} + 1\right) \quad (5.7)$$

Based on Equation 5.7 V_{oc} is increased when the photocurrent increases and reverse saturation current decreases. Short circuit current (I_{sc}) on the other hand, is identical to the photocurrent in ideal solar cells where the series resistance is very low and is equal to the maximum current that is produced by a solar cell. Based on Equation 5.8 I_{sc} is a factor of generation rate and the diffusion length of the electrons and holes where the former factor can be neglected if the thickness of the cell is much shorter that the diffusion lengths of the carriers.

$$J_{sc} = qG(L_n + L_p) \quad (5.8)$$

Equation 5.8 is valid only for a well-passivated surface with a shorter depletion region width that the diffusion lengths of the carriers.

Fill factor (FF) is a measure of the quality of the junction of a cell and the series resistance as well as recombination rate. Based on Equation 5.9 FF is defined by the ratio of the maximum power generated by the cell to the product of the open circuit voltage and the short circuit current.

$$FF = \frac{V_{max}I_{max}}{V_{oc}I_{sc}} = \frac{P_{max}}{V_{oc}I_{sc}} \quad (5.9)$$

5.3 Design and fabrication of P-N Junction

For designing the P-N junction, various parameters including the diffusion time and temperature were determined based on the desired junction depth.

In order to make the P-N junction phosphorofilm was introduced to p-doped textured mc-Si samples as n-type dopants. Prior to diffusion, Phosphorofilm was applied on the samples using a spin coating machine at 2000 RPM for 30 s. This step was followed by backing the samples in the oven at 110ºC for 1 min. The junction depth was designed to be 0.5 µm therefore, based on phosphorofilm data sheet the diffusion time was 1 hr at 900 ºC under 20% O_2 80% N_2 atmosphere. Since the diffusion furnace took 1hr to heat up and 1 hr to cool down, samples were totally kept for 3hr in the furnace, which is shown in Figure 5.1 and Figure 5.2.

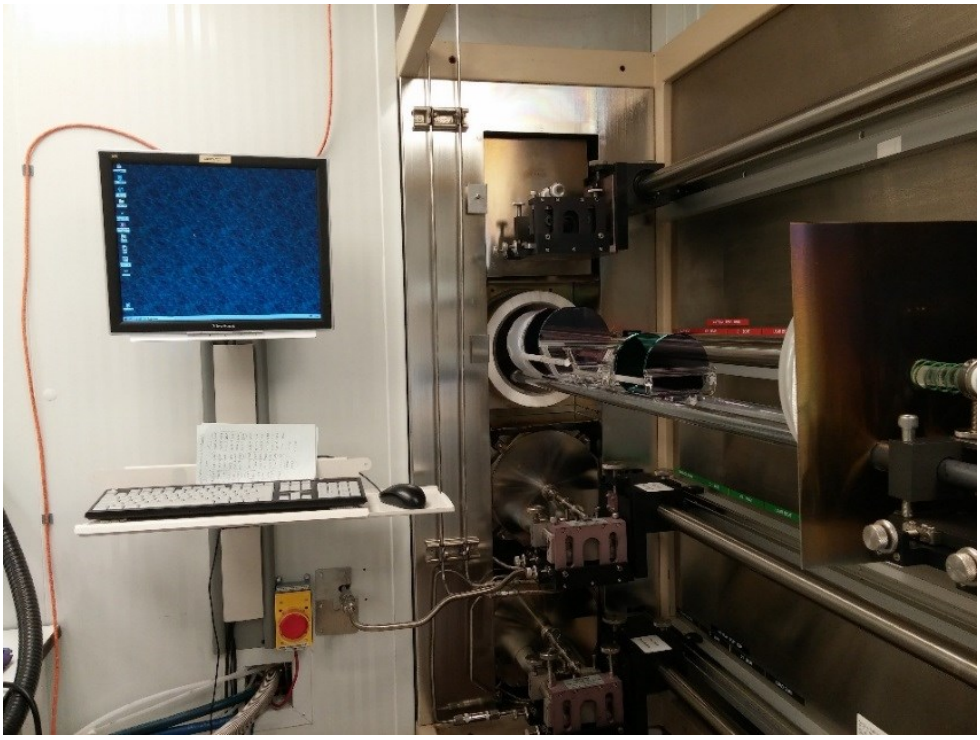

Figure 5.1 Diffusion furnace.

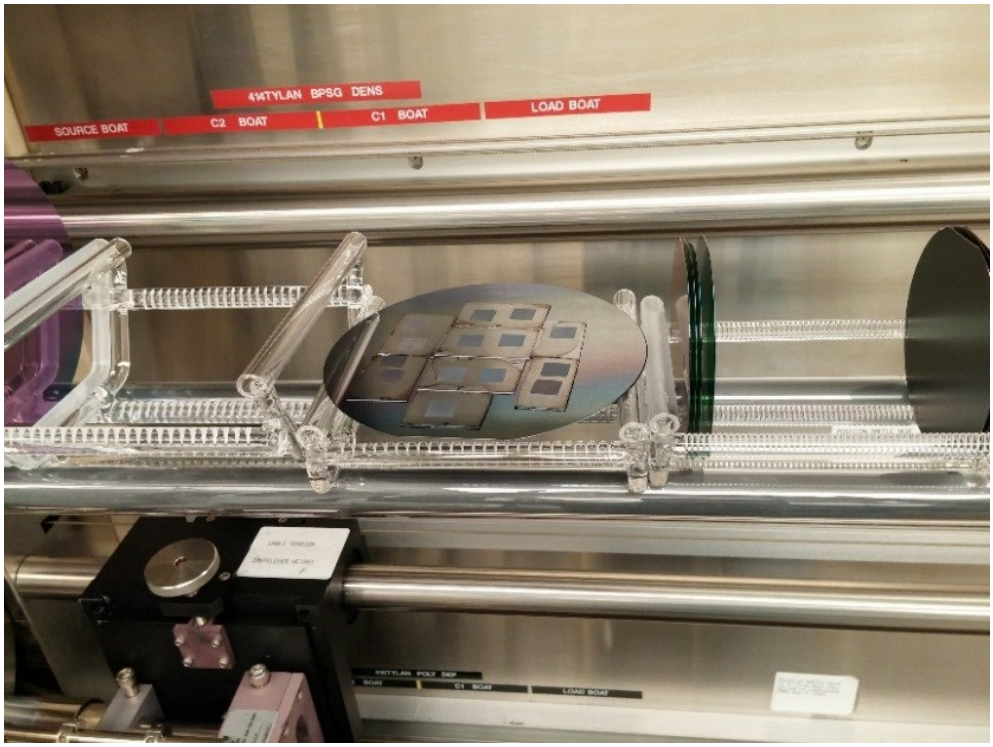

Figure 5.2 Samples loaded in the diffusion furnace

5.4 Fabrication of electrodes

Aluminum (Al) was used as the back contact and the transparent conductor indium tin oxide (ITO) as the front contact. In order to prevent any short-circuiting of the back and front contact, all sides of the samples were covered with Kapton tape. Samples were loaded in the metallization machine at pressure of 10^{-6} Torr to deposit a 250 nm layer of Al on the back sides of the samples. In order to make an intimate ohmic contact between Al and silicon, samples were kept in the oven for 40 min at 300ºC after the metallization step. After depositing a 350 nm layer of ITO on the front surface of the samples by the sputterer shown in Figure 5.3, they were kept in the oven for 15 min at 150 ºC.

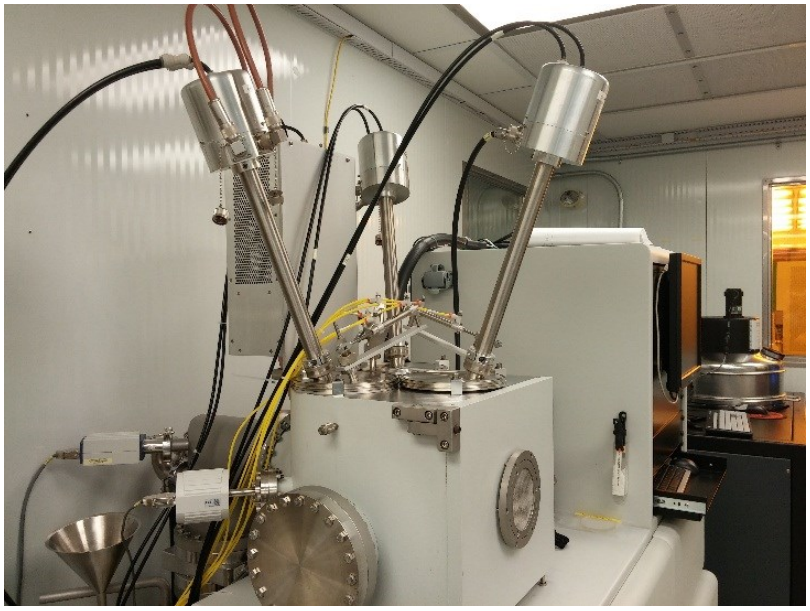

Figure 5.3 Sputterer.

5.5 I-V characterization

I-V characteristics of the fabricated solar cells was carried out with Solar Simulator model #SS50AAA from PET Photo emission Tech Inc. In order to calculate the FF based on the measured output power, the cells were exposed to AM 1.5 sun illumination. It is important to note that of the 14 textured wafers tested, the FF for wafers textured with overlap percentages 30% and 60%; and for number of scans 2 and 4; the results did not show any power output. Only for 0% overlap where the laser-induced damages were minimum we were able to measure the fill factor. Table 5.1 and

Table 5.2 summarize the measured output parameters and calculated values for P_{max} and FF, respectively. As shown in Figure 5.4, FF is the defined as the area of the smaller square (area P_{max}) divided by the area of the bigger square (area P_{total}).

Table 5.1 Measured parameters for the fabricated solar cell

	V_{oc} (V)	Isc (mA)	V_{max} (V)	I_{max} (mA)
Untextured sample	0.18	0.10	0.092	0.051
Textured sample 3	0.005	0. 015	0.002	0.006
Textured sample 4	0.10	0.08	0.060	0.027
Textured sample 5	0.013	0. 002	0.009	0.001

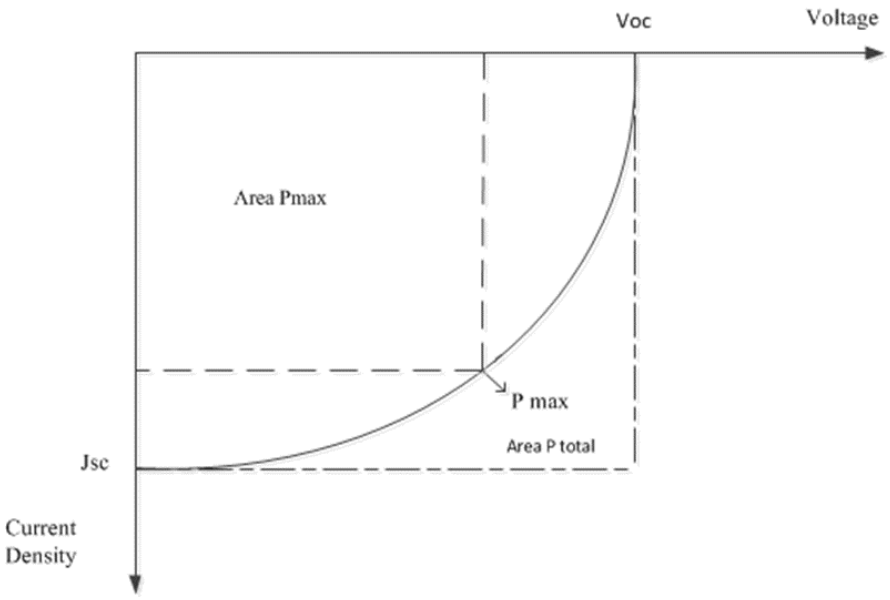

Figure 5.4 Schematic of the I-V characteristics of the solar cell.

Table 5.2 Calculated parameters for the fabricated solar cell.

	P_{max} (mW)	FF
Untextured sample	0.0047	26%
Textured sample 3	0.000012	16%
Textured sample 4	0.0016	20%
Textured sample 5	0.000014	53%

Table 5.3 Properties of the textured samples used for fabrication.

Sample	%SWR	depth(μm)	Ra(nm)	overlap	# scans	Fluence(J/cm^2)
Textured sample 3	2.107894	3.88	1060	0%	4	18
Textured sample 4	5.799918	1.6	371	0%	1	22
Textured sample 5	3.146552	2.55	553	0%	2	22

As shown in Table 5.2, sample 5 has the highest FF compared to other textured and untextured samples. From Table 5.3 we can see that except number of scans, other factors such as laser fluence and pulse overlap are the same in all three textured samples. By comparing the SWR values of the textured samples, we can see that more number scans leads to lower SWR values. However, we

know that, by increasing the number of scans the wafer is more deteriorated. On the other hand, to have a cell with a good FF value, we need to have the maximum light absorption and minimum recombination. However, based on Table 5.3 maximum light absorption is achieved when more number of scans are applied to the wafer and this in turn introduces more defects and consequently recombination sites to the wafer. Therefore, we can say that a medium condition where the SWR is not the least and defects are not the most, can be chosen as the best condition for a sample to be used as a solar cell. Though the fill factor for sample 5 is higher than that of untextured wafer, the P_{max} output from untextured wafer is still higher, which shows that better solar cell processing protocol needs to be followed.

5.6 Conclusion

The solar cell efficiency is not improved only by increasing the absorption, but also it is dependent to the recombination rate that affects the voltage. At the end of our research on laser texturing of mc-Si, we attempted to build solar cells based on our samples and distinguish the I-V characterization of the cells based on textured and non-textured mc-Si. Results show that there should be other important factors rather than the optical aspects that influence the electrical output of the device. One of the important parameters that affects the I-V characteristics of a solar cell and we ignored is the recombination issue that has to be minimized by etching textured wafers in a chemical solution. Therefore, considering this factor in the future works might hugely improve the electrical results of the fabricated devices.

CHAPTER 6. Conclusion and future work

6.1 Conclusion

In chapter 1, we went through different sc-Si and mc-Si texturing methods from the literatures and found laser texturing as the best approach for mc-Si texturing. Although, there are many works done to evaluate the effect of laser parameters on R_a and SWR, none investigated the optimum condition that results in minimum SWR along with the least energy consumption. To this aim, we implemented a statistical method to investigate the best condition that optimizes laser texturing experiment results.

In chapter 2, we designed the optical setup to carry out laser texturing experiments in two different ambients, air and acetone. In chapters 3 and 4 we investigated the effect of laser fluence, number of irradiations, pulse overlap and texturing ambient on morphology and optical properties of mc-Si. Interferometry microscope has been utilized in order to measure the R_a and depth of the micro/nano structures formed on the samples. ANOVA has been implemented to statistically evaluate the significance of laser texturing variables on R_a and depth. Implementing ANOVA in laser texturing takes the advantage of minimizing the huge amount of variables at a fixed number of experiments where the energy and time consumption are optimized. It was shown that, when texturing is conducted in air, overlap has the highest significance level and then the number of irradiations while laser fluence does not statistically alter the roughness and depth of the structures.

On the other hand, depth values demonstrate that at some certain overlap percentage and laser fluence values, increasing the number of irradiations is effective only up to a limit and further increasing this parameter does not enhance the depth. This is not true in wet treated samples where the highest number of irradiations results in higher depth values. Regression is used to test whether depth or R_a plays the major role in SWR reduction and it is understood that although both have statistically significant effect on the SWR, depth is more important when SWR below 2.44% is desired. Furthermore, due to the deposition of the ablated material on the textured area in dry laser texturing, shallower valleys are achieved compared to acetone-assisted experiments where the ablated material are taken away from the surface due to the bubble formation.

In chapter 5, we went through some theory about the semiconductor materials and electrical properties of the P-N junction devices. In addition, we explained the steps that we proceeded to

fabricate P-N junction based on our textured mc-Si samples along with investigating the I-V characteristics of the fabricated cells. Finally, we concluded that the laser textured mc-Si samples should undergo some chemical etching processes to remove the laser-induced damage and surface passivation should be implemented to tie up the dangling bonds, which are considered as another reason for low V_{oc} and I_{sc}.

6.2 Future work

Since we did not have the facilities to evaluate the effect of different laser wavelengths and pulse durations on the morphology and optical properties of the wafers, we suggest a statistical analysis work to investigate the effect of mentioned parameters on SWR. In this study we found that laser power does not play a major role in SWR reduction, therefore in future studies we can fix the laser power at a medium level and broaden the range of other factors such as overlap to see if better SWR is achieved within a the new range of variables.

On the other hand, further optimization in the fabrication steps is needed to improve the efficiency of the solar cell device. These reformations are mainly concerned with removing the recombination sites. Some of those optimization techniques are listed below:

- Etching the textured samples in alkaline solution for removing the laser-induced damage, which is one of the main sources of recombination. A per Dobrzanski et al. [20] this process can be done by using a 20% KOH solution at 80°C.
- Applying wet etching in diluted HF for removing the redundant phosphorofilm after the diffusion step.
- Surface passivation; Surface recombination is one of main reasons of having low V_{oc} and I_{sc}. Surface passivation is the process of tying up Si dangling bonds at the surface, which are considered as active sites for recombination. If the whole surface is to be covered with ITO as the front contact, wet oxidation is not the right passivation method because it is an insulator layer and in this case allowing the textured samples under N_2 and H_2 would be a better solution.

Finally, simulating the optical and electrical properties of the laser textured mc-Si structures with Sentaurus, which is the most commonly used modeling software in the PV industry. This software, uses finite element method to accurately model textured and untextured Si-based solar cell devices.

References

[1] J. Conti, “International Energy Outlook 2014,” 2014.

[2] N. S. Lewis, “Toward cost-effective solar energy use.,” *Science*, vol. 315, no. 5813, pp. 798–801, 2007.

[3] N. S. Lewis, G. Crabtree, A. J. Nozik, M. R. Wasielewski, and P. Alivisatos, “Basic Research Needs for Solar Energy Utilization,” *Basic Energy Sci. Work. Sol. Energy Util.*, p. 276, 2005.

[4] J. Zhao, A. Wang, M. a. Green, and F. Ferrazza, “19.8% Efficient ‘Honeycomb’ Textured Multicrystalline and 24.4% Monocrystalline Silicon Solar Cells,” *Appl. Phys. Lett.*, vol. 73, no. 14, p. 1991, 1998.

[5] W. Shockley and H. J. Queisser, “Detailed Balance Limit of Efficiency of p-n Junction Solar Cells,” *J. Appl. Phys.*, vol. 32, no. 3, p. 510, 1961.

[6] “ASTM G173 - Standard Tables for Reference Solar Spectral Irradiances: Direct Normal and Hemispherical on 37 Tilted Surface,” 2008.

[7] H. Nakaya, “Polycrystalline silicon solar cells with V-grooved surface,” *Sol. Energy Mater. Sol. Cells*, vol. 34, pp. 219–225, 1994.

[8] K. Tsujino, M. Matsumura, and Y. Nishimoto, “Texturization of multicrystalline silicon wafers for solar cells by chemical treatment using metallic catalyst,” *Sol. Energy Mater. Sol. Cells*, vol. 90, no. 1, pp. 100–110, 2006.

[9] T. Machda, “Development of low cost production technologies for polycrystalline silicon solar cells,” *Sol. Energy Mater. Sol. Cells*, vol. 48, no. 1–4, pp. 243–253, 1997.

[10] P. K. Singh, R. Kumar, M. Lal, S. N. Singh, and B. K. Das, “Effectiveness of anisotropic etching of silicon in aqueous alkaline solutions,” *Sol. Energy Mater. Sol. Cells*, vol. 70, no. 1, pp. 103–113, 2001.

[11] P. Papet, O. Nichiporuk, a. Kaminski, Y. Rozier, J. Kraiem, J.-F. Lelievre, a. Chaumartin, a. Fave, and M. Lemiti, “Pyramidal texturing of silicon solar cell with TMAH chemical anisotropic etching,” *Sol. Energy Mater. Sol. Cells*, vol. 90, no. 15, pp. 2319–2328, 2006.

[12] Y. T. Cheng, J. J. Ho, S. Y. Tsai, Z. Z. Ye, W. Lee, D. S. Hwang, S. H. Chang, C. C. Chang, and K. L. Wang, “Efficiency improved by acid texturization for multi-crystalline silicon solar cells,” *Sol. Energy*, vol. 85, no. 1, pp. 87–94, 2011.

[13] E. S. Marstein, H. J. Solheim, D. N. Wright, and A. Holt, "Acidic texturing of multicrystalline silicon wafers," *Conf. Rec. Thirty-first IEEE Photovolt. Spec. Conf. 2005.*, no. 2027, pp. 1309–1312, 2005.

[14] P. Panek, M. Lipiński, and J. Dutkiewicz, "Texturization of multicrystalline silicon by wet chemical etching for silicon solar cells," *J. Mater. Sci.*, vol. 40, no. 6, pp. 1459–1463, 2005.

[15] A. K. Volk, S. Gotscher, A. Brand, W. Wolke, M. Zimmer and H. Reinecke, "Laser assisted honeycomb-texturing on multicrystalline silicon for industrial applications," *28th Eur. PV Sol. Energy Conf. Exhib.*, pp. 1–5, 2013.

[16] Y. Nishimoto, "Investigation of Acidic Texturization for Multicrystalline Silicon Solar Cells," *J. Electrochem. Soc.*, vol. 146, no. 2. p. 457, 1999.

[17] U. Gangopadhyay, S. K. Dhungel, P. K. Basu, S. K. Dutta, H. Saha, and J. Yi, "Comparative study of different approaches of multicrystalline silicon texturing for solar cell fabrication," *Sol. Energy Mater. Sol. Cells*, vol. 91, no. 4, pp. 285–289, 2007.

[18] R. Younkin, J. E. Carey, E. Mazur, J. a. Levinson, and C. M. Friend, "Infrared absorption by conical silicon microstructures made in a variety of background gases using femtosecond-laser pulses," *J. Appl. Phys.*, vol. 93, no. 5, p. 2626, 2003.

[19] "PV education, Optical properties of Silicon" 2015. [Online]. Available: http://www.pveducation.org/pvcdrom/materials/optical-properties-of-silicon.

[20] L. A. Dobrzañski, A. Drygaa, P. Panek, M. Lipiñski, and P. Ziêba, "Development of the laser method of multicrystalline silicon surface texturization," *Int. Sci. J.*, vol. 38, no. 1, pp. 5–11, 2009.

[21] Z. Fu, B. Wu, Y. Gao, Y. Zhou, and C. Yu, "Experimental study of infrared nanosecond laser ablation of silicon: The multi-pulse enhancement effect," *Appl. Surf. Sci.*, vol. 256, no. 7, pp. 2092–2096, 2010.

[22] J. Jiménez-Jarquín, M. Fernández-Guasti, E. Haro-Poniatowski, and J. L. Hernández-Pozos, "IR and UV laser-induced morphological changes in silicon surface under oxygen atmosphere," *Phys. Status Solidi*, vol. 2, no. 10, pp. 3798–3801, 2005.

[23] X. Li, L. Chang, R. Qiu, C. Wen, Z. Li, and S. Hu, "Microstructuring and doping of silicon with nanosecond laser pulses," Appl. Surf. Sci., vol. 258, no. 20, pp. 8002–8007, 2012.

[24] A. J. Pedraza, J. D. Fowlkes, and Y.-F. Guan, "Surface nanostructuring of silicon," *Appl. Phys. A*, vol. 77, no. 2, pp. 277–284, 2003.

[25] C. H. Crouch, J. E. Carey, J. M. Warrender, M. J. Aziz, E. Mazur, and F. Y. Génin, "Comparison of structure and properties of femtosecond and nanosecond laser-structured silicon," *Appl. Phys. Lett.*, vol. 84, no. 11, p. 1850, 2004.

[26] M. Sheehy, L. Winston, and J. et al. Carey, “Role of the background gas in the morphology and optical properties of laser-microstructured silicon,” *Chem. Mater.*, vol. 17, no. 3, pp. 3582–3586, 2005.

[27] V. V. Iyengar, B. K. Nayak, K. L. More, H. M. Meyer, M. D. Biegalski, J. V. Li, and M. C. Gupta, “Properties of ultrafast laser textured silicon for photovoltaics,” *Sol. Energy Mater. Sol. Cells*, vol. 95, no. 10, pp. 2745–2751, 2011.

[28] S. Zhu, Y. F. Lu, and M. H. Hong, “Laser ablation of solid substrates in a water-confined environment,” *Appl. Phys. Lett.*, vol. 79, no. 9, pp. 1396–1398, 2001.

[29] S. Zhu, Y. F. Lu, M. H. Hong, and X. Y. Chen, “Laser ablation of solid substrates in water and ambient air,” *J. Appl. Phys.*, vol. 89, no. 4, pp. 2400–2403, 2001.

[30] J. Ren, M. Kelly, and L. Hesselink, “Laser ablation of silicon in water with nanosecond and femtosecond pulses.,” *Opt. Lett.*, vol. 30, no. 13, pp. 1740–1742, 2005.

[31] M. Sobhani and M. H. Mahdieh, “Comparison of sub-micro/nano structure formation on polished silicon surface irradiated by nanosecond laser beam in ambient air and distilled water,” *Laser Part. Beams*, vol. 31, no. 03, pp. 465–473, 2013.

[32] R. Karimzadeh, J. Z. Anvari, and N. Mansour, “Nanosecond pulsed laser ablation of silicon in liquids,” *Appl. Phys. A*, vol. 94, no. 4, pp. 949–955, 2009.

[33] J. H. Zhao, C. H. Li, Z. H. Lv, and Y. Xu, “Regular arrays of triangular-microstructure formed on silicon (111) surface via ultrafast laser irradiation in KOH solution,” *Surf. Interface Anal.*, vol. 45, no. July, pp. 1667–1672, 2013.

[34] M. Füle, “Ti:sapphire Laser Ablation of Silicon in Different Ambients,” *J. Laser Micro/Nanoengineering*, vol. 9, no. 2, pp. 119–125, 2014.

[35] M. Aghayan and S. Narayanswamy, “Morphology based statistical analysis of nanosecond pulsed laser texturing of the multicrystalline silicon,” *J. Laser Appl.*, vol. 27, no. 3, p. 032002, 2015.

[36] “Semrock” 2015. [Online]. Available: http://www.semrock.com/laser-damage-threshold.aspx.

[37] M. Hoeven, “Technology Roadmap,” *INTERNATIONAL ENERGY AGENCY (IEA)*, 2013.

[38] M. H. Kang, K. Ryu, A. Upadhyaya, and A. Rohatgi, “Optimization of SiN AR coating for Si solar cells and modules through quantitative assessment of optical and efficiency loss mechanism,” *Prog. photovoltaics*, vol. 19, no. 8, pp. 983–990, 2011.

[39] V. V. Iyengar, B. K. Nayak, and M. C. Gupta, "Optical properties of silicon light trapping structures for photovoltaics," *Sol. Energy Mater. Sol. Cells*, vol. 94, no. 12, pp. 2251–2257, 2010.

[40] M. Green, "Lambertian light trapping in textured solar cells and light-emitting diodes: analytical solutions," *Prog. Photovoltaics Res. Appl.*, vol. 10, no. 4, pp. 235–241, 2002.

[41] M. S. Brown and C. B. Arnold, "*Laser Precision Microfabrication*," Berlin, Heidelberg: Springer Berlin Heidelberg, vol. 135, 2010.

[42] G. G. Untila and M. B. Zaks, "Silicon-based photovoltaics: State of the art and main lines of development," *Therm. Eng.*, vol. 58, no. 11, pp. 932–947, 2011.

[43] A. Nijdam, J. van Suchtelen, J. . Berenschot, J. G. . Gardeniers, and M. Elwenspoek, "Etching of silicon in alkaline solutions: a critical look at the {111} minimum," *J. Cryst. Growth*, vol. 198–199, pp. 430–434, 1999.

[44] Y. Wang, W. Xu, Y. Zhou, L.-Z. Chu, and G.-S. Fu, "Influence of pulse repetition rate on the average size of silicon nanoparticles deposited by laser ablation," *Laser Part. Beams*, vol. 25, no. 01, pp. 9–13, 2007.

[45] P. Panek and C. Techniques, "Application of laser in multicrystalline silicon surface processing," *J. Achiev. Mater. Manuf. Eng.*, vol. 24, no. 2, pp. 179–182, 2007.

[46] J. F. Nijs, J. Szlufcik, J. Poortmans, S. Sivoththaman, and R. P. Mertens, "Advanced cost-effective crystalline silicon solar cell technologies," *Sol. Energy Mater. Sol. Cells*, vol. 65, pp. 249–259, 2001.

[47] L. Dobrzański and a. Drygała, "Laser processing of multicrystalline silicon for texturization of solar cells," *J. Mater. Process. Technol.*, vol. 191, no. 1–3, pp. 228–231, 2007.

[48] L. Dobrzański and A. Drygała, "Surface texturing of multicrystalline silicon solar cells," *J. Achiev. Mater. Manuf. Eng.*, vol. 31, no. 1, pp. 77–82, 2008.

[49] U. Zastrow, L. Houben, D. Meertens, a. Grohe, T. Brammer, and E. Schneiderlöchner, "Characterization of laser-fired contacts in PERC solar cells: SIMS and TEM analysis applying advanced preparation techniques," *Appl. Surf. Sci.*, vol. 252, no. 19, pp. 7082–7085, 2006.

[50] M. D. Abbott, T. Trupke, H. P. Hartmann, R. Gupta, and O. Breitenstein, "Laser Isolation of Shunted Regions in Industrial Solar Cells," *Prog. photovoltaics*, vol. 15, no. 7, pp. 613–620, 2007.

[51] C. Eisele, M. Berger, M. Nerding, H. P. Strunk, C. E. Nebel, and M. Stutzmann, "Laser-crystallized microcrystalline SiGe alloys for thin film solar cells," *Thin Solid Films*, vol. 427, no. 1–2, pp. 176–180, 2003.

[52] B. R. Wu, D. S. Wuu, M. S. Wan, H. Y. Mao, and R. H. Horng, "Fabrication of selective-emitter silicon heterojunction solar cells using hot-wire chemical vapor deposition and laser doping," *Thin Solid Films*, vol. 517, no. 17, pp. 4749–4752, 2009.

[53] K. S. Wang, B. S. Tjahjono, J. Wong, A. Uddin, and S. R. Wenham, "Sheet resistance characterization of laser-doped lines on crystalline silicon wafers for photovoltaic applications," *Sol. Energy Mater. Sol. Cells*, vol. 95, no. 3, pp. 974–980, 2011.

[54] M. Shen, J. E. Carey, C. H. Crouch, M. Kandyla, H. a Stone, and E. Mazur, "High-density regular arrays of nanometer-scale rods formed on silicon surfaces via femtosecond laser irradiation in water," *Nano Lett.*, vol. 8, no. 7, pp. 2087–91, 2008.

[55] J. Bonse, J. Krüger, S. Höhm, and a. Rosenfeld, "Femtosecond laser-induced periodic surface structures," *J. Laser Appl.*, vol. 24, no. 4, p. 042006, 2012.

[56] A. J. Pedraza, J. D. Fowlkes, and D. H. Lowndes, "Silicon microcolumn arrays grown by nanosecond pulsed-excimer laser irradiation," *Appl. Phys. Lett.*, vol. 74, no. 16, p. 2322, 1999.

[57] M. Halbwax, T. Sarnet, P. Delaporte, M. Sentis, H. Etienne, F. Torregrosa, V. Vervisch, I. Perichaud, and S. Martinuzzi, "Micro and nano-structuration of silicon by femtosecond laser: Application to silicon photovoltaic cells fabrication," *Thin Solid Films*, vol. 516, no. 20, pp. 6791–6795, 2008.

[58] M. Abbott and J. Cotter, "Optical and electrical properties of laser texturing for high-efficiency solar cells," *Prog. Photovoltaics Res. Appl.*, vol. 14, no. 3, pp. 225–235, 2006.

[59] S. Tao, B. Wu, Y. Zhou, and Y. Gao, "Thermal modeling and experimental study of infrared nanosecond laser ablation of silicon," *J. Appl. Phys.*, vol. 106, no. 12, p. 123507, 2009.

[60] S. W. Glunz, R. Preu, and D. Biro, "Crystalline Silicon Solar Cells: State-of-the-Art and Future Developments," *Comprehensive Renewable Energy*, vol. 1, pp. 353–387, 2012.

[61] K.-R. Kim, T.-H. Kim, H.-A. Park, S.-Y. Kim, S.-H. Cho, J. Yi, and B.-D. Choi, "UV laser direct texturing for high efficiency multicrystalline silicon solar cell," *Appl. Surf. Sci.*, vol. 264, pp. 404–409, 2013.

[62] P. V. Kazakevich, a. V. Simakin, and G. a. Shafeev, "Formation of periodic structures by laser ablation of metals in liquids," *Appl. Surf. Sci.*, vol. 252, no. 13, pp. 4457–4461, 2006.

[63] I. Sukhov, G. Shafeev, V. V. Voronov, M. Sygletou, E. Stratakis, and C. Fotakis, "Generation of nanoparticles of bronze and brass by laser ablation in liquid," *Appl. Surf. Sci.*, vol. 302, pp. 79–82, 2014.

[64] A. Kruusing, "Underwater and water-assisted laser processing: Part 1 - General features, steam cleaning and shock processing," *Opt. Lasers Eng.*, vol. 41, no. 2, pp. 307–327, 2004.

[65] K. L. Choo, Y. Ogawa, G. Kanbargi, V. Otra, L. M. Raff, and R. Komanduri, "Micromachining of silicon by short-pulse laser ablation in air and under water," *Mater. Sci. Eng. A*, vol. 372, no. 1–2, pp. 145–162, 2004.

[66] A. Kruusing, "Underwater and water-assisted laser processing: Part 2 - Etching, cutting and rarely used methods," *Opt. Lasers Eng.*, vol. 41, no. 2, pp. 329–352, 2004.

[67] W. Liu, O. Kosareva, I. S. Golubtsov, a. Iwasaki, a. Becker, V. P. Kandidov, and S. L. Chin, "Femtosecond laser pulse filamentation versus optical breakdown in H2O," *Appl. Phys. B Lasers Opt.*, vol. 76, no. 3, pp. 215–229, 2003.

[68] J. M. Vadillo, J. M. Fernández Romero, C. Rodríguez, and J. J. Laserna, "Effect of plasma shielding on laser ablation rate of pure metals at reduced pressure," *Surf. Interface Anal.*, vol. 27, no. 11, pp. 1009–1015, 1999.

[69] G. Daminelli, J. Krüger, and W. Kautek, "Femtosecond laser interaction with silicon under water confinement," *Thin Solid Films*, vol. 467, no. 1–2, pp. 334–341, 2004.

[70] K. Hadobás, S. Kirsch, a Carl, M. Acet, and E. F. Wassermann, "Reflection properties of nanostructure-arrayed silicon surfaces," *Nanotechnology*, vol. 11, no. 3, pp. 161–164, 2000.

[71] M. J. Huang, C. R. Yang, Y. C. Chiou, and R. T. Lee, "Fabrication of nanoporous antireflection surfaces on silicon," *Sol. Energy Mater. Sol. Cells*, vol. 92, no. 11, pp. 1352–1357, 2008.

[72] N. Bärsch, J. Jakobi, S. Weiler, and S. Barcikowski, "Pure colloidal metal and ceramic nanoparticles from high-power picosecond laser ablation in water and acetone.," *Nanotechnology*, vol. 20, no. 44, p. 445603, 2009.